UNIVERSITY OF CALIFORNIA, MERCED

CHARACTERIZING CHEMICAL CLEANERS USED IN REMOVING VARNISH IN GAS TURBINE ENGINES

by

Duval A. Johnson

A disertation submitted in partial satisfaction of the
requirements for the degree of
Doctor of Philosophy

in

Mechanical Engineering

Committee in charge:
Professor Ashlie Martini, Advisor
Professor Gerardo Diaz
Professor Po-Ya Abel Chuang
Dr. Zhen Zhou

The disertation of Duval A. Johnson is approved:

_____

Ashlie Martini, Advisor   Date

_____

Gerardo Diaz   Date

_____

Po-Ya Abel Chuang   Date

_____

Zhen Zhou   Date

University of California, Merced

This dissertation is dedicated to the people I cherish most in my life. My children have become a source of inspiration and motivation for me throughout my academic life. As a man ages, thoughts of legacy and contribution fill his mind. I submit this work as motivation for them to achieve great things and to gain an understanding of the valuable contributions they can make to the scientific community and society. My wife, Xiaoli, who also obtained her Ph.D. from Professor Ashlie Martini, is an incredible woman who supports our family and fills the role of taxi, chef, tutor and so much more. My mother was constantly available to help her grandchildren in anyway needed. This wouldn't have been possible without the combined contribution of my family. Reach for the stars and never give up.

CURRICULUM VITAE

EDUCATION

- B.S. in Mechanical Engineering, University of California, Merced, 2014.

WORK HISTORY

- 2018 Mechanical Engineer II and Tribologist, Jet Propulsion Laboratory, Pasadena, CA

- 2018 Teaching Assistant, Statics and Dynamics (ENGR 057), University of California, Merced, CA

- 2017 Graduate Student Researcher, Martini Research Group, University of California, Merced, CA

- 2016 Lecturer, Statics and Dynamics (ENGR 057), University of California, Merced, CA

- 2015 Lecturer, Statics and Dynamics (ENGR 057), University of California, Merced, CA

- 2015 Teaching Assistant, Capstone Design, University of California, Merced, CA

- 2014 Teaching Assistant, Statics and Dynamics (ENGR 057), University of California, Merced, CA

- 2014 Undergraduate Reader, Statics and Dynamics (ENGR 057), University of California, Merced, CA

- 2014 Lead Transmission Specialist, AAMCO Transmissions, Merced, CA

- 1991-1018 CEO and Founder, DJ Repair and Fabrication, Merced, CA

- 1986-1988 Medical Specialist, United States Army

HONORS AND AWARDS

- 2017-2018 Graduate Deans Dissertation Fellowship, University of California, Merced

- 2015-2016 Graduate Deans Dissertation Fellowship, University of California, Merced

- 2015 Bobcat Fellowship Award, University of California, Merced

- 2014-2015 School of Engineering Dean's Travel Award, University of California, Merced

- 2014 Outstanding Undergraduate Award, University of California, Merced

- 2013 Mechanical Engineering Graduate Fellowship Award, University of California, Merced

- 2012 Graduate Division General Fellowship, University of California, Merced

PUBLICATIONS

1. **Duval Johnson**, Characterizing Chemical Cleaners Used in Removing Varnish in Gas Turbine Engines, *Thesis, University of California, Merced*, (2018).

2. **Duval Johnson, Enrique Dominguez, Elizabeth Montalvo, Zhen Zhou, Ashlie Martini**, Quantifying Varnish Removal Using Chemical Flushes, *Tribology Transactions*, (2018).

3. **Paul Michael, Mercy Cheekolu, Pawan Panwar, Mark Devlin, Rob Davidson, Duval Johnson, Ashlie Martini**, Temporary and Permanent Viscosity Loss Correlated to Hydraulic System Performance, *Tribology Transactions*, (2018).

4. **Duval Johnson**, Simulation and Analysis of a Fractionally Controlled Active Suspension System Using Quarter Car Model, *ASME*, (2015).

TABLE OF CONTENTS

LIST OF FIGURES

xiii

LIST OF TABLES

ACKNOWLEDGEMENTS

ABSTRACT

Varnish is an undesirable by-product of using hydrocarbons as lubricants and hydraulic fluids. Oxidation of hydrocarbons is a natural process accelerated by heat, pressure, light and mechanical stressing. Varnish coats metal surfaces with a thin orange carbonaceous film that reduces clearances and, in extreme cases, causes stuck hydraulic valves in large frame gas turbine engines and automotive automatic transmissions, as well as failure of journal bearings and thrust surfaces from reduced clearances and high temperatures. These effects can cost down time for equipment causing lost revenue and expense to address varnish related failures. One method of removing varnish is the use of chemical cleaning compounds that are flushed through the system to soften, dislodge and remove varnish using filtration. However, comparisons of varnish removal effectiveness between cleaning compounds have not been possible because there is no consistent method used for evaluating varnish removal and, more generally, a poor fundamental understanding of removal mechanisms. This research included design and implementation of a varnish removal test system combined with a new method of characterizing cleaner fluid effectiveness. In the newly developed method, the fluids remove artificial varnish applied to a coupon within the test system and removal is characterized by mass loss, filter inspection and in situ imaging of the removal process. The results are analyzed in terms of varnish removal mechanisms based on multiple types of diffusion. This research allows cleaner fluids to be directly compared and provides a greater fundamental understanding of varnish and varnish removal mechanisms.

Chapter 1

INTRODUCTION

1.1 Lubrication History

The history of lubrication extends well over 7 millennia [15]. The knowledge accumulated during this time gives us the ability to design, build, and maintain some of the most sophisticated machines the world has ever seen. Machines that provide us with the ability to generate electricity, provide transportation, process materials, explore space, and a host of other comforts we have come to enjoy and rely on today.

Long ago man would rotate a stick in his palms while simultaneously pressing it against another piece of wood to generate enough friction to make fire. This pivotal idea began a quest to turn the stick more efficiently and apply pressure to the end more effectively. Figure 1.1.0.1 shows the pinnacle of this hand held device with the use of a bowstring to rapidly rotate the stick while applying pressure in the form of a cap. The bowstring and cap went through many iterations as materials were investigated that would endure the friction of rapid rotation. Consider-

Figure 1.1.0.1: Egyptian drill [1]

ing the cap, it is known that it was first made of bone, then stone, then soapstone, and then finally of bronze and iron. This cap was a prime example of *necessity being the mother of invention* as the first bearings were born [16].

It is believed that the idea of lubrication began in ancient Egypt during the early civilizations period [17]. Ancient Egypt, which is known throughout the world for its colossal construction projects, moved huge stone blocks for the building of pyramids and sphinxes that necessitated the use of a lubricant to lessen the force required to move the massive stone blocks. The Egyptians used tree trunks (effectively roller bearings) under these large blocks as well as hydrated calcium sulphate (otherwise known as gypsum) to place and move the blocks during final

assembly. Water is shown as a lubricant on paintings from Saqqara (circa 2400 BC) and El-Bersheh (c.1880 BC) as another method to facilitate moving large stone blocks [18].

Perhaps the most pivotal invention of all time, the wheel, set man on a path to find methods of reducing rolling resistance and mitigating the heat that occurred on the hub of the wheel. Lubricating the wheel hub began around 2600 B.C. when sled wheels, that belonged to Ra-At-Ka (Pharo king of Egypt), used beef or ram tallow to lubricate the axle [18]. Early experimentation used oils and fats common to the day and the Egyptians noticed that some of the more viscous liquids not only dissipated heat but also prevented much of the heat from being generated in the first place [19].

The first real scientific study of lubricants began when Sir Issac Newton (1643 - 1727) [20] found the proportional relationship shown as Equation 1.1.

$$\tau = \frac{F}{A} = \eta \frac{\partial U}{\partial y} \tag{1.1}$$

Equation 1.1 states that the force (F) required to move an object is proportional to the area (A), the local velocity gradient ($\frac{\partial U}{\partial y}$) [21], and the proportionality factor η (specifically, the dynamic viscosity). The shear stress (F/A) is frequently represented by the Greek letter (τ). What Newton found was that the viscosity of a fluid was an important characteristic of the fluid and was directly proportional to the force required to move the upper plate in Figure 1.1.0.2.

$$\frac{F}{A} = \tau = \eta \frac{dU}{dy}$$
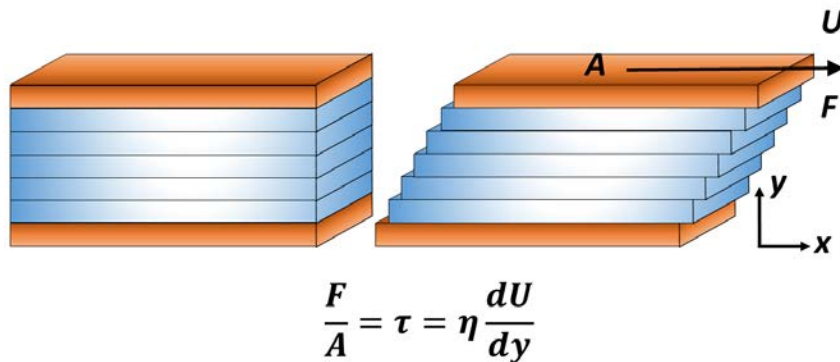
Figure 1.1.0.2: Two plate model

Scientists that followed Newton provided further characterization of fluid and material dynamics which allows today's machines to provide ever longer service life. James Watt's (1736 - 1819) development of the practical steam engine (c.1769)

introduced the industrial age [22]. The coming of new, more demanding machines marked the beginning of the search for improved lubricants to meet the requirements of devices operating at constantly increasing speeds and loads. The first substances to be used were mineral oils, which were obtained from naturally occurring surface pools and extended with the addition of known plant and animal oils. Beauchamp Tower (1845 - 1904) is credited with the discovery of substantial pressures in a half-bearing simulating the conditions found in railway axle-boxes of the day. Tower's investigations also found that the common methods of lubrication are so irregular in their action that the friction in a bearing often varies considerably. In order to achieve consistent results, the majority of Tower's investigations were carried out with the journal immersed, or at least dipped into, a bath of oil. This recognition of the importance of adequate lubrication was one of the major results of Tower's investigations [23].

Heinrich Rudolph Hertz (1857 - 1894) studied contact stresses and deformations that are basic to lubrication principals. Richard Stribeck (1861 - 1950) made significant contributions to the ball bearing industry and advanced our understanding of the friction in plain bearings. In the course of his life a vast ball-bearing industry was established and he became a world recognized figure for his contributions to the science and technology of plain and rolling element bearings [17]. Mayo D. Heresy (1886 - 1978) developed a mathematical formula to determine friction due to viscous shear, now called the Hersey number by engineers. He was considered among the world's foremost authorities on tribology, studying interacting moving surfaces such as gears, and related factors including corrosion, erosion, friction, lubrication, and viscosity.

Over years of research and development it was found that mineral oil was an excellent lubricant and helped to drive the search for easier and more efficient methods of extracting it. The world of oil as we know it today began when the first oil well was successfully drilled in Titusville, Pennsylvania, in 1859 [24]. By 1860 over 1000 barrels of oil per day were extracted from American soil and this number swelled to over 174 thousand barrels of oil per day by 1900 [25]. The Industrial Revolution, two world wars, and a monumental transportation industry has driven crude production to new heights. In 2016, the amount of oil produced was a staggering 9500 thousand barrels per day. While only 1 percent of this production produces lubricating oil their importance can't be underrated or undervalued [26].

If we consider just a couple of the most important luxuries enjoyed by machines today, electricity and transportation would certainly be ranked high. In 2016 about 4.08 trillion kilowatthours (kWh) of electricity were generated in the United States [27] and the number of registered highway vehicles has swelled to over 263,610,219 on the road in 2015 [28]. This would not be possible without the work of tribology and material progenitors. From the earliest humans to the work performed today within research institutions, the drive to rotate and slide materials over one

another ever more efficiently, with less wear, will provide the next generation with superior machines.

1.2 Lubrication Basics

At the heart of the typical mechanical system lies surfaces which slide or roll against each other. Tribology, therefore, is central to the understanding of lubricated systems and provides technological advances for a wide range of applications. The science of decreasing wear, friction and oil degradation while increasing component life, oil change intervals and our basic understanding of lubricated systems has fallen to mechanical engineers, chemists, physicists and materials scientists. While tribology encompasses much more than the study of friction, it is central to the performance of mechanical systems [11]

Work done in overcoming friction in bearings and gears is dissipated as heat, and by reducing friction we can achieve an increase in overall efficiency of machines. A key method of reducing friction, and often wear, is to introduce a lubricant into the system. Additionally, due to the close proximity of the lubricating oil to the source of friction, the lubricating oil becomes the most convenient mechanism for removing heat from the system. This heat is transferred to the atmosphere through radiators typically mounted with cooling fans thereby providing oil temperatures conducive to the longevity and performance of the system. Furthermore, the lubricating oil provides a way to remove foreign and domestic contaminates from the system, through filtration, as well as coating the internal surfaces of the system with oil to minimize corrosion. Lubricating oils also serve as work mediums in hydraulic systems by transmitting work from one form to another. Few systems have the ability to provide such a wide ranging list of benefits and abilities.

1.2.1 Friction

Engineered surfaces, when viewed under magnification, are all found to possess irregularities. A plethora of methods have been used to study surface topography, including electron, light and atomic force microscopy [29]. Several quantitative measures are used to characterize the irregularities from one surface to another. The most commonly reported measure of surface roughness is the *roughness average* (R_a) and is shown as Equation 1.2.

$$R_a \cong \frac{1}{N} \sum_{i=1}^{N} |Z_i| \qquad (1.2)$$

where Z_i is the height of the ith point and N is the number of points measured along the sampling length [30]. Another widely used measure of surface roughness is the *root mean squared* (*rms*) roughness and is defined as Equation 1.3. A list of typical R_a values are shown in Table 1.2.1.1.

4

$$R_q \cong \sqrt{\frac{1}{N}\sum_{i=1}^{N} z_i^2} \qquad (1.3)$$

Machining type	R_a (μm)	R_a (μin)
planning, shaping	1.6 - 12.5	62.9 - 492
milling	0.8 - 6.3	31.5 - 248
drawing, extrusion	0.8 - 3.2	31.5 - 126
turning, boring	0.4 - 6.3	15.7 - 248
grinding	0.1 - 1.6	3.94 - 62.9
honing	0.1 - 0.8	3.94 - 31.5
polishing	0.1 - 0.4	3.94 - 15.7
lapping	0.05 - 0.4	1.97 - 15.7

Table 1.2.1.1: Typical roughness average values of engineered surfaces finished by different processes. Table from Reference [11]

Engineered surfaces are commonly finished using the processes shown in Table 1.2.1.1 and, although machined metal surfaces might seem smooth to the unaided eye, they resemble mountain ranges when looked at more closely. A lathed metal surface, with an expected roughness average of R_a of 0.8μm (31.5μin), was placed under a scanning electron microscope (SEM) and magnified 1000 times as shown in Figure 1.2.1.1. It is apparent that even carefully prepared metal surfaces contain peaks (called asperities) and valleys. Due to these asperities the actual area of contact between two surfaces is very small. The contact area can increase due to applied loads causing plastic deformation of the material [31]. When sliding occurs the frictional area is very small and surface temperatures, at the asperities, can reach very high values. This heating can cause structural changes to the asperities and cause melting and welding of the two surfaces. The frictional force is mainly the force required to shear these junctions [32].

A widely used model for sliding friction stems from the work of Bowden and Taylor. Their model assumes that frictional forces originate from two sources: an *adhesion force* developed at the asperity junctions, and a *deformation force* needed to plough the asperities [33]. The resultant frictional force F is then taken to be the sum of the two contributing terms, F_{adh} and F_{def}. Other factors, not considered in the Bowden and Taylor model, contribute to the overall frictional force F. They include *work hardening* and *junction growth* [11]. Work hardening and junction growth will tend to increase the friction of adhesion to the point that the force of deformation (F_{def}) becomes a minor contribution leading to expressions for overall friction that only include F_{adh}. The contribution to the coefficient of friction from the adhesive force can be represented as Equation 1.4
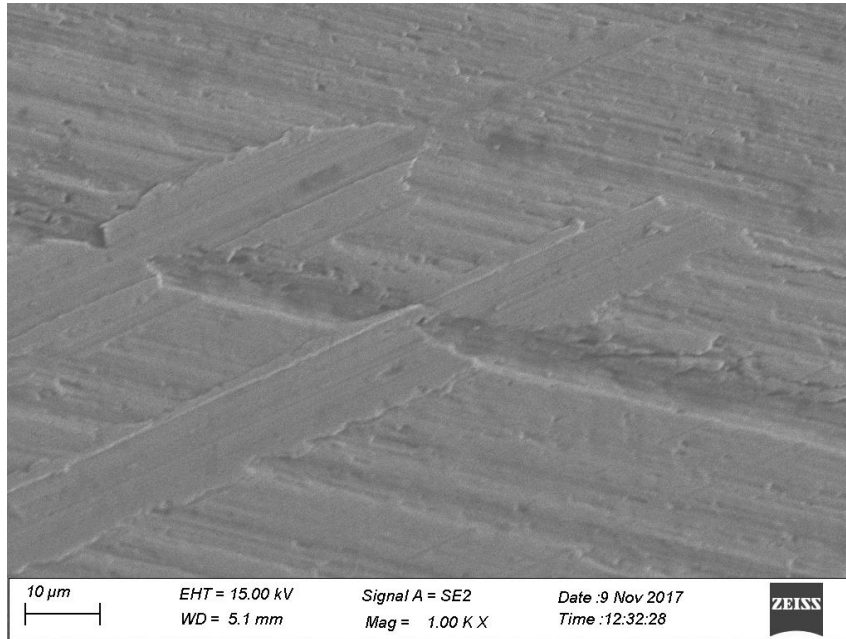
Figure 1.2.1.1: A surface of 52100 steel, with expected roughness of R_a of 0.8μm (31.5μin) magnified 1000 times with a scanning electron microscope

$$\mu_{adh} = F_{adh}/W \cong \tau/H \tag{1.4}$$

where τ is the shear stress of the junction, H is the surface hardness and W is the applied load. From Equation 1.4, it follows that for low friction the sliding materials must have low shear strength and high hardness. If a film of low shear strength can be applied between two surfaces, then the coefficient of friction can be lowered. This is the underlying principal of lubricants and is exploited in the design of some journal bearings by using one soft material and one hard [34, 35].

1.2.2   Mechanisms of Wear

The loss of material from a surface is defined as wear. For sliding contacts this can occur from processes such as adhesion, abrasion, corrosion and contact fatigue. To summarize the effect of each type of wear mechanism, a wear chart has been constructed that shows a normalized wear rate diagram for the different mechanisms discussed in this paper and is shown as Figure 1.2.2.1.

It is apparent that abrasion, adhesion, and fatigue are the three largest factors in decreasing machinery life. In Figure 1.2.2.1, the term *design wear rate* has a value of 1 for the conditions that will achieve the manufacturer's projection for machine life. Increasing or decreasing wear rates can substantially affect the mean
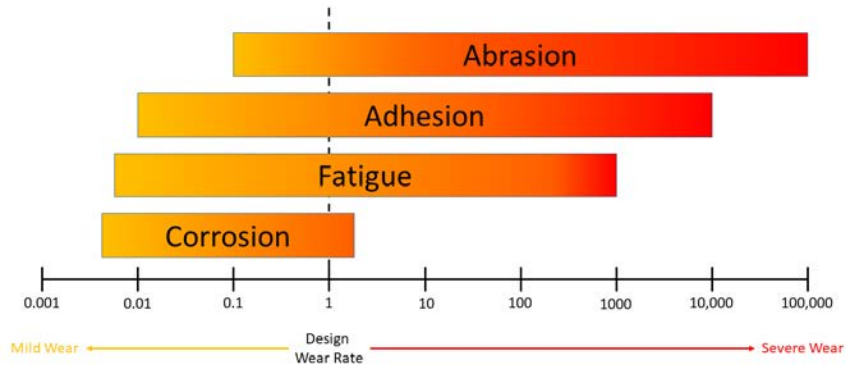
Figure 1.2.2.1: Normalized wear rates for industrial machinery (wear volume/distance) x (hardness/load). Figure from Reference [2]

time between failures (MTBF) which is, on average, about 40,000 hours. Lubricants play a vital roll in limiting each of these wear mechanisms.

1.2.2.1 Abrasive Wear

Abrasive wear is caused by the presence of hard particles in the contact area and is exemplified by abrasive operations such as cutting, grinding or polishing. The process of abrasion extensively work hardens the material causing structural changes over time [11]. Frictional hardening is well documented and can be predicted from phase diagrams of metals [36, 37]. Most engineering materials are a mixture of elements with considerable differences in hardness. Therefore, the size of the abrasive particle will determine whether the alloy becomes more or less resistive to abrasive wear [38].

When two sliding surfaces contact each other, the process is called *two body* abrasion. Two-body abrasion is detrimental to the life of the surface by causing premature wear, heat, gouging, plowing, and possible debris. The actual definition of two-body abrasion is still open to some interpretation but most agree that the main elements of two-body abrasion include a first body and a second body. The first body is generally understood to be the body being worn and is of most concern. The second body is generally understood to be any counterface body and is not of immediate concern. The second body is in relative motion to the first body and in direct or indirect contact such that forces can be transmitted to the first body [39]. When asperities begin to shear off and fall into the spaces between the two mating surfaces it promotes even further interaction between them. This would leave differently sized pieces of domestic material within the running clearance of the

7

system. This process is called *three body* abrasion and includes a third body called the interfacial element which is any material (whether autogenously generated or foreign matter) such as wear debris, lubricants, entrained solid particles, and reactive chemicals [40]. Two and three-body abrasion are shown in Figure 1.2.2.2.
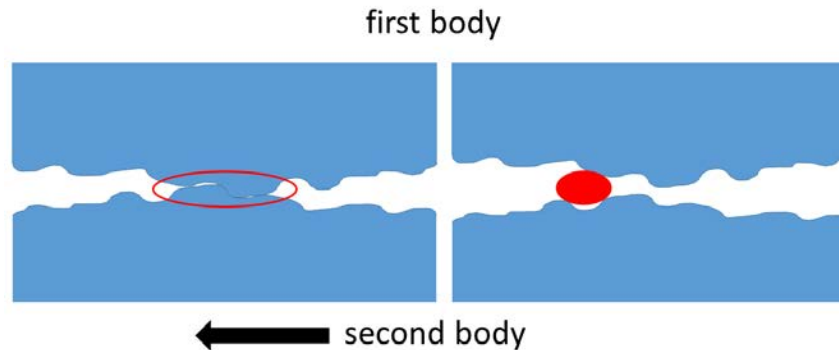
Figure 1.2.2.2: Left: red ellipse outlining asperity contact causing two-body abrasion. Right: interfacial element causing three-body abrasion

Three-body abrasion can cause a plethora of problems depending upon the characteristics of the third body particle, such as size, shape, and hardness [41]. It is known that abrasive wear of engineering and agricultural machine components is a major industrial problem [42]. If the particle is roughly the same size as the oil film thickness, the particle will cause further abrasion between the surfaces. If the contaminant is larger than the running clearance, the particle might become embedded in one of the surfaces causing scratching, gouging, or ploughing [43]. When this happens, the result is parallel furrows, like might be seen in a freshly plowed field, in the direction of relative motion between the components. When the contaminant is smaller than the oil film, mild abrasion occurs that may result in a polished look of a satiny, matte appearance [38]. Abrasion is extremely damaging to machine surfaces and creates a vicious cycle of destruction due to increased surface interaction and is known to be the most frequent, and often the most rapid, wear mechanism affecting machinery components [44]. Abrasion can be limited by increasing the hardness of the rubbing surfaces, design journal bearings with soft coatings to embed debris, improve oil filtration, increase the oil film thickness and reducing the surface roughness.

Not all abrasion is bad. Processes where the surface characteristics get maximum attention are called ultra-precision machining operations and rely on abrasive

properties. They are often used to alter surface attributes such as roughness, waviness, flatness and roundness without significant material removal from the workpiece. Typical examples are the lapping and polishing of optical lenses, computer chips or magnetic heads, honing of cylinder liners, and micro-finishing of bearing races [45].

1.2.2.2 Adhesive Wear

Adhesive wear occurs when bonding, or cold welding, occurs at the asperity tips of loaded surfaces. Thus, work hardening can occur at the bonded, or welded, tip section and be strengthened. This can cause the material to shear well below the asperity tip junction [46]. This process can cause one surface to become bonded, or welded, to the other. It can also cause the sheared material to break off and become an abrasive particle when the elastic energy just exceeds the surface energy [47]. When sheared material comes loose a fresh surface is exposed. This surface is more reactive than the original surface and must be quickly covered with additives to prevent detrimental effects [32]. Many wear process begin as adhesive wear and end as abrasive wear because of the sheared off material [48]. Abrasive wear can be limited by metal combinations which don't bond together easily, improving the low shear strength of additive layers and by increasing the oil film thickness.

Adhesion is a common problem when there is a lack of lubrication supplied to frictional surfaces. It commonly occurs when high temperatures, or pressures, cause the lubricant film to decrease enough for asperities to contact each other and spot weld together. Adhesion occurs in the mixed and boundary lubrication regimes typically due to insufficient lubrication supply, improper viscosity choice, clearance problems, machining issues, or incorrect assembly of equipment. Some adhesion is expected when new components typically go through a break-in period when first used [49].

1.2.2.3 Contact Fatigue

There are two main types of contact fatigue: surface and subsurface [50]. Contact fatigue tends to predominate in rolling contacts where slip is small and contact stresses are high. *Pitting* in gears and bearings, and *squats* in railway track are examples of surface initiated contact fatigue cracks [51]. Plastic deformation, caused by high contact stresses, can initiate surface cracks. Material defects, such as scratches or dents, can also initiate surface cracks [52]. Subsurface fatigue is generally found in rolling element bearings and gear teeth. The long term, repeated, exposure to load cycles and stress cause elastic deformation of the material. This elastic deformation can reach subsurface flaws and cracks in the material and begin a cycle of propagation of the crack to the surface [53, 54]. This is common and is the result of a bearing, or gear, surviving its normal life expectancy. The eventual result is pitting and spalling of the material's surface [55]. Fatigue damage can be limited by increasing the oil film thickness, minimizing the influence of entrained air

and dissolved water and with the addition of fatigue limiting additives such as zinc or phosphate.

1.2.2.4   Corrosive Wear

Corrosive wear loses material by chemical reaction and can be very detrimental to the service life of materials. For example, the acidic corrosion of cylinder liner materials caused by oil degradation and combustion components can prematurely wear these materials [56, 57]. However, if it is controlled, it can be beneficial. The formation of low shear strength boundary lubricant films such as extreme pressure (EP) and anti wear (AW) additives are a form of chemical corrosion [11]. A lubricated system contains many corrosive species such as oxygen, water, carbon dioxide, sulphur compounds, acidic combustion products, acidic oil oxidation products and anti wear and extreme pressure additives. Corrosive species, like those listed previously, have a tendency to attack metals. Normal sliding, and rolling, motions can exacerbate this chemical attack by removing protective corrosive coatings. This exposes fresh surface material and can increase surface temperatures causing increased diffusion and reaction rates [58]. Corrosion can be limited by using corrosion inhibitors, using additives that prevent adhesion, limiting corrosive species and neutralizing acidic species by using over based detergents.

1.2.3   Surface Types

There are two basic types of surfaces encountered within the typical machine, conformal and non-conformal surfaces, shown in Figure 1.2.3.1. Conformal surfaces will fit snugly into each other so that the load is carried over a relatively large surface area. This surface area remains essentially constant while the load increases on a conformal surface. The loading on conformal surfaces ranges from 1MPa - 7MPa which causes no elastic effects on the mating surfaces [59]. Components with conformal surfaces include fluid film journal bearings, slider bearings, and thrust surfaces.
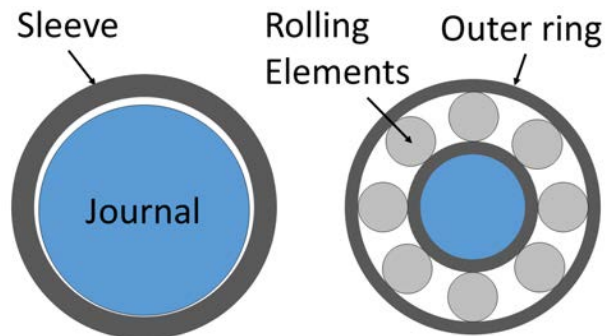
Figure 1.2.3.1: Left: conformal surface. Right: non-conformal surface

Nonconformal surfaces do not conform to each other very well and the load must be carried by a very small contact area. The contact areas between nonconformal surfaces enlarge considerably with increasing load but are still small when compared with the contact areas between conformal surfaces. The loading on nonconformal surfaces can exceed 700MPa even at modest applied loads causing elastic deformation of the materials such that elliptical contact areas are formed on the mating surfaces [60]. Components with nonconformal surfaces include mating gear teeth, cams, followers and rolling element bearings. It is important to note that it is common practice in engineering to have one hard surface and one softer (sacrificial) surface with conformal surfaces and two hard surfaces with non-conformal surfaces.

1.2.4   Lubrication Regimes

Knowing that we have to deal with surface asperities we must find another way of controlling surface contact if machines are to endure. The answer to this dilemma is to provide a lubricating oil between the surfaces as to minimize surface contact. Depending on how this lubricating oil is maintained between the surfaces there are three different types of lubrication conditions that exist as shown in Figure 1.2.4.1. The three lubrication types are boundary lubrication, mixed lubrication, and full film lubrication.
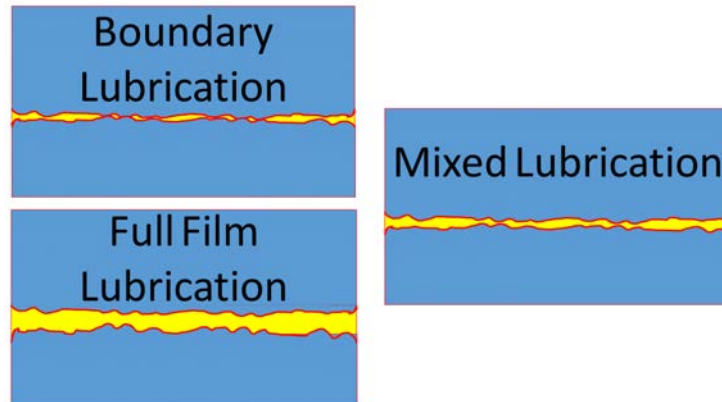
Figure 1.2.4.1: Lubrication regimes

Boundary lubrication occurs when the solid surfaces are so close together that appreciable contact between opposing asperities is possible. The friction and wear in boundary lubrication are determined predominantly by interaction between the solids and between the solids and the liquid. The bulk flow properties of the liquid play little or no part in the friction and wear behavior [61]. Mixed lubrication occurs when surface asperities significantly affect the performance of the contact [62]. Full film lubrication is the lubrication regime where, through viscous forces, the load is

fully supported by the lubricant between the surfaces in relative motion. Full film lubrication consists of both hydrodynamic (conformal surfaces) and elastohydrodynamic (non-conformal surfaces) lubrication [59].
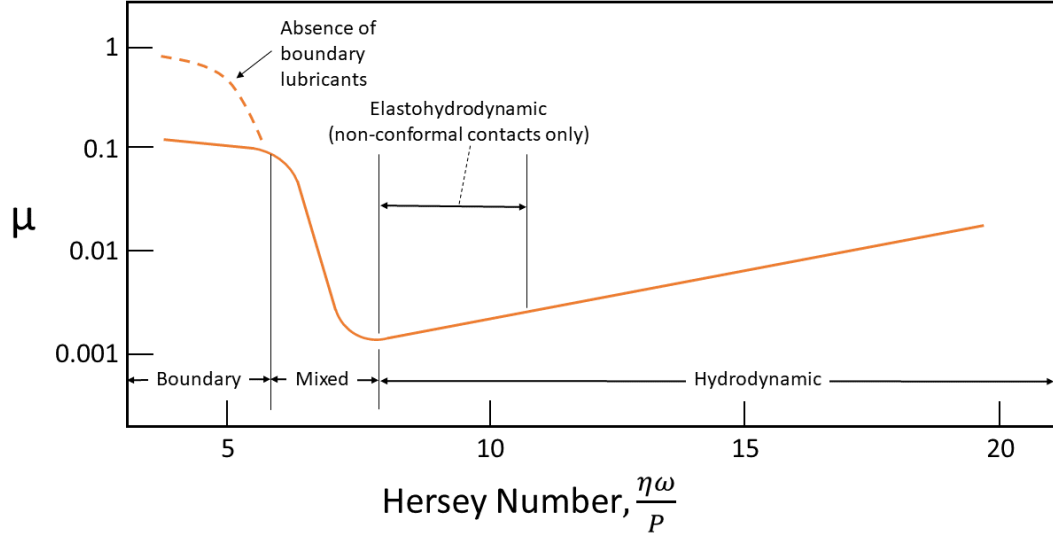
Figure 1.2.4.2: Stribeck curve

A frequently used method to identify the lubrication regime a system will operate in is known as the Stribeck curve (named after Richard Stribeck) and is shown in Figure 1.2.4.2. The abscissa of the Stribeck curve uses the dimensionless Hersey number (Mayo D. Hersey) which relates the dynamic viscosity η (Pa· s), the rotational velocity ω (rps), and the pressure P (Pa) applied within the contact zone (Shown as Equation 1.5).

$$H_s = \frac{\eta\omega}{P} \tag{1.5}$$

When friction is plotted against the Hersey number, the Stribeck curve is the result. High Hersey numbers usually mean a relatively thick lubricant film while low Hersey numbers would indicate a very thin film. It is apparent from Figure 1.2.4.2 that at low Hersey numbers no substantial lubricant film can develop, resulting in significant asperity contact and high friction values, and indicating the system is operating in the boundary lubrication regime. The first drop in friction indicates a movement from boundary lubrication to the mixed lubrication regime. In the mixed lubrication regime a variety of operating conditions exist that are dependent on temperature, pressure, and speed. As the Hersey number increases,

friction reaches a low point and then steadily, and slowly, increases marking the next regime of hydrodynamic lubrication. At this point the surfaces are effectively separated by the lubricant and asperity contact has negligible effect on load support and friction [59].

While the Stribeck curve gives a method to define system lubrication regimes given operational parameters, it isn't readily apparent that the Hersey number contains the complexities inherent in viscosity, which exhibits unique, and unexpected behaviors. The dynamic viscosity, which was first defined in Equation 1.1 and Figure 1.1.0.2, is also contained in the numerator of the Hersey equation shown in Equation 1.5. Viscosity can be highly dependent upon the operating temperatures of the system, the local pressures within the contact zone and upon the shear rate ($\dot{\gamma}$) the fluid experiences.

1.2.5   Viscosity Shear Rate Dependence

If we look again at Figure 1.1.0.2 we can impose two conditions that allow for accurate calculation of viscosity-related variables. The first is a no slip condition along the length of the plates that the fluid is in contact with and the second is that laminar flow conditions exist within the layers of the fluid. The second variable that can be defined from Equation 1.1, is shear rate ($\dot{\gamma}$). To obtain shear rate the velocity of the upper plate of Figure 1.1.0.2, is divided by the distance between the plates giving the unit of reciprocal second. This provides a second equation for dynamic viscosity shown as Equation 1.6. The shear rate is an important parameter in defining viscosity and a substance's flow behavior [3].

$$\eta = \frac{\tau}{\dot{\gamma}} \tag{1.6}$$

Using Equations 1.1 and 1.6, two plots can be constructed that help to define the behavior a fluid at a constant temperature and pressure. Figure 1.2.5.1 (left) shows the flow curve generated from the relationship between shear stress and shear rate while 1.2.5.1 (right) shows a viscosity curve using the viscosity and shear rate relationship. Using the plots from Figure 1.2.5.1 we can define a Newtonian and a non-Newtonian liquid. A Newtonian liquid, although varying with temperature and pressure, does not vary its viscosity with deformation rate or time [3, 63].

Line 2 in Figure 1.2.5.1 would be identified as the Newtonian fluid while curves 1 & 3 would be identified as non-Newtonian fluids and exhibit shear thickening and shear thinning respectively [63]. Lubricating base oils are typically categorized as Newtonian fluids and behave as expected between shear rates of 10^0 - 10^8 s^{-1}.
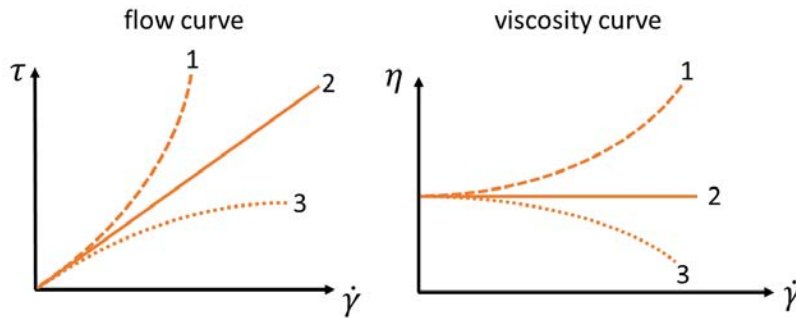
Figure 1.2.5.1: Left: flow curve showing stress vs shear rate. Right: viscosity curve showing viscosity vs shear rate.

1.2.6 Viscosity Temperature Dependence

The viscosity of all simple liquids decreases with increase in temperature and generally the higher the viscosity, the greater is the rate of decrease [63]. For example, while the viscosity of water decreases by about 3% per degree Celsius at room temperature, motor oils decrease by about 5% per degree, while bitumens decrease by 15% or more per degree [3]. There are several methods of determining the viscosity-temperature relationship such as the Reynolds, Andrade-Erying, Slotte, and Vogel relationships [64, 65].

One of the most frequently used methods for comparing the viscosity temperature variation between different oils is the dimensionless number known as the viscosity index (VI). The kinematic viscosity of the sample oil is measured at two different temperatures (40°C and 100°C) and the viscosity change is compared with an empirical reference scale. The original reference scale was based on two sets of lubricant oils derived from separate crude oils: a Pennsylvania crude, arbitrarily assigned a VI of 100, and a Texas Gulf crude, assigned a VI of 0 [66]. The higher the VI number, the less the effect of temperature on the viscosity of the sample.

The ASTM (American Society for Testing and Materials) suggests using viscosity index (VI) to describe the viscosity-temperature relationship (ASTM D2270) [67] and gives their corresponding viscosity temperature diagram as shown in Figure 1.2.6.1 [68]. The relationship is given as Equation 1.7 where ν is the kinematic viscosity (dynamic viscosity divided by density or $\nu = \mu/\rho$), T is the absolute temperature, and α, b and d are constants with the values α = 0.6 - 0.75, b = 1 and d = 10.

14
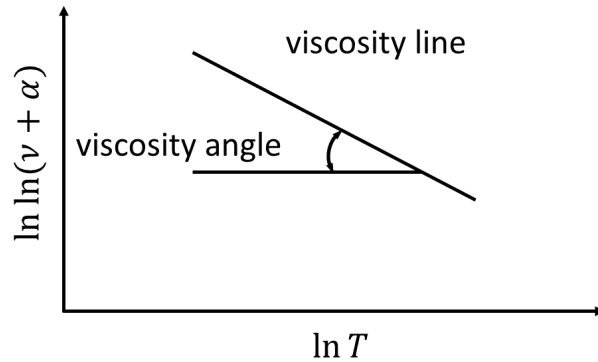
Figure 1.2.6.1: ASTM viscosity temperature diagram.

$$(\nu + \alpha) = bd^{1/T} \tag{1.7}$$

For double logarithmic coordinates and single logarithmic abscissa, the formula is a straight line as shown in Figure 1.2.6.1. Then, Equation 1.7 becomes

$$ln\ ln(\nu + a) = A - BlnT \tag{1.8}$$

The advantage of Equation 1.8 is that only two viscosities, with corresponding temperatures, need to be measured in order to determine the constants A and B. Then a straight line can be plotted to find other viscosities at any temperature. For a typical mineral oil, an ASTM diagram is very effective. Furthermore, the viscosity angle in Figure 1.2.6.1 can be used as an index to evaluate the viscosity-temperature feature of a lubricant [68].

1.2.7   Viscosity Pressure Dependence

For most liquids, viscosity increases with increasing pressure because the molecules can move less freely and the internal friction forces increase. Compared to the temperature influence, liquids are influenced very little by the applied pressure. The reason is that liquids (unlike gases) are almost incompressible at low or medium pressures. For most liquids, a considerable change in pressure from 0.1 to 30 MPa causes about the same change in viscosity as a temperature change of about 1 K (1°C) [65]. Equation 1.9 (known as the Barus equation) shows the exponential relationship between viscosity under pressure where η_0 is the viscosity at STP (standard temperature and pressure), α is a pressure coefficient for the oil, and P is the pressure.

$$\eta_p = \eta_0 e^{\alpha P} \tag{1.9}$$

Viscosities can double when the pressure is increased from atmospheric pressure to 100 MPa (1000 bar or atmospheres) [3]. For pressure differences of 0.1 to 200 MPa, the viscosity increase for most liquids amounts to a factor 3 to 7 only [63]. For pressures approaching 400 MPa, the viscosity increase can be 100 times greater. For components such as gears, the pressures are enormous during the very short times at the points of contact, and the viscosity of oil then becomes as high as that of bitumen at normal pressure. For example, lubricants in cogwheels or gears can be subjected to pressures of 1 GPa and higher as shown in Figure 1.2.7.1. For a lubricating oil at 1 GPa, the viscosity could easily be 10^7 times greater than its original value [3].
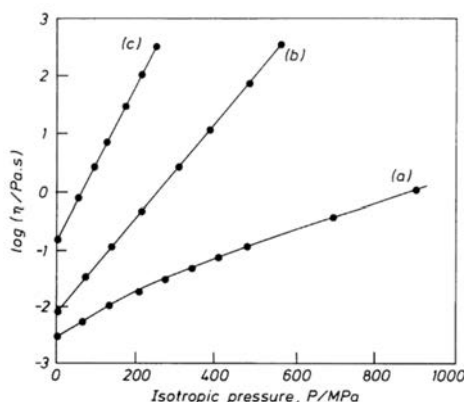
Figure 1.2.7.1: Variation of viscosity with pressure: (a) Di-(2-ethylhexyl) sebacate; (b) naphthenic mineral oil at 210°F; (c) naphthenic mineral oil at 100°F. Figure from Reference [3]

1.2.8   Summary

Lubrication occurs though a complex set of processes with many influencing factors. A lubricant is responsible for decreasing friction by limiting abrasive and adhesive forces. Moreover, it must carry all of the required additives, such as antiwear and extreme pressure coatings, to ensure surface protection and limit corrosion through anti-corrosive agents. Furthermore, the lubricant must deal with temperature fluctuations and extreme pressures associated with gears and bearings. No other system is tasked with such a plethora of vitally important jobs. Because lubricating oils are tasked with such a wide ranging list of objectives an understanding of their physical traits and chemical composition is vitally important. Lubricants will be discussed in the following section.

1.3 Lubricants

The majority of a lubricating oil consists of a base stock that is the foundation of the lubricant. The base stock material can have different origins such as mineral oil, synthetic oil or vegetable oil. Mineral oil, which is derived from crude oil, is produced with a wide range of characteristics depending on the refining process. Synthetic oils are produced through a synthesis process (man-made oligomers) and come in even a wider range of chemical compositions depending on their intended purpose. Vegetable oils are a very small percentage of lubrications and won't be discussed in this work.

Base stocks can have very different physical and chemical properties and possess characteristics that will determine their performance for a variety of lubrication challenges. Mineral oils obtain these specific characteristics from the refining process. Synthetics oils have come to address characteristics that are not achievable with mineral oils [13]. Modern lubricants are formulated from a range of base stocks and chemical additives. The base stock has several functions but its primary use is to provide the fluid layer to separate moving surfaces. Many properties of the lubricant are enhanced, or created, by the addition of special chemical additives to the base fluid. For example, stability to oxidation and degradation in an engine oil is improved by the addition of antioxidants while extreme pressure anti-wear properties, needed in gear lubrication, are created by the addition of special additives. The base stock acts as the carrier for these additives and therefore must be able to maintain them in solution under normal working conditions [69].

1.3.1 American Petroleum Institute Base Stocks

The 20th century implemented a number of improvements in the refining process used for mineral oils along with the introduction of a variety of synthetics. By the early 1990s, the American Petroleum Institute (API) had developed a classification system for lubricant base stocks, as identified in API Publication 1509 Annex E [12]. The definitions have evolved to the present five group standard, set in 1995, which categorize base oils for their origins (mineral or synthetic) and their method/process of production as well as the range of their viscosity index and the percentage of saturated hydrocarbons as shown in Table 1.3.1.1.

1.3.1.1 Group I

Group I base stocks are manufactured using solvent extraction techniques, solvent or catalytic de-waxing, and hydro finishing techniques [70]. The solvent refining process is a selective separation process that isolates compounds present in the crude without the formation of new molecules.

First, to remove undesirable aromatics, polar solvents such as furfural or phenol are used to attract and remove heavy aromatics from the vacuum distillate.

group	sulphur (%)	saturates (%)	VI	manufacturing method
I	> 0.03	< 90	80 - 119	solvent refined
II	≤ 0.03	≥ 90	80 - 119	hydro-processed
III	≤ 0.03	≥ 90	120 +	severely hydro-processed
IV	polyalphaolefin			oligomerization
V	all others			various
VI	polyinternalolefins			oligomerization

Table 1.3.1.1: Categories of base oils according to the API. Table from Reference [12]

Next, wax is crystallized by the addition of a solvent such as ketone at refrigerated temperatures. The ketone serves as an anti-solvent for the wax so it can be recovered by filtration. As a final step to making Group I base stocks, both color and stability may be improved through hydrofinishing [13]. Ultimately, 10 - 40% aromatic components remain after solvent processing [13, 69, 71]. These are mostly single-ring aromatics with some sulfur containing compounds. These components are unaffected by hydrofinishing and remain in the oil.

Group I base stock characteristics include good solvency, good compatibility with seals, better additive solubility and natural long term oxidation control. Group I base stocks are available in very high viscosities (≥ 30cSt at 100°C). Typical use includes marine and diesel engine oils, hydraulic oils, heat transfer oils, industrial gear oils, conventional greases, paper machine oils, compressor oils, machine tool way and slide lubricants [13].

1.3.1.2 Group II

Group II base oils are typically manufactured by hydroprocessing and solvent or catalytic de-waxing processes [4]. This treatment removes impurities that affect oxidation stability. Group II base stocks have improved antioxidant properties, since most of the hydrocarbon molecules are saturated. Group II base stocks are available in viscosities up to 12cSt at 100°C. Typical uses include passenger car and commercial engine oils, natural gas engine oils, automatic transmission fluid, turbine oils and automotive gear oils [13].

1.3.1.3 Group III

Group III base oils are manufactured by special processes such as isohydromerization or severe hydrocracking. High severity hydro-processing eliminates ring structures beyond Group II causing poor solvency. These oils are extremely pure, which make them non-polar, and often require the addition of an ester or aromatic compound to increase solvency to a sufficient point to hold additives in solution [4]. Group III oils are available in viscosities up to 8 cSt at 100°C. Typical

uses include premium passenger car motor oils (such as SAE 0W and 5W viscosity grades), automatic transmission fluids, food grade lubricants and white oil quality lubricants [13].

1.3.1.4 Group IV

Polyalphaolefins (PAOs) are synthetic, paraffin like, liquid hydrocarbons with a unique combination of high temperature viscosity retention, low volatility, very low pour point (the ability to flow at low temperatures), and a high degree of oxidation resistance. The VI of these base stocks can range from 125 to more than 200 with pour points down to 85°F (65°C) [4]. These characteristics result from the wax-free combination of relatively unbranched molecules of predetermined chain length. These properties made them ideal base stocks for high performance lubricants.

Group IV characteristics include excellent performance at high temperatures with superior oxidation stability. Typical uses include high performance engine, gear, compressor, hydraulic and circulating oils, high performance greases, heavy duty transmissions and industrial bearing lubricants [13].

1.3.1.5 Group V

Group V naphthenic base stocks are produced from naphthenic crude. The refining process is similar to that of Group I except that naphthenic crude contains essentially no paraffins. Therefore, they don't require solvent dewaxing although many naphthenic stocks are finished by hydrotreating. Naphthenic base stocks are characterized by having very low pour points (down to $-80°F$ or $-62°C$) and low VI (typically in the range of $20-85$) compared to Group I base stocks. These base stocks make them suitable for a number of specialized applications such as metalworking, process oils, refrigeration compressor oils, and automatic transmission oils.

The properties and manufacture of nonconventional synthetic Group V base stocks vary widely. These cover a broad range of materials, each having relatively unique properties that make them suitable for a number of specialized industrial, automotive, and aviation applications. Characteristics include very good low temperature performance, high solubility and are available in a wide viscosity range. Typical uses include products that operate in a narrow temperature range, at low temperatures and/or require high solubility such as transformer and process oils and grease.

1.3.1.6 Group II+ and III+

Group II+ and Group III+ base stocks are not officially part of the API classification but many companies manufacture them. These *plus* base stocks all have VIs on the high end of the API guidelines. Sulfur and saturate specifications remain the same from the official group classification. Among *plus* producers, the

minimum VI falls somewhere between 130 and 140. In addition to the high VI benefit, these stocks generally have lower volatility and lower pour points. [69].

1.3.2 Base Stock Application

Base stock makes up a significant portion of the finished lubricant (ranging from 70% of automotive oils and diesel engine oils to 99% of some industrial oils [69]) and proper selection is essential to the manufacture of high-quality finished lubricants. The base stock is a major factor in a broad range of areas including viscosity, volatility, thermal stability, additive/contaminant solubility, oxidation stability, air release, foaming resistance and demulsibility. The remainder of lubricant formulations consist of the addition of performance improving additives, selected according to the needs of the product being manufactured. Table 1.3.2.1 identifies whether the base stock or the additive has the greatest influence on key properties of a lubricant.

Lubricant Property	Base Stock Impact	Additive Impact
viscosity	primary	secondary
viscosity stability (VI)	primary	secondary
thermal stability	primary	-
solvency	primary	-
air release	primary	-
volatility	primary	-
low temperature flow	primary	secondary
oxidation stability	primary	primary
deposit control	secondary	primary
demulsibility	secondary	primary
foam prevention	secondary	primary
antiwear/extreme pressure	secondary	primary
color	secondary	primary
emission control	secondary	primary

Table 1.3.2.1: Base stock and additive impact on lubricant properties. Table from Reference [13]

Table 1.3.2.1 clearly demonstrates that both the base oil and the additives share responsibility for the overall performance of the finished lubricating oil. Modern lubricants are used in a great number of applications and no one single base oil is able to satisfy all product requirements. For example, some heavy duty diesel engines require higher viscosity base stocks available only in Group I. In contrast, to satisfy low-temperature Society of Automotive Engineers (SAE) 0W passenger car engine oils, Group III or IV base stocks are preferred. Moreover, some products under severe service require Group IV or V synthetic oils to withstand extreme stresses encountered in service.

1.3.3 Crude Oil

Crude oil is a complex mixture of many hydrocarbons ranging in molecular size from simple gases such as methane to very high molecular weight asphaltic components. Crude is characterized by the virtual absence of unsaturated hydrocarbons consisting mainly of saturated, predominantly straight-chain alkanes, small amounts of slightly branched alkanes, cycloalkanes, and aromatics [72]. Only some of these crude oil constituents are desirable in a lubricant base fluid and a series of physical refining steps separate desirable and undesirable lubrication characteristics. Other process steps, involving chemical reactions, are also used to enhance properties of the oil. Despite the wide range of hydrocarbons, and other organic molecules found in crude oils, the main differences between crudes are not the types of molecules but rather the relative amounts of each type that occur in each crude oil source [4]. The standard components of crude oil are shown in Table 1.3.3.1.

component	content by weight (%)
carbon	83 - 87
hydrogen	11 - 14
sulphur	0 - 8
nitrogen	0 - 1
oxygen	0.5
metals	0.02

Table 1.3.3.1: Standard component analysis of crude oil. Table from Reference [14]

1.3.3.1 Chemical Composition

Petroleum contains a wide range of organic functionality and molecular size. In general terms, petroleum, heavy oil, bitumen, and residue are a complex composition of oxygen, nitrogen and sulfur compounds as well as hydrocarbons and metallic constituents. The isolation of pure compounds from petroleum is an exceedingly difficult task, and the overwhelming complexity of the hydrocarbon constituents of the higher molecular weight fractions, as well as the presence of compounds of sulfur, oxygen, and nitrogen, are the main causes for the difficulties encountered.

1.3.3.2 Hydrocarbons

Hydrocarbons range in size from the simplest methane molecule, which contains one carbon atom and four hydrogens, to heavy asphaltic resins [13]. Furthermore, as the number of carbon atoms in a molecule increase, the number of different ways that a molecule can be structured increases. Although many different arrangements of molecules are possible, petroleum hydrocarbons are generally subdivided

into alkanes, alkenes, alicyclics and aromatics [4], Examples of just a few of these combinations are shown in Figure 1.3.3.1.
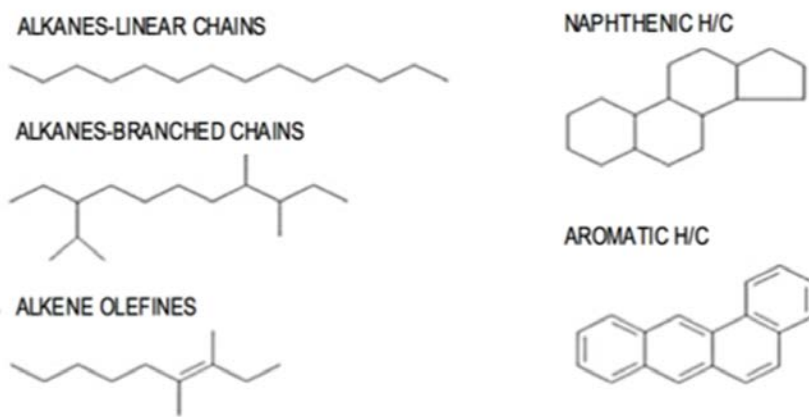
Figure 1.3.3.1: Examples of straight- and branched-chain aliphatic, alkenes, alicyclic and aromatic hydrocarbon structures. Figure from Reference [4]

As lubricating oils are exposed to heat, entrained air, metals and other degradation mechanisms, hydrocarbon characteristics are important to understand. Alkanes, alicyclics and aromatics of the same molecular weight have very different physical and chemical characteristics. Physical characteristics affect the viscosities of the lubricant, and the chemical stability of each class to oxidation and degradation is very important in use [73]. Of the three main classes, alkanes have relatively low densities and viscosities for their molecular weights and boiling points. They have good viscosity temperature characteristics and show relatively little change in viscosity with change in temperature compared to cyclic hydrocarbons. However, there are significant differences between isomers as the degree of alkane chain branching increases [70].

Linear alkanes, the *normal*, or *n*-paraffins in the lubricant boiling display good viscosity temperature characteristics but their high melting points cause wax issues at lower temperatures. In contrast, highly branched alkanes are not waxy but have less desirable viscosity temperature characteristics. Alkanes have good pressure viscosity characteristics and are fairly resistant to oxidation and respond well to oxidation inhibitors [14].

Alicyclics have higher densities and viscosities for their molecular weights when compared to alkanes. An advantage of alicyclics over alkanes is that they tend to have low melting points and so do not contribute to wax. However, one disadvantage is that alicyclics have inferior viscosity temperature characteristics.

Single ring alicyclics with long alkyl side chains, however, share many properties with branched alkanes and can be highly desirable components for lubricant base oils. Alicyclics tend to have better solvency power for additives than pure alkanes but their stability to oxidative processes is inferior [4].

Aromatics have densities and viscosities which are higher than alkanes and alicyclics. Viscosity temperature characteristics are rather poor however melting points are low. Although they have the best solvency power for additives, their stability to oxidation is poor [4].

Severely hydrotreated base stocks, as well as GTL (gas-to-liquid) basestocks and PAO (polyalphaolefins) are often regarded as *dry* base oils because they only contain fully saturated non-polar hydrocarbon (isoparaffin) molecules [74]. The complexities of molecular performance demonstrate the need for qualified tribologists to correctly formulate and blend lubrication oils.

1.3.3.3 Non-Hydrocarbons

Other elements are found in crude oil and are generally contained within the ring structures or as functional groups. Within the base oil lubricant boiling range almost all organosulphur and organonitrogen compounds are heterocyclic molecules as shown in Figure 1.3.3.2 [14].
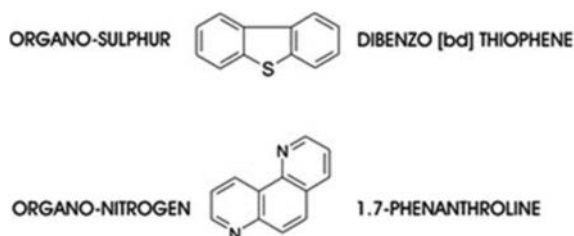
Figure 1.3.3.2: Non-hydrocarbon examples of sulphur and nitrogen heterocyclic structures. Figure from Reference [4]

1.3.4 Crude Refining

Approximately 90 percent of the current lubricant market share is comprised of conventional (mineral-based) oils which are derived from crude oil [75]. In order to get a lubricating oil from a crude oil, the crude oil must be sent through a refinery. In oil refineries, the crude oil is subjected to fractional distillation and a number of other processes, which result in different types of fuels, base oils, paraffin, asphalt and even some secondary products. The production of base oils consists of distillation, removal of aromatics, dewaxing and finishing [76]:

Crude oil is sent through a furnace where it is heated, partially vaporized and sent to a fractionating column. The fractionating column separates hydrocarbons based on their boiling and condensing points, which are a direct result of their molecular size [14]. As the vaporized hydrocarbons travel up the column they cool and condense. The condensation happens at different heights allowing separation based on molecular size. The smallest of the hydrocarbons (5 to 10 carbon atoms) will rise to the very top of the column. They will be processed into products like gasoline. Condensing just before reaching the top, compounds containing 11 to 13 carbon atoms will be processed into kerosene and jet fuel. Larger atoms, with 14 to 25 carbon atoms in the molecular chain, are diesel and gas oils. Compounds with 26 to 40 carbon atoms are a tribologists main concern. This is the material used for the creation of lubricating oil. At the bottom of the column, the heaviest and largest of the hydrocarbons (40-plus carbon atoms) are taken and used in asphaltic based products [70].

Aromatics are then removed by solvent extraction to improve characteristics of the lubricating oil. Wax is then removed by cooler temperatures and filtration [77]. The return on the base oil from the distillation column of the refinery depends on the proportion of desirable components in the range of the lubricants boiling points [78].

1.3.5 Synthetic Oils

Synthetic lubricants first appeared in the early 1930s, as synthetic hydrocarbon and ester technologies were developed at the same time in Germany and the USA [79]. The increasing demand of lubricants to perform in expanding temperature ranges (mainly driven by the developments in the engines of the military aircrafts) will ensure continuing development of synthetic lubricant technology [80, 81].

Today, synthetic lubricants are used in virtually all fields and applications that require lubrication. Industries such as automotive, shipping, industry, aviation and aerospace all use synthetic oils in high temperature applications. A plurality of base oils has been investigated for their use as potential synthetic base oils of final lubricants, out of which the most prevalent ones are alkylated aromatics, esters, PAOs, polybutenes and silicones [4]. Below is a list of the most common synthetic oils:

- Alkylated aromatics: include dialkyl benzenes and alkyl aromatics [4]

- Esters (100% synthetic): include diesters and polyesters [82]

- Polyalphaolefins (PAO), (100% synthetic): derived from the polymerization of an alpha-olefin [79]

- Polybutenes (PIB)

- Polyglycols (PAGs): produced by oxidation of ethylene and propylene [4]

24

- Silicones: typically contain a Si=O functional group such as PDMS [80]

1.3.6 Chemical Additives

The various base stock manufacturing processes can all produce base stocks that have characteristics conducive to formulating finished lubricants with desirable performance. The lubricant oil base stock is the building block to which chemical additives or improvers, which enhance their physicochemical characteristics and properties, are added. Additives give the final product properties and characteristics required for individual application [83]. Some additives impart new and useful properties to the lubricant, some enhance properties already present and some act to reduce the rate at which undesirable changes take place in the oil during its service life. The key to achieving good performance in finished lubricants is understanding the interactions of base stocks and additives and combining them to meet the requirements of machinery and operating conditions. Modern passenger car engines, automatic transmissions, hypoid gears, railroad and marine diesel engines, high speed gas and steam turbines, and industrial processing machinery, as well as many other types of equipment would have been greatly lagging in their development were it not for lubricant additives and the performance benefits they provide [70].

Additives for lubricating oils were used first during the 1920s, and their use has continued to increase [84]. Additives, in improving the performance characteristics of lubricating oils, have aided significantly in the development of the transportation industry and industrial machinery. Over a period of many years, oil additives were identified that solved a variety of engine problems: corrosion inhibition, ability to keep particles such as soot dispersed, ability to prohibit acidic combustion products from forming varnish on engine surfaces, and the ability to minimize wear by laying down a chemical film on heavily loaded surfaces [80]. Furthermore, engine oils became so specialized that requirements for diesel engine oils began to diverge from requirements for gasoline engines, since enhanced dispersive capability was needed to keep soot from clumping in the oil of diesel engines. Today, practically all types of lubricating oils contain at least one additive, and some oils contain many different types of additives. Additives can also have detrimental effects if too much is added or there are undesirable interactions with other additives. The amount of additives used in a finished lubricant varies from a few hundredths of a percent to 30% or more [70]. The main chemical additives are listed below, with additional detail on antioxidants, which are the most relevant to this research, in the following section:

- Anti Foaming: chemicals that lower air droplet surface tension allowing release of air [85]

- Corrosion Inhibitors and Rust Preventatives: a tenacious film that prevents water from reaching the metal surface [86]

- Detergents: metal salts of organic acids that frequently contain excess base [84]

- Dispersants: interfere in agglomeration by associating with individual resin and soot particles [87]

- Extreme Pressure: compounds containing sulfur, phosphorus, chlorine, borate, or metals, either alone or in combination [88]

- Friction Modifiers: used for smooth transition from static to dynamic condition as well as reduced noise, frictional heat, and startup torque [89]

- Viscosity Index (VI) Improvers: long chain, high molecular weight polymers that function by increasing the relative viscosity of an oil more at high temperatures than they do at low temperatures [90]

1.3.6.1   Antioxidants

Through the natural oxidative process, or accelerated by the presence of oxidative mechanisms, oxidative degradation occurs in the lubricating oil. As a result of this oxidation, the oil viscosity and concentration of organic acids in the oil both increase, and varnish deposits begin to form on hot metal surfaces exposed to the oil. Varnish deposits may be further oxidized to form hard carbonaceous materials. The rate at which oxidation proceeds is affected by several factors. As the temperature increases, the rate of oxidation increases exponentially and a general guide is that for each 10°C (18°F) rise in temperature, the oxidation rate will double (Arrhenius rate rule) [91]. Greater exposure to air (and the oxygen it contains), or greater mixing with it, will also increase the rate of oxidation. Many materials, such as metals (particularly copper and iron) and organic and mineral acids, may act as catalysts or oxidation promoters [92].

Before the mechanisms of hydrocarbon oxidation were well known, researchers observed that some oils provided greater resistance to oxidation than others. This resistance was eventually identified as naturally occurring antioxidants, which varied depending on crude source or refining techniques. Some of these natural antioxidants were found to contain sulfur or nitrogen bearing functional groups [4]. Therefore, certain additives that are used to impart special properties to the oil, such as sulfur bearing chemicals, were found to provide additional antioxidant stability. The discovery of sulfurized additives providing oxidation stability was followed by the identification of similar properties with phenols, which led to the development of sulfurized phenols. Next, certain amines and metal salts of phosphorus or sulfur containing acids were identified as imparting oxidation stability [93]. Today, nearly all lubricants contain at least one antioxidant for stabilization and other performance enhancing purposes. Since oxidation has been identified as the primary cause of

oil degradation, it is the most important aspect for lubricants that the oxidation stability be maximized.

Oxidation produces harmful species, which eventually compromise the designated functionalities of a lubricant, shortens its service life, and to a more extreme extent, damages the machinery it lubricates. The internal combustion engine is an excellent chemical reactor for catalyzing the process of oxidation with heat and engine metal parts acting as effective oxidation catalysts [94]. Thus, in service engine oils are probably more susceptible to oxidation than most other lubricant applications. For the prevention of lubricant oxidation, antioxidants are the key additive that protects the lubricant from oxidative degradation, allowing the fluid to meet the requirements for use in engines and industrial applications.

Several effective antioxidant classes have been developed over the years and have seen use in engine oils, automatic transmission fluids, gear oils, turbine oils, compressor oils, greases, hydraulic fluids, and metal working fluids. The main classes include oil soluble organic and organometallic antioxidants of the following types [95]:

- sulfur compounds

- sulfur-nitrogen compounds

- phosphorus compounds

- sulfur-phosphorus compounds

- aromatic amine compounds

- hindered phenolic (HP) compounds

- organo-copper compounds

- boron compounds

- other organometallic compounds

Antioxidants are formulated into modern lubricants in order to inhibit the oil oxidation mechanism and extend the lubricant life. However, these antioxidants are gradually consumed causing the oil to increase the oxidative process.

1.3.7   Summary

Formulating a finished lubricant that meets the demands of a given system is a challenge. This challenge includes choosing a base stock based on its physical and chemical characteristics, and then selecting an additive package. Synthetics base

stocks are known to provide better thermal and oxidative stability, viscosity performance and friction properties. They would seem an obvious choice if it weren't for their lower solubility to additives and high cost [80]. Group I, II and III offer a good viscosity index, good solvency and lower cost. Group V offers very specific characteristics from the naphthenic content and are widely used for locomotive engine oils, refrigerant oils, compressor oils, transformer oils and process oils [75].

The operating envelope of the machine is important in identifying the proper lubricating oil and additive package to ensure long and efficient life. There is no one lubricating oil that meets the demands for all applications so lubricating oils can be tailored to meet the specific demands within a given system. Lubricating environments that endure extreme pressures or temperatures can be chemically composed to provide adequate performance for these extreme environments. Additive packages that incorporate viscosity modifiers, foam inhibitors, extreme pressure additives, detergents, rust and corrosion inhibitors, antioxidants, and friction modifiers all help to tailor the oil to a specific system.

It is important to understand that even with a healthy lubrication system environmental contaminants, fuel contamination due to blow-by in internal combustion engines, antifreeze contamination, and additive shearing can create engine lubrication problems. Oil change intervals can greatly affect the performance of any type of machinery and several parameters are usually tested to check the health of lubrication oil. The viscosity, acid number, additive elements, oxidation number, and other tests can help to ensure proper oil change intervals and keep machinery running smoothly.

The leading cause of oil degradation is oxidation. Anti-oxidants are a widely researched area of lubrication and every oil consists of some type of anti-oxidant additive. The result of the oxidation process is varnish and sludge. Varnish is a leading cause of servo valve sticking in the gas turbine industry and has been a problem in the ring-pack of the internal combustion engine. Varnish coats surfaces and robs efficiency by decreasing working clearances and clogging pumps and sumps. This work directly addresses the varnish problem and the following chapter is devoted to the detrimental effects of varnish, varnish formation and mitigating varnish.

Chapter 2

VARNISH

2.1 Introduction

Varnish is formed as hydrocarbon base fluids degrade through oxidation. Oxidation is accelerated by exposure to increased temperatures, mechanical stresses, ultraviolet light, entrained air, electrostatic discharge and wear materials (metals) found in typical machines [73, 80]. Varnish is formed as soluble primary oxidation products, such as acids, water and alcohols, follow condensation and polymerization reactions to form insoluble products [4]. These products are polar, causing varnish to adsorb on metal surfaces where further agglomeration thickens the varnish [96]. Varnish typically has a gold-orange appearance that darkens as the thickness increases. However, varnish appearance can vary with factors such as base stock and additive package constituents, temperature, atmospheric content and surface material [97].

Varnish deposits are one of the most detrimental by-products of hydrocarbon oxidation [98, 99]. Varnish fills the tight clearances between the valve and bore in hydraulic circuits causing erratic valve operation and in some cases fully seized valves [98]. Varnish contributes to decreased efficiency, increased wear and corrosion, impaired oil cooler performance and inadequate hydrodynamic lubrication. Journal bearings that experience varnish build up have increased shear rates, increased operational temperatures and, in extreme cases, bearing failure [100]. A sticking inlet guide vane valve of large frame gas turbines, such as those used in the power generation industry, can produce a fail to start, or shut-down event [101].

More efficient combustion processes have been achieved by increasing combustion temperatures [102]. This has strained the capabilities of materials and the lubricants that separate them. For temperatures greater than 100°C, each increase of 10°C doubles the rate of oxidation, which directly contributes to the inevitable formation of varnish and the eventual depletion of anti-oxidant compounds [11]. Internal combustion engines are well known for creating environments conducive to varnish formation where, in the ring pack of the piston, temperatures can exceed 250°C [103]. Air compressor temperatures can exceed 250°C, causing varnish formation which decreases the working clearances of rotor blades and robs efficiency [13]. The rapid compression of entrained air can produce temperatures in excess of 500°C and electrostatic discharge creates localized temperatures upwards

of 10,000°C, causing thermal degradation of the fluid [104]. Temperatures such as these lead to accelerated rates of varnish formation and decrease the working life of the fluid.

2.2 Varnish Formation

While reactions of oxygen with many organic materials are important, such as the O_2/CO_2 cycle, reactions of oxygen with liquid hydrocarbons (lubricants) are undesirable [105]. These reactions lead to the degradation of the lubricating oil in a process commonly referred to as oxidation (a process where a material gives up electrons such as when the material combines with oxygen). All oxidative process have a common reaction pattern due to oxygen's reactivity and ability to combine with other elements [106]. The most common mechanisms of varnish and sludge formation include oxidative reactions and are shown in Figure 2.2.0.1.
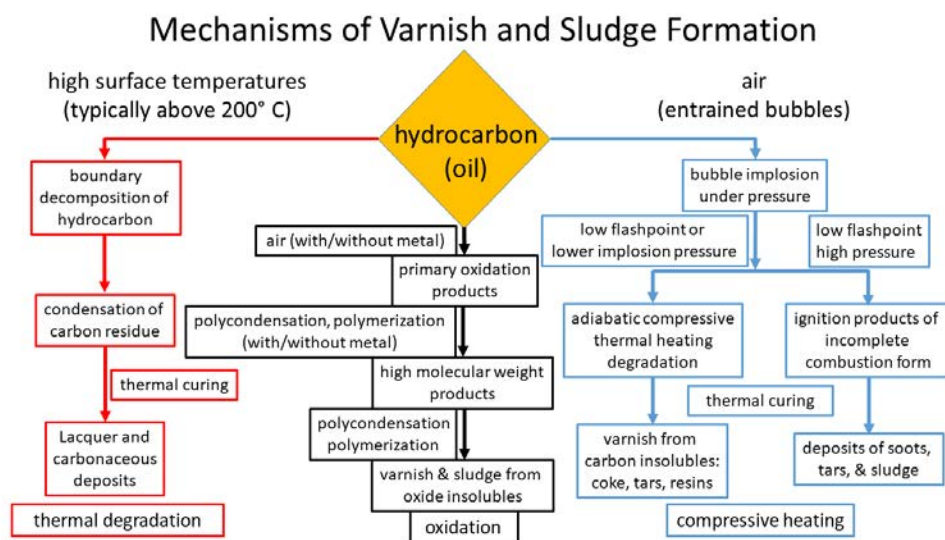
Figure 2.2.0.1: Mechanisms of varnish and sludge formation. In black: base oil oxidation. In red: high temperature decomposition including electrostatic discharge. In blue: compressive degradation. Figure recreated from Reference [5]

Oxidation is the initiating process of varnish formation and has been identified as the primary agent of lubricating oil degradation [4, 6, 100, 107]. Oxidation is the major source for viscosity increase, varnish formation, sludge and sediment formation, additive depletion, base oil breakdown, filter plugging, loss in foam properties, acid number increase, rust and corrosion. Oxidation involves a series of

chemical reactions that form varying by-products depending on base stock, additives, pressure, temperature, atmosphere, filtration, and metal content within the system [108].

Upon formation, the soluble oxidation products will condense and polymerize together to form higher molecular weight objects. Depending upon the concentration, chemistry and temperature, these oligomers eventually reach the saturation point of the fluid and precipitate out of solution to form insoluble particles. The particles are known as soft contaminants and have a median size of approximately 0.08μm [109]. These soft contaminants are polar and are attracted to each other in the non-polar (fully saturated hydrocarbon molecules) environment of modern lubricating oils [74, 110]. They are also attracted to metal surfaces by the high permanent dipole moment [111, 112].

Lubricant oxidation reactions, resulting in varnish formation, can be catalyzed by metal surfaces. The degree of catalysis is affected by the metal surface composition, the rate of surface corrosion by the lubricant to produce soluble metal products and the susceptibility of the surface to adsorption by surface coatings formed by lubricant components like tricresyl phosphate [113–115]. A simplified illustration describing this process of varnish and sludge formation is shown in Figure 2.2.0.2.

Oxidative reactions proceed through several well-known mechanisms. Base oil oxidation is a continual process occurring simply due to exposure to oxygen and normal use. This process is accelerated when high temperatures or pressures, typical of modern mechanical systems, overcome bond dissociation energies and increase the rate of formation of varnish and sludge precursors. Finally, electrostatic discharges, capable of extremely high temperatures, contribute to the oxidative degradation of base oil. Oxidation not only degrades the base oil, it also degrades and depletes the additive package used to maintain functionality of the blended oil.

2.2.1   Base Oil Oxidation

The self accelerating oxidation of hydrocarbons is called autoxidation and consists of four reaction steps: chain initiation, chain propagation, chain branching and chain termination [105, 116]. Chain initiation is characterized by the formation of alkyl (R ·) and hydroperoxide (HOO ·) radicals from the breakdown of hydrocarbon (RH) bonds [95]. Initiation reactions can begin by exposure to oxygen, heat, ultraviolet (UV) light, or mechanical shear stress and are shown as Reactions 2.1 and 2.2 [117].

$$RH \xrightarrow{O_2} R\cdot + HOO\cdot \tag{2.1}$$

$$R - R \xrightarrow{Energy} R\cdot + R\cdot \tag{2.2}$$
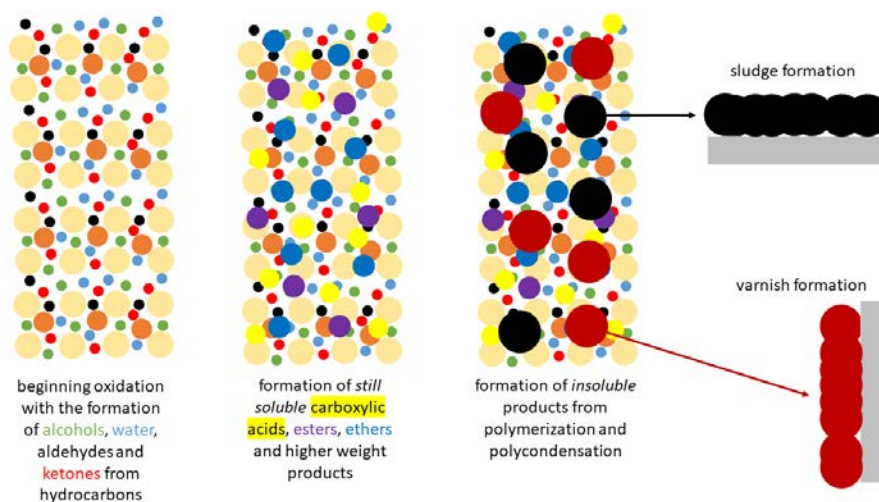
Figure 2.2.0.2: From left to right: fully formulated lubricant including hydrocarbons (yellow). Soluble impurities - low molecular weight products such as alcohols, ketones and carboxylic acids. Insoluble suspensions - high molecular weight products such as polymerised or polycondensed products. Deposit formation - varnish on polar metal surfaces and sludge forming on low flow areas. Figure recreated from Reference [6]

These reactions are typically very slow under ambient conditions but proceed at accelerated rates with higher temperatures and exposure to catalytic metal ions [4]. A second class of initiation reactions (hydroperoxide decomposition reactions) are catalyzed by the presence of iron (or other metals typically found in lubricated systems [118]) at much lower temperatures [4,95]. The typical catalytic decomposition reaction for iron is shown as Reactions 2.3 and 2.4.

$$Fe^{3+} + ROOH \rightarrow Fe^{2+} + ROO \cdot + H^+ \tag{2.3}$$

$$Fe^{2+} + ROOH \rightarrow Fe^{3+} + RO \cdot + HO^- \tag{2.4}$$
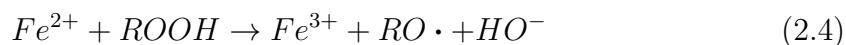
This type of reaction will increase the amount of hydroperoxide available to the point that hydroperoxide decomposition initiation reactions start to predominate [116]. Propagation involves the alkyl radicals, formed during initiation, reacting with oxygen to form alkylperoxy radicals as shown in Reaction 2.5.

$$R \cdot + O_2 \rightarrow ROO \cdot \tag{2.5}$$
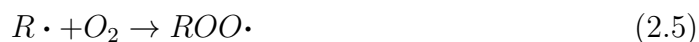
This reaction happens very fast, with low activation energy, and is independent of temperature [4]. The alkylperoxy radicals then abstract hydrogen from other hydrocarbon molecules to form hydroperoxide and additional alkyl radicals as shown in Reaction 2.6.

$$ROO \cdot + RH \rightarrow ROOH + R\cdot \tag{2.6}$$
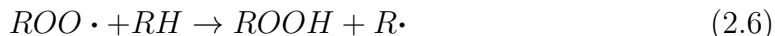
This reaction is slow, depending on the type of hydrocarbon, and is a rate determining step for chain propagation. The new alkyl radicals can then react with oxygen to form additional alkyl peroxide radicals (Reaction 2.5). This leads to an increased rate of formation of various types of hydroperoxide, which results in a reinforced autocatalytic degradation of hydrocarbons [4].

Low temperature (< 120°C) chain branching either homolytically cleaves (low concentrations), or through bimolecular reaction (high concentrations) the various hydroperoxides, formed during the early stages of autoxidation, to yield alkoxy and hydroxy radicals as shown in Reactions 2.7 and 2.8 [4].

$$ROOH \rightarrow RO \cdot + HO\cdot \tag{2.7}$$

$$ROOH + ROOH \longleftrightarrow ROO \cdot + RO \cdot + H_2O \tag{2.8}$$
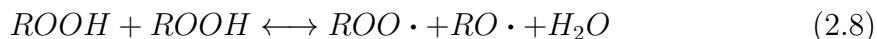
Reaction 2.7 has high activation energy and is only significant at higher temperatures or under catalysed conditions. The resulting radicals follow a number of possible reactions as shown below [95]:

- alkoxyl radicals abstract hydrogen from a hydrocarbon to form a molecule of alcohol and a new alkyl radical

- hydroxyl radicals abstract hydrogen from a hydrocarbon molecule to form water and a new alkyl radical

- secondary alkoxyl radicals may decompose to form an aldehyde

- tertiary alkoxy radicals may decompose to form a ketone

As a consequence of hydroperoxide accumulation and reaction, the concentration of free radicals initiating new chains increase. The lower molecular weight aldehydes and ketones generated will immediately affect the physical properties of the lubricant by decreasing oil viscosity, increasing oil volatility and increasing polarity [95, 116].

High temperature (> 120°C) chain branching begins with the same radical chain reactions as discussed under low temperature conditions with reduced selectivity and increased reactions rates. At high temperature the cleavage of hydroperoxide

plays the most important role. Reaction 2.7, now with plenty of energy, leads to an abundance of hydroxy radicals, which non selectively abstract hydrogen atoms [4]. Carboxylic acids are formed using the hydroperoxy peroxy radicals and aldehydes that were formed earlier. Carboxylic acids can react with the alcohols (formed under low temperature chain branching) to form esters and when the rate of oxidation becomes diffusion limited, ethers are formed [4]. As oxidation proceeds, acid or base catalyzed Aldol reactions take place leading to the formation of oligomers and high molecular weight oil soluble products (molecular weight about 2000 amu) [80, 116]. When diffusion becomes limited, by the increase in oil viscosity, polycondensation and polymerization (initiated by alkoxy radicals) reactions of these high molecular weight intermediates form products which are no longer soluble in the lubrication oil. These high molecular weight products contribute to oil viscosity increase and can eventually combine to form oil insoluble products resulting in sludge and varnish [95].

Chain termination reactions might include limited diffusion, from increased viscosity, that cause two alkyl radicals to combine forming a hydrocarbon molecule or an alkyl radical combining with a alkylperoxy radical to form a peroxide [4]. Termination reactions might proceed through primary and secondary peroxy radicals but at temperatures above 120°C these peroxy radicals also interact in a non terminating way to give primary and secondary alkoxy radicals [95]. These radicals again contribute to the formation of cleavage products. During the chain termination processes, formation of carbonyl compounds and alcohols may also take place on the peroxy radicals that contain an extractable α-hydrogen atom [116]. Termination may be effected by the combination of radical species such as peroxy radicals to yield ketones and alcohols leading to the formation of higher molecular weight compounds.

In summary, the uncatalyzed oxidation of hydrocarbons at temperatures of up to 120°C leads to peroxides, alcohols, aldehydes, water and ketones [80]. Under metal catalyzed conditions or at higher temperatures (> 120°C), degradation leads to a complex mixture of final products that include varnish and sludge deposits [4].

2.2.2 Thermal and Compressive Base Oil Degradation

Thermal breakdown occurs when a mechanical system's temperature begins to increase beyond the point of thermal stability of the base oil. When the temperatures of a mechanical system exceed 200°C (400°F) thermal decomposition (cracking) of the base oil will occur producing lower molecular weight volatile products [70]. Furthermore, thermal cracking can initiate side reactions, induce polymerization, produce gaseous by products, destroy additives, and generate insoluble by products [80].

Fluids exposed to high temperatures experience a substantial reduction in viscosity. This decrease in viscosity is accompanied by a further increase of temperature as hydrodynamic and mixed regime lubrication surfaces begin to have increased asperity contact. Furthermore, lubricating oils entrain air easily and the amount of air absorbed (or dissolved) increases significantly with temperature for all petroleum products [119]. Moreover, the oxidation rate of hydrocarbons will approximately double for every 10°C (18°F) increase in temperature following the Arrhenius equation for chemical reaction rates [120]. One of the most significant change in fluid properties caused by thermal decomposition of lubrication oil is an increase in vapor pressure caused by the shearing of molecules into smaller, more volatile fragments [121].

Compressive oil degradation occurs when fluids are aerated and high pressures are experienced. The condition is referred to as pressure induced dieseling (PID), or microdieseling, and can occur in both hydraulic and lubrication systems [122]. Air entrainment may be caused by leaking suction lines, agitated reservoirs, plunging return lines, leaking seals, undersized reservoirs and fluid turbulence. Air entrainment affects the ability of the oil to perform as a lubricant and limits the ability for hydraulic fluid to transmit energy. Temperatures can reach 1000°C (1800°F) when entrained air is pressurized during pumping which is more than enough heat to cause thermal degradation of the oil as shown in Figure 2.2.2.1. [100, 123].

Zone	Pressure	Temperature
A	Atmospheric (pump inlet)	100°F
F	1000 psi	1410°F
H	2000 psi	1820°F
I	3000 psi	2100°F
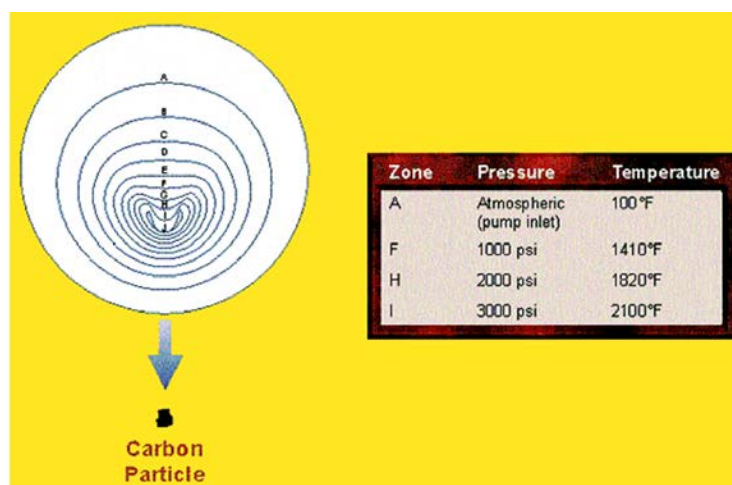
Figure 2.2.2.1: Left: entrained air bubble with contour lines showing decreasing volumes due to compression ending with an oxidative carbon particle. Right: Contour lines represented as temperature zones due to compression. Figure from Reference [5]

When vapor bubbles are rapidly pressurized, such as in a pump, destructive micro-jets of oil can collide with machine surfaces at very high velocities [124, 125].

35

This causes deformation of the pumping material and can lead to debris, pumping losses, and even failure of the pump. Furthermore, the temperature reached with PID leads to microscopic ignition (called partial combustion) of the oxygen rich oil vapors. The problem is exacerbated with low viscosity oils such as turbine oils [6]. Low viscosity fluids have low flash points, which contribute to the vaporization of the light oil fractions that mix with air at the bubble boundaries. PID can cause pressures in the area of micro-explosion to reach 5-6 times normal working pressure as well as very high temperatures. The end result is carbonized oil at the bubble interface leading to varnish and sludge deposits as well as increased oil degradation.

2.2.3   Electrostatic Discharge

Electrostatic charge generation occurs in fluid systems as a result of friction between the fluid and system components [6]. The magnitude of charge depends on many interrelated factors such as flow rates, composition of base oil, film thickness, surface roughness and environment [126]. Charges can occur during filtration of hydraulic and lubricating oils as well as diesel and gasoline fuels. Electrostatic discharge manifests itself as an audible noise (clicking sound) as charge accumulation causes sparking internally within the system as well as charge dissipation of the electrical charge downstream of the filter to a grounded surface [127].

Spark discharges can reach temperatures as high as 10,000 to 20,000°C and are usually short lived, being extinguished by the fluid [128]. This can result in etching of the discharged surface, possibly removing microscopic particles and leaving carbon deposits on the surface. Voltage potentials are directly related to the flux through the filter media and voltages exceeding 10 kV have been measured [128]. The high temperatures experienced during electrostatic discharge cause accelerated rates of hydrocarbon decomposition [127]. Electrostatic discharge has been shown to increase oxygen uptake (furthering oxidation) of test samples stored in light free, ambient temperature environments [104].

2.3   Removing and/or Mitigating Varnish

The first steps in minimizing hydrocarbon oxidation are implemented at refineries where techniques are employed to remove undesirable components that are easily oxidized, such as unsaturated hydrocarbons, polar components and wax, from crude oil [4]. Synthetic oils are widely produced to combat thermal degradation by producing molecular chains that are fully saturated, uniform and predictable during formation. Further oxidative resistance is provided through the use of strong anti-oxidation compounds designed to work synergistically with other additives, thereby providing superior performance and degradation resistance [70].

Unfortunately, additives can be harmful to the environment and emission related controls. For example, modern catalytic converters are highly effective in reducing emissions, however, they are vulnerable to the deteriorating effects of sulfur,

phosphorus, and ash derived from engine oils and fuels [80]. Due to this, the API has limited the allowable concentrations of elements like sulfur and phosphorus in blended oils. Therefore, initiatives have been made to reduce the Zinc dialkyldithiophosphates (ZDDP) content in engine oils. The current ILSAC GF-4 specification has limited the sulfur and phosphorus levels to a maximum of 0.7 and 0.08 wt%, respectively, and these numbers are likely to be even lower for future engine oils [129].

Varnish mitigation methods are also implemented by removing primary oxidation products using electrostatic and adsorption methods. Electrostatic varnish mitigation takes advantage of the polar nature of varnish combined with dielectrophoresis to remove varnish and varnish pre-cursors. Adsorption typically uses filter media with pores small enough to retain oxidation by-products. While these methods are successful in removing degradation by-products, they require extended durations for optimal performance and that no shut down time occurs, allowing temperatures to be maintained in a range that allow varnish to remain in suspension and be removed by filtration. Furthermore, caution must be used when choosing filter media, which can inadvertently remove beneficial additive compounds from the fluid [130].

Varnish removal can also be performed using chemical flushing compounds. While the electrostatic and adsorption methods are re-active to the formation of varnish, the chemical flush is pro-active in removing varnish. Chemical flushing comprises compounds that soften varnish, allowing it be suspended in the fluid and removed by filter media. This process can be very fast, depending on the chemicals used, and allows the system to remain fully functional while the cleaning process occurs. Moreover, the removal of additive package compounds by filtration is not a concern since a full oil change will occur when the process is complete, allowing very fine filter media to be used.

2.3.1 Full or Partial Oil Changes

The full, or partial, oil change method of varnish mitigation is a leading preventative measure in the transportation industry. New oil has typically not begun the oxidation process so it should not be expected to cause new deposits when added to the system. However, the benefit of this method is severely limited by the quantity of varnish deposits within the system. When new oil is placed in-service it will suspend some of the varnish and sludge contaminants already present in the system. This causes premature oxidation and saturation of the oil negating the benefits of a complete oil change. This is only the case when oil change intervals are not adhered to causing an abundance of varnish and sludge in the system.

While this approach could be beneficial if the oil is maintained in a less than saturated condition, it requires frequent testing to ensure oil condition. Moreover, oil consumers may not be sensitive to the rate of varnish accumulation in the new oil, limiting the benefit of this method. However, the approach would produce a net

benefit if performed periodically, as the cleanliness of the system in terms of existing varnish deposits can be improved with time.

2.3.2 Electrostatic Purification

The electrostatic method, operating in a *kidney loop* mode off the main tank, subjects the fluid to an electrical field, which causes the varnish precursors to charge and agglomerate into larger particles that are then captured by a filter mat or attracted to a charged, disposable surface [120]. There are several designs based on variants of the electrostatic charging principle to accomplish this goal.

The electrostatic type devices are reported to remove varnish precursors from the fluid phase, and as the fluid is cleaned up, soft varnish deposits from surfaces are re-entrained in the fluid and removed, thus resulting in the cleaning up of deposits accumulated over a period of time [100]. Since the removal of varnish from system components is a relatively slow process, these devices are recommended to be operated over a long period of time or to be installed permanently. The electrostatic type devices are reported to be sensitive to elevated moisture levels in the fluid and also to the presence of high levels of metal wear particles [131].

Electrostatic charge purification can be problematic for several reasons. When hydrocarbons pass by nonconductive filtration material there is the potential for discharge within the filer and media [132]. The use of grounded filter housings and pipelines does not stop the charge generation or internal damage to the filter or other components [131]. Furthermore, mineral based oils generate positive charges on filter media causing a negative charge to be carried downstream while synthetic oils showed just the opposite. Electrostatic charge purification is also limited to stationary systems and implementation in the transportation industry is not realistic due to cost and size constraints.

2.3.3 Adsorption Using Filter Media

The adsorption method utilizes adsorbent media with a large surface area to collect varnish and sludge. This method also requires a high void volume in the filter media, relatively low fluid flow and in some cases an electro chemical affinity for varnish and sludge precursors [120]. Many materials can be used as adsorbents, including compressed cellulose, cotton linters and macro-porous media such as resin beads, Fullers earth, activated carbon and others [127].

Physisorption, also known as physical adsorption, is characterized by the physical bonding of varnish and sludge precursors to the surface of the filter media at low temperatures in the absence of chemical bonds. The electronic structure of the adsorbate does not change upon adsorption and varnish molecules are believed to be attracted to the adsorbent through weak molecular forces such as hydrogen bonding (van der Waals forces) [120].

The down side to the adsorption method is the possibility of inadvertent removal of additives from the oil as well as placement of the filter media that will determine the effectiveness of the system [130]. Furthermore, this type of system must be implemented for extended durations (> 8 weeks) and is highly dependent on the amount of varnish and sludge previously in the system [120].

2.3.4   Chemical Cleaning or Flushing

The chemical cleaning/flushing method for removing varnish utilizes cleaning chemicals that are typically circulated through the system to dislodge, dissociate, or soften varnish and sludge from components [133]. The flushing action suspends the deposits in the fluid which are then removed by filtration and with the fluid when it is drained from the system. This process is usually performed for several hours or several days, depending on the system size and the extent of the varnish build up on components [134].

Once the flush and chemical treatment is completed, the system must be flushed again with an appropriate flushing fluid (such as base stock) to remove residual chemicals and to ensure no contamination finds its way into the new lubricating oil [135]. Although this process is more intensive, it does allow for quicker removal of varnish deposits, especially in a large systems. The quick removal rates are the defining aspect of this process. It is known to be cost effective when compared to other methods and only requires flushing when the system exhibits an abundance of varnish buildup. It does required close monitoring and entails lost production due to system downtime.

2.4   Summary and Motivation

Varnish is a natural process exacerbated by heat, light, contaminants and mechanical stresses. Because varnish is an unavoidable by-product of hydrocarbon degradation, understanding the factors that cause its formation is important to the scientific community as well as the end user. If steps can be taken to minimize the formation of varnish for in-service systems, efficiencies and longevities will increase. This is beneficial from both economic and environmental perspectives. Manufactures, as well as end users, have an obligation to provide the best possible stewardship over in-service equipment.

The mitigation of varnish for in-service equipment is possible because of our understanding of the mechanisms of varnish formation. Different types of varnish mitigation systems are available which are relevant to each type of industry. For example, the transportation industry's method of mitigating varnish will be very different than that used by the power generation industry. Moreover, the amount of oil in a given system, as well as whether that system is mobile or stationary, will dictate the most beneficial method of varnish mitigation. Historically, varnish has been the major factor in recommended service intervals and remains so to this day.

This work will focus on varnish removal from gas turbine engines used in the power generation industry using chemical cleaners. Gas turbines are stationary units that can hold up to 40,000 gallons of lubricating oil which makes full oil changes a daunting task both economically and environmentally. Implementing the use of chemical cleaners, combined with proper filtration, can extend the life of system components and the lubricating oils that separate them. Therefore, properly characterizing the performance of chemical cleaner is of utmost importance.

The largest concern using chemical cleaners is the lack of standard methods to characterize removal amounts and rates. This is in sharp contrast to the many standards that are available to characterize an oils resistance to oxidation, the precursor to varnish formation, e.g. ASTM D974 [136] or D664 [137], ASTM D2272 [138], ASTM D445 [139], ASTM D92 [140]. Testing lubricating oils before and during use is invaluable to the end user and, due to the fact that varnish formation is usually inevitable, it is also very important to quantify and standardize varnish removal methods. Standards that consistently quantify the removal potential of chemical cleaners are needed to ensure performance data will be available to the scientific community, as well as the end user.

To address this, a test has been designed that will allow varnish removal using chemical cleaners to be quantified. This test system has been designed to allow control of flow rates and temperatures across a flat steel sample containing an artificial varnish. This varnish is produced using common oxidative mechanisms and characterized to ensure the product accurately simulates varnish produced within the gas turbine engine. The varnish is subjected to chemical flushes at flow rates and temperatures designed to mimic conditions within a typical gas turbine engine. Testing metrics include mass loss and time-lapse photographic data, where the latter is analyzed numerically to determine parameters including the maximum rate of varnish removal. The novel test method developed in this research is described in detail in the next chapter.

Chapter 3

EXPERIMENTAL DESIGN

3.1 Design Introduction

To characterize chemical cleaners, a test system was needed to provide an environment where varnish would be exposed to the simulated conditions of in service systems. Furthermore, the test system needed to provide ease of testing, controllability, and reproducibility. To provide this, several design constraints were considered when designing the varnish test system. The system needed to operate effectively with a minimal amount of fluid, providing an efficient use of blended chemicals. Moreover, the design required that temperature control be a paramount feature, with the ability to ensure precise, accurate temperatures throughout testing. Furthermore, accurately controlling the flux of the test fluids through the system was of utmost importance, thereby allowing a broad range of testing to be done with consistency and confidence. The design also needed to provide easy flushing of chemicals between testing as well easily accessible locations for filling and draining fluids.

The test system needed to deliver operational envelopes for a wide range of industrial, commercial and transportation environments to ensure that conditions within journal bearings, heat transfer units, pumping lines, thrust washers and other engineered systems could be simulated. It was imperative that the test system provide a safe working environment both physically and environmentally. The total tabletop area of the test system needed to be kept to a minimum to allow location in confined spaces. The following sections will describe the components, sub-components, further design criteria and operational envelope of the varnish test system.

3.2 Test Coupon

A method of supplying a varnished surface, that could be repeated with confidence, was needed for the varnish test system. Stamping uniformly sized, rectangular metal coupons, were decided upon and varnish would be applied on the surface. A test coupon specimen, dimensioned as shown in Figure 3.2.0.1, was implemented.

The test coupon would need to slip fit into the test chamber, be held tightly to minimize movement during testing, and allow for easy removal when coated with
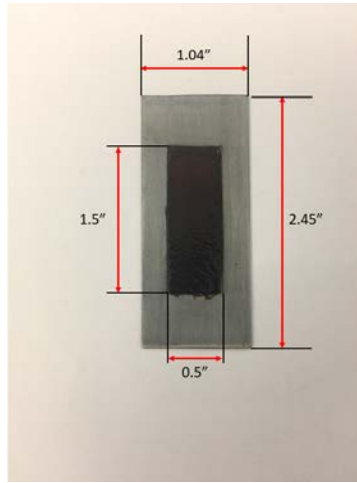
Figure 3.2.0.1: Test coupon with dimensions.

oil. The test coupon would eventually have varnish coated on its surface, which would need to be positioned in such a way that it would have maximum exposure to the flow of oil. The coupon shown is 1.04in (2.64cm) wide, 2.45in (6.22cm) long and 0.02in (508μm) thick, while the varnish stain is 0.5in (1.27cm) wide, 1.50in (3.81cm) long and an average of 0.003in (76.2μm) thick. This will be standard for each coupon and varnish stain.

3.2.1 Artificial Varnish

The varnish used on the coupon will be created in a lab using common oxidative mechanisms such as ASTM D7873 [141]. The varnish is exposed to conditions, that will allow an accurate representation of gas turbine oil varnish, such as common metals and atmospheric content. To ensure that the varnish is close to the composition observed from in service systems methods such as Fourier Transform Infra-Red (FTIR) spectroscopy can be used to identify species contained in the varnish. FTIR analysis (ASTM E2412-04 [142]) is a routine and useful tool that offers a snapshot of the molecular species present in the lubricant. Thermal oxidation byproducts may be tracked at specific IR wavenumber regions as shown in Figure 3.2.1.1. Figure 3.2.1.1 shows that the artificial varnish (left) is an accurate representation of actual varnish (right). This artificial varnish will hereafter be referred to as just varnish.

Using these methods many different types of artificial varnish can be formed. For the work done in this dissertation four different types of varnish were formed and will be referred to as Varnish A, B, C and D. Table 3.2.1.1 gives a brief overview of the compositions of the varnish used in this work.

The varnish produced is stored in a glass beaker, under ambient conditions, away from light sources. After production of the varnish it has to be applied to
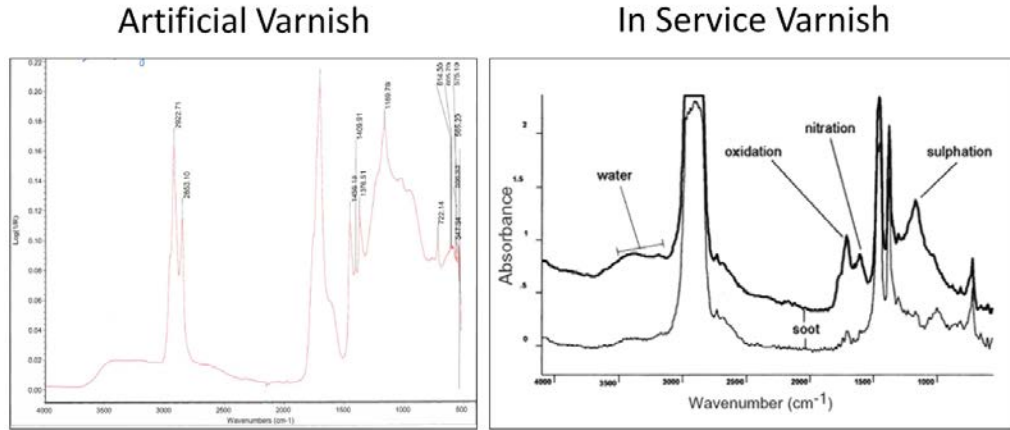
Figure 3.2.1.1: Left: FTIR of artificial varnish made for testing. Right thin line: FTIR of new engine oil. Right thick line: FTIR of used engine oil. Right Figure taken from [7].

Varnish Batch	C-O Molar Ratio	C-H Molar Ratio	Metal Content (%)
Varnish A	4.03	0.595	0.243
Varnish B	3.05	0.776	10.73
Varnish C	4.42	0.595	0.053
Varnish D	4.03	0.659	0.247

Table 3.2.1.1: Composition of artificial varnish used in this work.

the metal coupon. This method of application is to mark out the dimensioned area as shown in Figure 3.2.0.1 and apply slightly more varnish than is necessary to fill this area. The varnish is then cured under varying conditions of temperature and time. These parameters can vary from 130-160°C and from 3-7 hours respectively, and have a large impact of the final varnish product for testing. Four preparation conditions were used in this work as outlined in Table 3.2.1.2.

The varnish coupons were prepared under varying conditions, as signified by the first two digits (PX) and the either left exposed to the atmosphere or covered in a neutral base oil as labeled by the last digit (PXX). The four preparation conditions were used to identify the best varnish to eliminate trends and physicochemical changes in the varnish as outlined in Chapter 5.

Preparation Conditions	Temp °C	Time (hours)
P1A	135	3
P1O	135	3
P2O	135	6
P3O	150	3

Table 3.2.1.2: Preparation conditions for application of varnish to coupon.

3.3   Design Components

3.3.1   Flux Over Varnish Stain

To reproduce an environment where varnish is formed, it was imperative that flow over the coupon could range from the low flow laminar regime (Re < 2300), to the high flow turbulent regime (Re > 4000). This would allow simulated flow over a wide variety of engineered mechanical systems typically found in modern machines.

To provide flow across the entire varnish stain on the coupon the geometry perpendicular to the coupons surface must be found. Moreover, the geometry under consideration must be free from sharp edges and transitional surfaces that might cause turbulence. When considering pipe flow geometry two distinct parameters need to be considered: the area (A) and the perimeter (P_w), which is known as the *wetted* perimeter in pipe flow. Using the area and wetted perimeter, the parameter known as the hydraulic diameter (d_h) can be found by using Equation 3.1.

$$d_h = \frac{4A}{P_w} \tag{3.1}$$

The volumetric flow rate through any geometric area is shown as Equation 3.2

$$\dot{V} = VA \tag{3.2}$$

where V is the velocity of the fluid and $\dot{V}$ is the volumetric flow rate. The Reynolds number, the non-dimensional velocity, can be defined as the ratio of the inertia force ($\rho V d_h$) and the viscous, or frictional, force (η). It can also be expressed as the ratio of dynamic pressure (ρV^2) and the shearing stress ($\eta V/d_h$). By dividing out the density (ρ) of the fluid the Reynolds number can be expressed as shown in Equation 3.3

$$Re = \frac{V d_h}{\nu} \tag{3.3}$$

where ν is the kinematic viscosity. By combining Equations 3.1 and 3.2, an equation that uses Reynolds numbers, flow rates, viscosities (based on temperatures) and wetted perimeters can be found and is shown as Equation 3.4.

$$Re = \frac{4\dot{V}}{\nu P_w} \quad or \quad \dot{V} = \frac{Re \; \nu P_w}{4} \tag{3.4}$$

3.3.2 Test Cell Port Geometry

One of the most important parameters in the varnish test system is the test cell port geometry. The test cell port geometry will determine the range of Reynolds numbers available based on the flow rates generated by the pump and the viscosity of the fluid. The test cell port shape will be influenced by the machinability of the selected material and the blending of shapes as the fluid moves from the round piping system to the shape of the port. This port shape must minimize turbulence by creating a smooth flow transition while tolerances are kept to a minimum. The port shape must also completely cover the varnish on the coupon ensuring flow across the entire varnish stain. The port shape geometry is that of two semi-circles, of radius r, separated by a linear distance l_1 as shown in Figure 3.3.2.1.
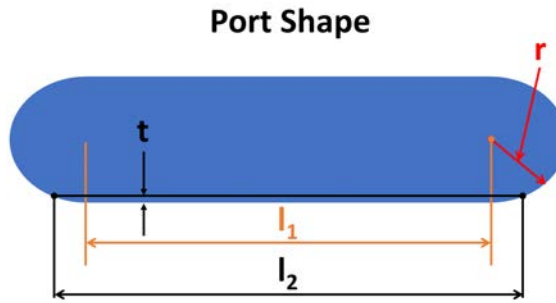
Figure 3.3.2.1: Port shape showing the length between semi-circles (l_1), the width allotted for varnish width variations (l_2), the thickness allotted for varnish height variations (t) and the radius of the semi-circles (r).

When locating the coupon (Figure 3.2.0.1) in the test cell, the bottom of the port will be located such that it sits at the same level as the top of the coupon. This will allow the varnish stain to protrude into the fluid flow exposing the leading edge. This will help to simulate varnish that forms on metal surfaces thereby mimicking real world varnish growth.

Looking again at Figure 3.3.2.1, l_2 needs to be slightly larger than 0.5in (1.27cm), to accommodate slight variations in varnish width and provide full exposure of the varnish to fluid flow, t (representing the thickness of the varnish stain) will be set at 0.005in (127μm) to allow for variations in varnish thickness, l_1 will be 0.375in (0.953cm) and r will be 0.125in (0.318cm). These values give a port area of 0.143in^2 (0.922cm^2), a wetted perimeter of 1.54in (3.90cm) and, using Equation 3.1, a hydraulic diameter of 0.372in (0.945cm).

3.3.3 Pump Selection

To properly size the oil pump a common oil (ISO VG-46), 46 centistokes (cSt) at 40°C and 8.2 cSt at 100°C, was selected to enable temperature related viscosities to be used in flow rate calculations. Using Equation 3.4, Reynolds numbers were found for flow rates ranging from 0 - 180 in^3/s and for viscosities at 40, 70 and 100°C. The results are shown in Figure 3.3.3.1. Based on the desired operational parameters of laminar to turbulent flow, a pump capable of 180 in^3/s is required.
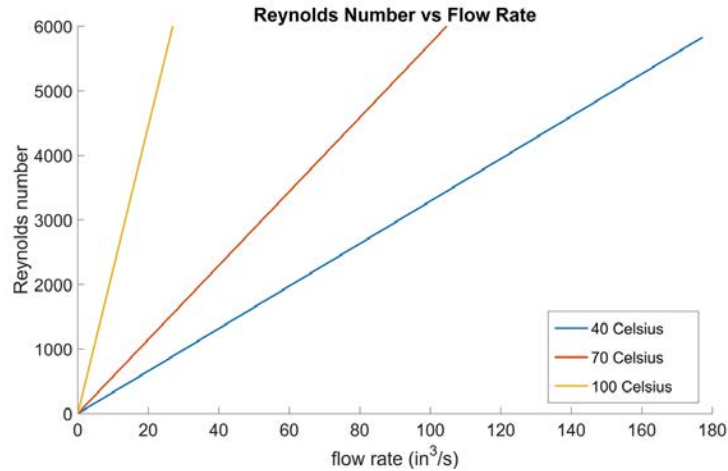
Figure 3.3.3.1: Reynolds numbers based on flow rate using ISO VG-46 base oil.

There are several types of pumps available to move fluid and they include positive displacement pumps, impulse pumps, velocity pumps, gravity pumps, steam pumps, and valveless pumps [143]. Because only positive displacement pumps are capable of providing constant flow, for a given pressure, the remaining pump types will not be considered. A Positive Displacement Pump has an expanding cavity during suction and a decreasing cavity during discharge providing constant geometric pumping volumes for each revolution. The positive displacement pumps can be divided into two categories of pumps: reciprocating and rotary.

Reciprocating pumps can be configured in to two main types of pumps; the plunger, and the diaphragm pump as shown in Figure 3.3.3.2. Because the operation of the reciprocating pump relies on a pulsed cycle, a constant flux across the varnish coupon is not possible without the addition of an accumulator or multiple plungers. Likewise, diaphragm pumps operate on a similar pulsed cycle but are typically found in dual diaphragm configurations to alleviate much of the pulsing. Due to the pulsing nature of reciprocating pumps they were not considered for use in the varnish test system.

Rotary pumps can be configured in many different ways including gear, lobe, vane, piston, progressive cavity pumps, peripheral pumps, and screw pumps. The
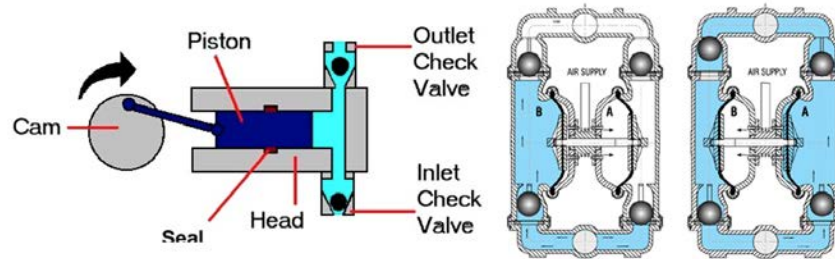
Figure 3.3.3.2: Left: plunger pump [8]. Right: diaphragm pump [9]

progressive cavity pump principle is ideal for handling slurries, viscous, shear sensitive or two or tri-phase mixtures or when applications require, significant suction lift capabilities. The characteristics of the peripheral pump make them suitable for use in a wide range of industrial sectors where small volumes are to be pumped against high pressures [144]. They can also be installed in applications where there is low intake head without creating cavitation problems.

Screw pumps offer the highest flow rate of positive displacement pumps which makes them a great choice for hard to move liquids that need to be move as quickly as possible. Screw pumps are frequently used in applications such as moving fuels, oils, and other high viscosity liquids [145]. Screw pumps are also used for two phase liquid and gas mixtures. However, with the exception of single screw pumps, they are not ideal for moving clean liquids at steady paces. In addition, the complexity of screw pumps often comes with increased maintenance and shorter equipment life spans when compared to other pumps.

The simplest gear-type pump uses a pair of mating gears rotating in an oval chamber to produce flow. As the gears rotate, the changing size of the chambers, created by the meshing and un-meshing of the teeth, provides the pumping action. Another gear design uses an external rotating ring that mesh with an internal gear as it rotates. As the inner gear rotates, the tooth engagement creates chambers of diminishing size between the inlet and outlet positions to create flow [143].

All gear-type pumps have a fixed displacement. These pumps are relatively inexpensive compared to piston and vane type pumps with similar displacements, but tend to wear out more quickly and are not generally economically repairable. Gear pumps are very common in constant flow/constant pressure applications on mobile equipment because of their low cost and dirt tolerance [146]. They are also

widely used as charge pumps to pressurize the inlets of piston and vane pumps because of their excellent inlet vacuum tolerance. A typical external gear pump is shown in Figure 3.3.3.3.
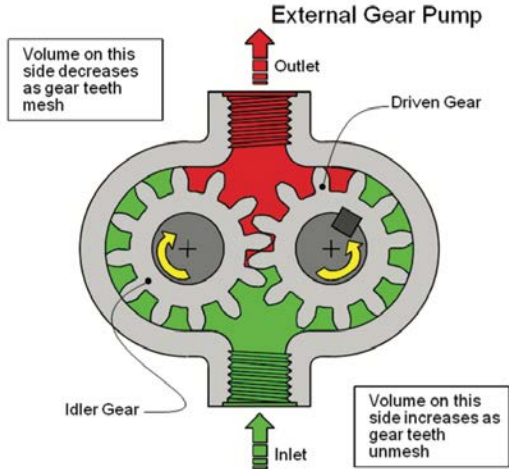
Figure 3.3.3.3: Typical external gear pump [10].

The most commonly encountered vane-type pump generates flow using a set of vanes, which are free to move radially within a slotted rotor that rotates in an elliptical chamber. The changing volume of the cavity between adjacent vanes creates the pumping action as the rotor rotates [143]. A unique feature of vane pumps is the ability to vary the displacement by varying the position of the elliptical chamber relative to the rotor providing minimized power consumption during low flow requirements. This application is widely used in the automotive industry in automatic transmission oil pumps. Moreover, vane pumps can be hydraulically balanced, which greatly enhances efficiency [147]. Furthermore, vane pumps have the rotating group contained in a cartridge making replacement very easy and cost effective. Vane pumps are also known for being very quiet in operation and producing very little vibration. They also have the unique attribute of allowing a soft start because vane type pumps typically do not achieve full output at speeds below about 600 revolutions per minute (RPM). This characteristic can significantly reduce the starting current requirements of electric motors which extends motor life. A vane pump is shown in Figure 3.3.3.4.

Piston pumps can have the pistons arranged in a radial or axial fashion. Radial types tend to be specialized for applications requiring very high power, while axial piston pumps are available in a wide range of displacements and pressure capabilities that make them suitable for many mobile and industrial tasks [143]. Axial-piston pumps consist of a set of pistons that are fitted within a cylinder block and driven by an angled swash plate powered by the input shaft. As the swash plate
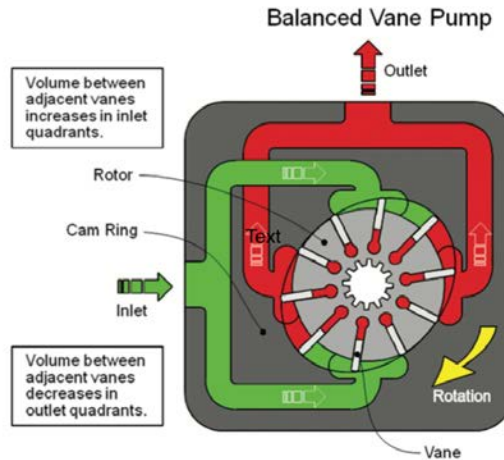
Figure 3.3.3.4: Typical balanced vane pump [10].

rotates, the pistons reciprocate in their respective cylinder block bores to provide the pumping action. A unique characteristic of a piston pump is that the displacement can be changed simply by changing the angle of the swash plate. Any displacement between zero and maximum is easily achieved with relatively simple actuators to change the swash plate angle. A piston pump is shown in Figure 3.3.3.5.
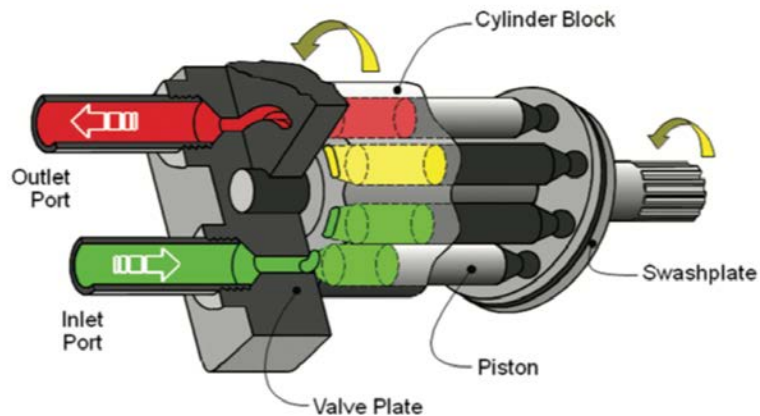
Figure 3.3.3.5: Typical piston pump [10].

The three types of pumps under consideration are the vane, gear, and piston pump which are well known for operational efficiency, longevity, availability, and cost effectiveness [143]. They will be compared in a few categories, that are important in the aspects of research in a lab environment, to provide a method of choosing

the best pump for the test system. Table 3.3.3.1 shows common attributes and characteristics considered when purchasing a pump for specific uses.

pump rating from 1 - 3 with 1 being the most desirable			
	piston pumps	vane pumps	gear pumps
pressure	1	2	2
input Speed	1	2	2
power density	1	2	2
conversion efficiency	*1*	*2*	*3*
dirt tolerance	3	2	1
inlet vacuum tolerance	3	2	1
noise and vibration	*2*	*1*	*3*
size and weight	3	2	1
fluid compatibility	1	2	1
life expectancy and reparability	*2*	*1*	*3*
cost	*3*	*2*	*1*
totals for factors in italics	8	6	10

Table 3.3.3.1: Pump characteristics and ratings for piston, vane, and gear types of pump [10].

Table 3.3.3.1 has four rows that are italicized showing the categories that were important for this project such as conversion efficiency, noise and vibration, life expectancy and reparability, and cost. When totaled, the vane pump became the preferred choice for the varnish test system based on the chosen criteria. To select the appropriately sized vane pump, we refer again to Figure 3.3.3.1. A pump that can flow 180in^3 per second is required to reach the high end of the turbulent flow regime at 40°C. Vane pumps are typically rated for either volumetric flow rate in gallons per minute (GPM), at 1200 RPM, or geometric flow per revolution in^3/rev (cm^3/rev). Converting 180in^3 per second gives a maximum volumetric flow of 46.8 GPM. To find a geometric flow per revolution the speed of the pump needs to be determined.

With a 60 cycle power supply the synchronous speeds available for electric motors are 3600 RPM, 1800 RPM, 1200 RPM and 900 RPM. Induction motors develop their torque by operating at a speed which is slightly less than synchronous speed. Typically they will operate at 3500 RPM, 1750 RPM, 1160 RPM or 875 RPM. Choosing a very common speed of 1800 RPM, the geometric flow is found to be 6in^3 per revolution. The final choice of pump was found through Eaton Vickers pump manufacturing. The pump is shown in Figure 3.3.3.6 with specifications.

Eaton vane pump # 02-137136-1:
- seals: viton fluorocarbon seals
- series: 35v series
- thru drive: none
- pilot designation: standard pilot
- geometric displacement: 30 usgpm at 1200 rpm (5.91 in^3/rev)
- port connections: sae 4 bolt flange inlet/outlet
- mounting: flange mounting
- shaft: straight keyed
- port orientation: opposite inlet port, as viewed from end of pump
- rotation: right hand clockwise, as viewed from shaft end of pump
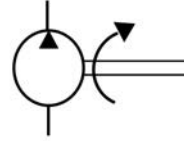
Figure 3.3.3.6: Hydraulic pump for varnish test system.

3.3.4   Electric Motor and Control Selection

There are many aspects to consider when selecting a motor, such as intended application, operational parameters, mechanical loading, and environmental issues. A constant or variable torque/horsepower will be required for the motor depending on the type of load the motor is driving. The size of the load, the required speed, and acceleration/deceleration (particularly if it's fast and/or frequent) will define the torque and horsepower that is required. Requirements for controlling motor speed also need to be considered such as duty cycle, service factor and efficiency.

The first calculation that needs to be addressed is the power requirement for pumping 50 GPM, which is a factor of volumetric flow and pressure developed within the system. This relationship is given by Equation 3.5

$$P_{hp} = \frac{\dot{V} \cdot P_{psi}}{1714 \cdot eff} \tag{3.5}$$

where P_{hp} is the horsepower required, P_{psi} is the pressure developed in pounds per square inch (psi) and eff is the effective efficiency of the electric motor. Electrical motors lose efficiency due to primary and secondary resistance losses, iron losses, stray losses and mechanical losses [148]. Electrical motors, constructed according to NEMA (National Electrical Manufacturers Association) design B (Single Speed 1200, 1800, 3600 RPM, Open Drip Proof (ODP) or Totally Enclosed Fan Cooled (TEFC) motors 1 hp and larger (that operate more than 500 hours per year), must meet the efficiencies shown in Table 3.3.4.1.

If the pressure in the system is limited to 300 psi, by using a variable pressure relief valve, and using 100% efficiency initially, the power requirement for the motor can be calculated at 8.6 hp. Using the information from Table 3.3.4.1 an efficiency of 84.0% needs to be included in the recalculation to find a total power requirement of

power (hp)	minimal nominal efficiency %
1 - 4	78.8
5 - 9	84.0
10 - 19	85.5
20 - 49	88.5
50 - 99	90.2
100 - 124	91.7
> 125	92.4

Table 3.3.4.1: Minimum nominal efficiencies according to NEMA design B.

10 hp. Formulas for finding required amperage, for various electrical power supplies, is shown in Table 3.3.4.2.

direct current	single phase	two-phase four wire	three phase
$\frac{hp \cdot 746}{V \cdot eff}$	$\frac{hp \cdot 746}{V \cdot eff \cdot PF}$	$\frac{hp \cdot 746}{2 \cdot V \cdot eff \cdot PF}$	$\frac{hp \cdot 746}{1.73 \cdot V \cdot eff \cdot PF}$

Table 3.3.4.2: Finding required amperage for direct and alternating current electric motors.

where V is the voltage, eff is the efficiency of the motor, PF is the power factor and hp is the horsepower. The efficiencies are again found in Table 3.3.4.1 and the power factor is found using Table 3.3.4.3.

power (hp)	speed (rpm)	power factor		
		1/2 load	3/4 load	full load
0 - 5	1800	0.72	0.82	0.84
5 - 20	1800	0.74	0.84	0.86
20 - 100	1800	0.79	0.86	0.89
100 - 300	1800	0.81	0.86	0.91

Table 3.3.4.3: Typical motor power factors for 3 phase motors.

A 208 volt, 3 phase, 30 amp, power supply was available within the working area where the varnish test system would be housed so further calculations will be used with those parameters. Using 208 volts, an efficiency of 85.5% and a power factor of 0.86, the required full load amperage is found to be 28.2 amps. The final choice of motors is shown in Figure 3.3.4.1 with specifications.

A 3 phase induction motor is a constant speed motor. This means that for the entire loading range, the change is the speed of the motor is quiet small. The speed control of induction motor is done at the cost of decreased efficiency and lower

U.S. Electric Motors #
S10P2AC:
• Model # DJ63
• Phase: 3
• Voltage: 208-230/460
• Frame: 215TC
• Weight: 120 lbs
• Full load efficiency: 91.7%
• Full load amps: 26.5

Figure 3.3.4.1: Electric motor for varnish test system.

electrical power factor. To control the speed at which a 3 phase induction motor operates can be done from the stator or rotor using various methods. To control the speed from the stator side requires changing either the applied voltage, the frequency (using the constant voltage/frequency (V/F) method), or changing the number of poles in the stator. Controlling speed from the rotor side can be done either by rheostat control, using cascade operation or by injecting electromotive force (EMF) in the rotor circuit.

With the V/F method, if the ratio of voltage to frequency is kept constant, the flux remains constant. By keeping V/F constant, the developed torque remains approximately constant. This method gives higher run time efficiency. Therefore, the majority of AC speed drives employ constant V/F method for speed control. Moreover, along with wide range of speed control, this method also offers *soft start* capability. The choice of inverter control is fairly basic requiring only the choice of brand. For the varnish test system a V/F base inverter was chosen from Fuji Electric capable of providing power requirements for a 10hp electric motor. The FRENIC-multi, part number FRN010E1S-2U, was selected based on its compact design, ease of control and ease of installation. This will allow speed control from 0 - 100% of rated maximum speed. The inverter is shown in Figure 3.3.4.2.

3.3.5 Motor to Pump Couplings and Mounting

The hydraulic pump needs to be driven by the electric motor and both required solid mounting on a table top. Typically hydraulic pumps are mounted to the engine that drives them while the motor is mounted to a frame of some kind. That was the followed procedure for this test system and the pump was mounted to the motor using an aluminum adapter manufactured by Lovejoy ®(part number BHN-182 24-C H, L = 6.81in). To drive the pump two adapters, one mounted to the motor and one to the pump, are fitted to the shafts of each unit. The electric

Frenic-Mulit part # FRN010E1S-4U
- Phase: 3
- Voltage: 230
- Power rating: 10 hp

Figure 3.3.4.2: VF inverter controller for varnish test system.

motor has a 1-3/8in shaft while the pump has a 1-1/4in shaft, each coupled with a Lovejoy adapter. These adapters are then joined together with a replaceable hard urethane coupler, which insulates and dampens vibration from one unit to the other, also from Lovejoy (part number L099/L100SOX). Each shaft is machined to accept a keyway style transmission of power from the shafts to the adapters so keystock was also needed to complete the coupling (precision brand 14299 5/16in x 5/16in x 12in). The coupling system is shown in Figure 3.3.5.1 with specifications.

LOVEJOY part #s L100X1, L100SOX, L099X1
- Jaw material: steel
- Isolator material: urethane

LDI Industries part # 1955
- Material: Aluminum

Figure 3.3.5.1: Adapters and couplers for transmission of power from electric motor to hydraulic pump.

The motor/pump combination also needs to be mounted to the surface it will reside on. To accomplish this, two aluminum C-channels (2in x 1-1/4in x 1/4in) were cut 36in long to provide the base for the combination. These C-channels were connected together by aluminum angle (1-1/2in x 1-1/2in x 1/8in) while aluminum flat (1-1/2in x 1/8in) was used to help support the hydraulic pump. The C-channel

54

was spaced 7 inches apart and the aluminum angle was bolted in two places to maintain this spacing. The electric motor was bolted directly to the C-channel while the pump was fixed to the electric motor by the adapter. Two supports, from one of the angle braces on top of the C-channel, were cut and bolted directly to the pump to support its weight.

3.3.6 Test Cell

The test cell needs to house the test coupon and allow for connection to the piping of the test system. It also needs to provide a blended transition from round pipe to the port shape shown in Figure 3.3.2.1. The entrance and exit connection to the test cell will be done with a 1-1/4in CD-61 fitting that matches the 1-1/4in CD-61 fitting on the exit of the vane pump. The dimensions of this fitting (shown in Figure 3.3.6.1) are A = 2.6in and B = 3.2in, and uses a bolt size of a 7/16-14 UNC thread.
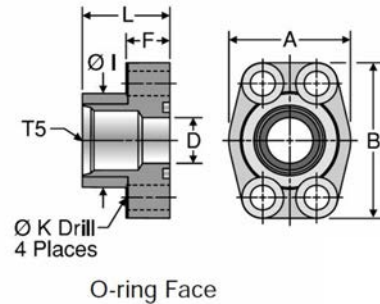
Figure 3.3.6.1: Standard CD-61 fitting schematic.

The test cell width and height was sized at 3.2in x 2.5in to allow the CD-61 fitting's o-ring to seal properly and allow for enough thickness within the bolt mounting area of the test cell. The length of the test cell needed to be the sum of the length needed for the test coupon (2.45in), the entrance region length and a blended section which connects the port shape to the round piping of the system. Using computer aided drafting (CAD) a test cell was designed, based on the parameters listed previously, and a preliminary design was dimensioned and is shown in Figure 3.3.6.2.

After extensive discussions with several machinists it was decided that the maximum depth, dimension B in Figure 3.3.6.2, that could be machined using 316 stainless steel was 2-3/8in using a 1/8in tooling bit. This would make the overall length of the test cell 7in and provide an entrance length of 1.25in.

Figure 3.3.6.2 shows the test coupon, located in the middle-center of the test cell, along with an entrance region blended into a 1-1/4in round pipe configuration. This will match the CD-61 fitting allowing for a smooth transition from the system
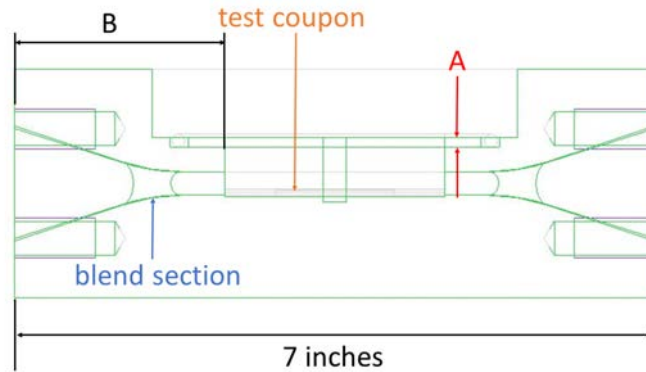
Figure 3.3.6.2: Side view of the preliminary test cell design showing the entrance and blended section (B), the o-ring land (A) and the location of the test coupon.

to the test cell. The four mounting bolts are shown drilled and tapped to standard depths. Dimension A shows the o-ring required to seal the test cell's lid to the body when testing. The lid of the test cell not only needed to seal the system from leaks, it had to maintain the shape of the port throughout the length of the test coupon area. This was done by using the same dimensions referenced in Figure 3.3.2.1 and by using dimension l_2 as the bottom width for the lid. This would allow for variations in the varnish height as well as providing an area for round o-rings to be located (black arrows in Figure 3.3.6.3), with 1/16in black o-ring cord, to ensure a force of 20N holding the test coupon to the bottom of the test cell to minimize movement of the coupon.

The o-ring dimensions, which seals the lid to the test cell body (dimension A, Figure 3.3.6.2), needed to be found. In the varnish test system this o-ring will be subject to no movement making it a static seal. In a static seal the mating gland parts are not subject to relative movement except for small thermal expansion or separation by fluid pressure. The choice of seal material is based on chemicals in the system, temperature range of system, pressure experienced and mating surface roughness. The depth, and width, of the o-ring grove need to be calculated to allow for the proper amount of crush while allowing the o-ring to swell during operation. The volume of the o-ring grove needs to allow for expansion of the o-ring when the lid comes into contact and begins to compress it. The o-ring grove in the test cell body was calculated to be 0.2 inches wide x 0.104 inches in height and have an overall diameter of 3.395in. This would house an o-ring whose dimensions are a 0.139in cross section and have an inside diameter of 3.109in. These dimensions provide a 25% crush on the o-ring while allowing for a 35% swell. The material of the o-ring seal is that of viton rubber.
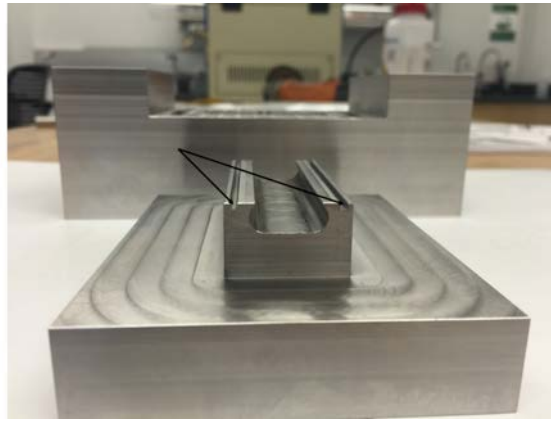
Figure 3.3.6.3: Front view of the test cell lid with arrows pointing out areas for o-rings to be housed to ensure a force holding test coupon to bottom of test cell.

Initially, one test cell lid was machined out of 316 stainless steel and beginning at test 41, a vapor polished, polycarbonate lid was machined to allow real time data of the varnish removal process. Due to the difference in thermal expansion between 316 stainless steel (16.0μm/(m·K)) and polycarbonate (65-70μm/(m·K)), slight dimensional differences in the lid were necessary. These differences were applied to the CAD model and files were sent out for machining. Figure 3.3.6.4 shows test cell assembly with dimensions and specifications.
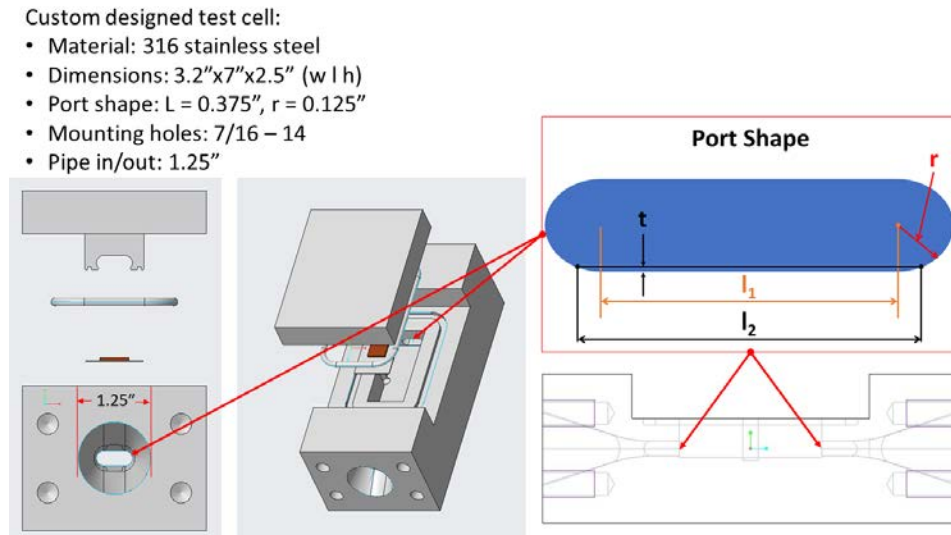
Figure 3.3.6.4: Test cell dimensions and specifications.

3.3.7   Flow Meters

While it is easy to calculate the geometrical flow rate of the pump it does not take into consideration several factors such as pump efficiency, wear, major and minor losses and other factors. Since flow rate is directly related to finding the Reynolds number, pressure drops, and pipe losses, a method of correlating the geometrical output and actual output is desired. In the varnish test system two flow meters are required to allow both high and low Reynolds number measurements. The main line of the test system must allow for the complete measurement of flow from the pump which can be as high as 50 GPM while the bypass line of the test system is designed to measure flow rates from 0.1 - 20 GPM very accurately.

The main flow line will always measure the total output from the pump while the by-pass line will measure low flow conditions. The entire output of the pump, during low flow conditions, will run through the main line flow meter and to a 3 way ball valve that will either flow to the test cell or to the by-pass line. With the 3 way ball valve directing the entire flow to the by-pass line a second measurement will provide very accurate flow measurements through the system. The ball valve will then be slightly moved to direct flow towards the test cell. The difference between the by-pass line measurements is the flow through the test cell. So it is imperative that a very accurate by-pass flow meter be used. The flow meters must also accommodate a range of viscosities from 5 - 100 cSt, be capable of 150 psi, and handle temperatures up to 120 degrees Celsius.

There are several types of flow meters that can handle oil based liquids along with temperature and pressure variations. Hedland variable area flow meters were initially chosen for both flow meters. However, increased accuracy was desired for the bypass line and an Omega, positive displacement, flow meter was installed in place of the variable area Hedland. The combination of these flow meters will ensure accurate and repeatable measurements. The flow meters are shown in Figure 3.3.7.1 with specifications.

3.3.8   Heater

The varnish test system is required to provide a temperature range of 20 - 120°C. To accomplish this a heater that is capable of rasing the temperature of the fluid from ambient to 90°C as quick as possible was desired. One of the operational parameters of the test system was to operate on a minimal amount of fluid. Because 5 gallon pails are a common standard in industry it was proposed to calculate heater requirements based on a 5 gallon system. Furthermore, the heater system needed to work with the standard 120V, 20amp, outlet. With the standard power outlet available there is only a total of 2400 Watts to be used to heat a fluid with an average specific heat (c) of 2.18 J/gK, average density (ρ) of 861000 g/m^3, a volume (V) of 0.004m^3 and a desired temperature increase (δT) of 70°C. We also need to consider

Omega part # FPD3034-D
- Accuracy: +- 0.5% of reading
- Repeatability: +-0.03%
- Minimum Viscosity: 1cPs
- Maximum Viscosity: 1000cPs
- Mounting: shafts in horizontal plane
- Size: ¾" NPT
- Temperature: 20 – 100C
- Flow: 0 – 20 gpm

Headland (McMaster part # 4263K75):
- Size: 1-1/4"
- Connection: NPT
- Body material: Aluminum
- Fittings: 303 stainless steel
- Seals: fluoroelastomer
- Pressure range: 50 – 150 psi
- Temperature range: -20 – 240 F
- Max pressure: 3,500
- Length: 12.25"
- Accuracy: +- 2%

Figure 3.3.7.1: Left: positive displacement flow meter located in the by pass line of the test system. Right: variable area flow meter located in the main line of the test system.

convection to the atmosphere, conduction to the table-top and any radiation emitted from the components of the system.

The only component that will be in direct contact with any surface is the reservoir, therefore conduction will be limited. Likewise, radiation at the temperatures the test system will operate at will be minimal. This leaves convection as the dominate method of heat dissipation. To find the power lost to convection the surface area of the test system must be estimated. The current area estimation for the test system (including test cell, piping, reservoir, filter, pump, flow meters etc.) is estimated to be 2.5m^3. Using an average convection coefficient (10 W/mK for still air), and a temperature difference of 70°C, the power requirements to overcome convection are calculated at 1750 Watts. The time to raise the temperature of the remaining oil is found using Equation 3.6.

$$T_{min} = \frac{60W}{C_p \rho V \Delta T} \tag{3.6}$$

Using the total available power of 2400W this time is found to be 20 minutes. Contacting Durex Industries, an immersion heater in a sheet metal enclosure was purchased. This heater will thread into the return line and the element will protrude into the reservoir to ensure effective heating. Recalculating the time to heat, using 2000W, gives a time of 50 minutes. The heater is shown in Figure 3.3.8.1 with specifications.

3.3.9 Filter

When the varnish is removed from the coupon it was decided that a filter system was needed to help characterise the particle sizes and would allow insight

Durex Industries Heater part # MS20S4-A13H3-2000ZA-01:
- Type: Immersion heater
- Fitting: 2 inch NPT steel screw plug
- Power: 2 kW
- Voltage: 120 V
- Phase: 1 Ph
- Length: 13.5 inches
- Element: 3 0.475 inch incoloy 840 element
- Flux: 28W/in^2 max
- Enclosure: NEMA 4 sheet metal
- Thermostat: 85-230f SPST
- Temperature range: 20 – 120 Celsius
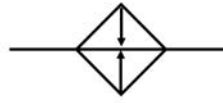
Figure 3.3.8.1: Heater for varnish test system with specifications.

into the mechanisms of removal. To accomplish this a Ron-Vik filter system was installed downstream from the test cell. This filter system is composed of three pieces: the top, the bowl and the filter. The top is made from 6/6 white nylon with 1-1/2in NPT fittings, the bowl is constructed of clear nylon and uses a viton seal, while the filter is a 15 micron 304 stainless steel mesh. The temperature/pressure capabilities of the filter system are rated at 150 psi at 90°C and nylon is known to be resistant to hydrocarbons, aromatic solvents, fuels, motor oils and refrigerants. The pressure drop across the filter, when clean, is 0.5 psi and the filter will be mounted in the return line of the system. The filter is shown in Figure 3.3.9.1 with specifications.

Ron-Vik Filter Company:
- P/N 10696 – Top 1-1/2" FNPT white nylon 6/6
- P/N 10521 – Bowl large clear nylon 6/6
- P/N 17497 – Filter element 15 micron 165x800 mesh, 20x20 backup mesh with PVC seals
- P/N 10539 – Viton bowl seal
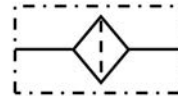
Figure 3.3.9.1: Filter for varnish test system.

Initially the filter was used with just the stainless steel mesh screen. In later testing the filter was lined with polypropylene paper with an average filtering capability of 5 micron. The filter paper allows for quick and easy examination of the

removed varnish. Strips of filter paper are cut to fit inside the steel mesh filter and have a 1in^2 box and test ID labeled in black permanent marker. Upon completion of the test the paper is removed and laid flat for inspection.

3.3.10 Reservoir

A reservoir does more than just hold fluid. A reservoir must allow for thermal expansion of the fluid and transfer heat to the atmosphere. A reservoir must have enough volume in reserve for fluid when service items, such as filters, are changed. Reservoirs must also allow for air to escape and sediment to settle to the bottom. The test system reservoir will have none of these things. The recommended practice NFPA/T 3.16.2 [149] addresses basic minimum design and construction features for reservoirs.

Due to the requirement of a low volume test system, the reservoir of the varnish test rig will be substantially undersized by industry standards. This might require several modifications to our test system to compensate for the undersized volume of fluid contained in the reservoir. The main challenge will lie with removing air from the fluid. A traditional reservoir provides the opportunity for air to escape from fluid before it is drawn into the pump inlet. A low volume reservoir could allow aerated fluid to be drawn into the pump, which could cause cavitation and eventual damage or failure of the pump. An issue of even more concern in the varnish test coupons case would be removal of varnish due to entrained air that could not be quantified.

The final shape of the reservoir is that of a square with a total volume of 3 gallons. It will be fabricated from 12 gauge 316 Stainless steel, have 1 suction port, 3 return ports, and a flanged open top. The ports will be fabricated using NPT weldable bungs and the suction port will be located on the bottom center of the reservoir and be a 2 inch NPT fitting. The main return line will be located in the center of one side of the reservoir and be a 2 inch NPT fitting. The two other return lines will be located on an adjacent side from the main return line and be 1-1/4in NPT weldable bungs. The reservoir will be located in such a way that only 1/2 gallon of fluid will drain back to the reservoir when the lid of the test cell is opened. A baffle will be installed in the reservoir to channel fluid from the main return line to the suction port to ensure that vortices will not be able to form during high flow rates causing entrained air. A 100 mesh stainless steel screen will be located on the suction port to safeguard against foreign material from entering the pump. The reservoir for the varnish test system is shown in Figure 3.3.10.1 with specifications.

3.3.11 System Piping and Components

To ensure that laminar flow exists within the piping of the system we can use Equation 3.4 with the highest flow rates developed by the pump, at various

Custom built reservoir:
• Size: 8"x10"x10" (l w h)
• Material: C1008/1010 CRS
• Suction port: 2"
• Return port: 2"
• Drain line off suction port: 1"
• Relief valve return port: 1-1/4"
• Bypass flow control return port: 1-1/4"
• Lid: Clear Lexan
• Volume: 3.46 gallons
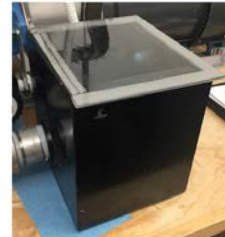
Figure 3.3.10.1: Reservoir for varnish test system with specifications.

temperatures, using the discharge port size from the pump, which is given as a 1-1/4in CD-61 fitting. Using the inside perimeter for 1-1/4in 316 stainless steel pipe the maximum flow rates for various temperatures can be found and are shown in Figure 3.3.11.1. The maximum flow rates, for laminar flow in 1-1/4in 316 stainless steel pipe, are 48 GPM at 40°C, 31 GPM at 70°C, 15.6 GPM at 90°C and 8 GPM at 100°C. Care must be taken to ensure system operation is maintained within the testing regime intended.
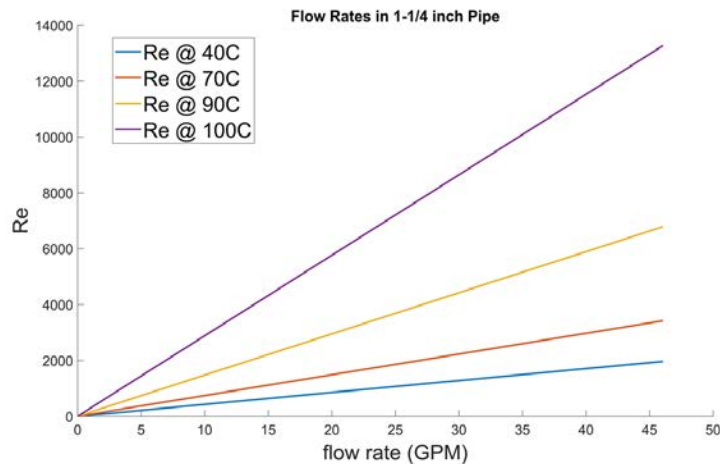
Figure 3.3.11.1: Re numbers based on 1-1/4 inch 316 stainless steel pipe.

The first step in finding the piping of the system is to layout where each component will be located. The piping needs to be kept as short as possible allowing

a compact design. To accomplish this a CAD model was produced to allow for quick manipulation and location of each component. An image of the proposed layout of the varnish test system is shown in Figure 3.3.11.2.
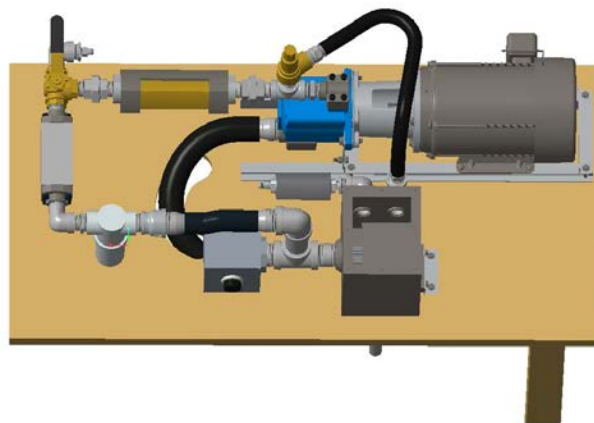
Figure 3.3.11.2: Layout of the varnish test system to ensure minimal piping.

The pump has a CD-61, 1-1/4in, discharge port and a CD-61, 2in, suction port. The suction port will use a 90 degree 2in CD-61 to 1-1/4in NPT connected to 2in rubber hose that leads to the reservoir. The discharge port will connect with a 90 degree CD-61 to 1-1/4in NPT fitting and have a gauge block between the pump and the CD-61 fitting to allow a pressure gauge, and a small ball valve to allow air to be injected into the system to facilitate flushing, to be mounted near the pump. These components are shown in Figure 3.3.11.3 with specifications.

McMaster-Carr part # 46325K27
- Size: 3/8"
- Connection: NPT
- Pressure range: 800 psi
- Temperature range: 0 – 450 F
- Length: 1-3/4"
- Vacuum rating: 28.95 in. of Hg
- Shape: Straight
- Seat: PTFE
- Seal: Fluoroelastomer
- O-ring: Fluoroelastomer
- Body: 316 stainless steel
- Ball: 316 stainless steel

Perma-Cal Industries, Inc. part # 123NIR06A21-LZ
- Accuracy: -+ 0.5% mid scale
- Connection: NPT
- Material: 316 stainless steel
- Dial size: 2.5"
- Graduation marks: 2 psi
- Numeric increments: 20 psi
- Pressure range: 0 – 200 psi
- Temperature range: -65 – 600 F

Figure 3.3.11.3: Left: 2 way ball valve. Right: pressure gauge.

The discharge line will then proceed to a 1-1/4in tee to allow mounting of a variable pressure relief valve (shown in Figure 3.3.11.4 left) , which returns to the reservoir to ensure system pressure dose't exceed 150 psi. The pressure line then enters the 50GPM Hedland flow meter and exits to a 1-1/4in, 3 way, brass, ball valve (shown in Figure 3.3.11.4 right). The ball valve diverts flow either to the by-pass flow meter or to the test cell.

Black Mountain Inc. Kunkle Valve
part # 913BEFM73-ME:
- Size: 1-1/4"
- Connection: NPT
- Material: Bronze
- Seal: 316 Stainless steel
- Pressure range: 50 – 150 psi

Bonomi North America Inc. part # 365N
- Size: 1-1/4"
- Connection: NPT
- Pressure range: 0 - 400 psi
- Temperature range: -4 – 340 F
- Length: 4-3/8"
- Vacuum rating: 29 in. of Hg
- Shape: Tee
- Inlet location: center port
- Flow pattern: L-pattern
- Seat: PTFE
- Seal: Fluoroelastomer
- O-ring: Fluoroelastomer
- Body: Brass
- Ball: chrome plated brass

Figure 3.3.11.4: Left: pressure relief valve. Right: 3 way brass ball valve.

The fluid that diverts through the low flow meter is then channeled back to the reservoir. The fluid through the test cell then enters the filter and returns to the reservoir passing over the heater coils. All of the 1-1/4in piping in the system is made from 316 stainless steel with a pressure rating of 150 psi. Moreover, there are 2in 316 stainless steel piping used through the heater assembly as it returns to the reservoir. Finally, there are various sizes of hydraulic hoses used to facilitate the connections between pump and reservoir, diverter valve and low flow meter, and filter and piping for heater. A complete hydraulic schematic for the varnish test system is shown in Figure 3.3.11.5 with specifications.

3.4 Summary

The most important component of the test system is the test cell. This is where the coupon will be housed and where the flow will interact with the varnish on the coupon. The coupon was chosen first and the test cell was sized to house the coupon. The main components of the test system, as shown in Figure 3.3.11.5, have been discussed. Each component is necessary for the test system to operate and allow characterization of fluids. While most of the components worked as expected
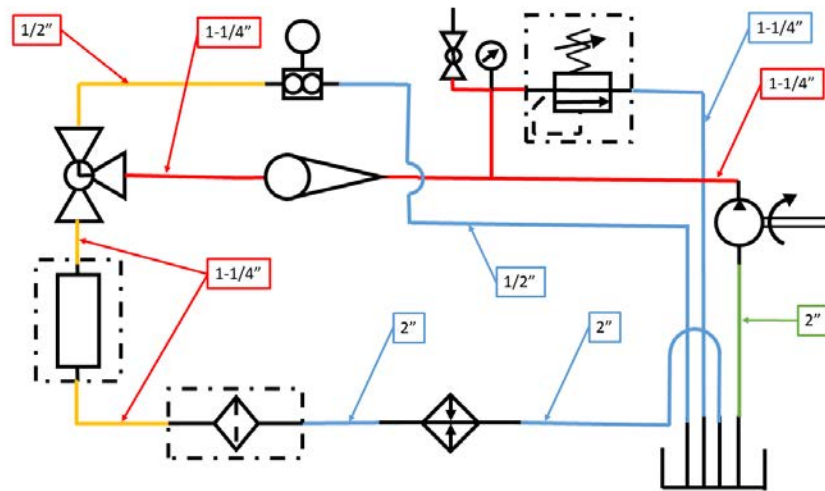
Figure 3.3.11.5: Complete hydraulic diagram of test system: red is fluid pressure, blue is return fluid, green is suction and yellow is low pressure fluid. System symbols are given in the figures in each section.

the reservoir proved the challenge for the test system. Initially air entrainment was a problem due to the high flow rates the system is capable of. A baffle was fabricated and installed to direct the return fluid directly to the suction line. This eliminated any air entrainment. When the test system was up and running, developing methods of utilizing its capabilities and finding the best testing parameters and metrics was the next step. The testing procedures and methods will be addressed in the following chapter.

Chapter 4

TEST METHODS AND METRICS

4.1   Test Fluids

There were nineteen fluids tested during the course of this work. These included two base fluids and seventeen cleaner fluids with removal capabilities. The differing chemicals used in each cleaner gave the fluids a range of colors. The final eight fluids used in this work are shown in Figure 4.1.0.1.
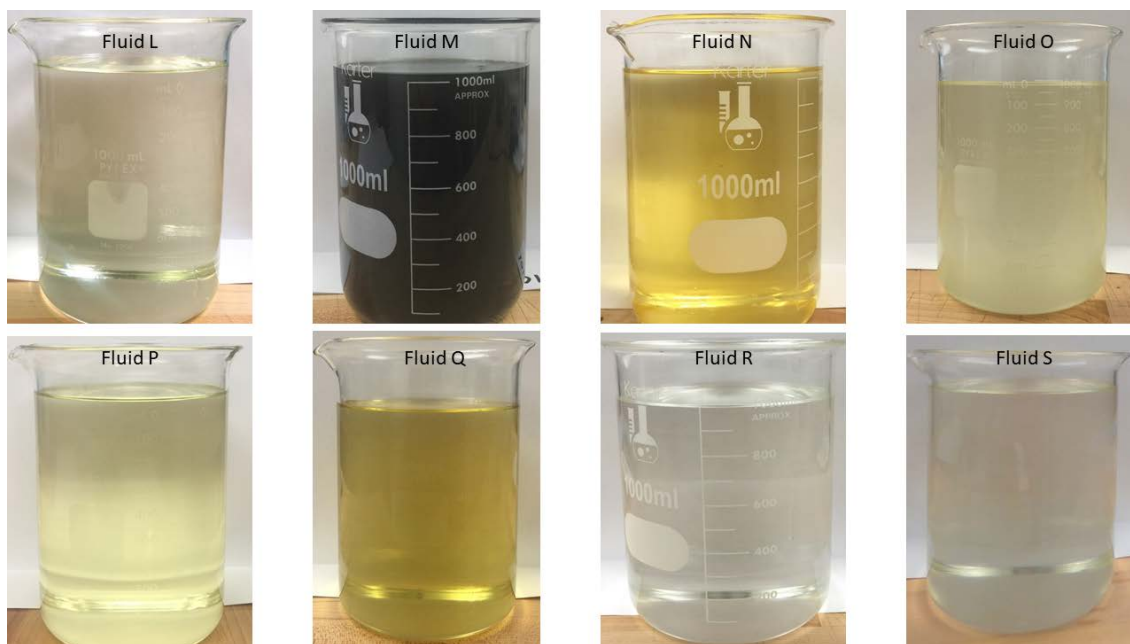
Figure 4.1.0.1: Cleaner fluid color for Fluids L, M, N, O, P, Q, R, S.

The chemical composition and solubility have an effect on several parameters of varnish removal which will be discussed in Chapter 6. The initial odor of each fluid was noted and, while some fluids maintained a typical base fluid hydrocarbon smell, other were very strong. For the most part, the color of the fluid was a good indicator of the strength of the fluid smell. Darker colors usually had a very strong chemical smell while lighter colors were less strong. Fluid odor might become an

issue for cleaner agents when used in confined areas and end users will be interested in the severity of the smell and whether it volatile organic compound (VOC) could be an issue for them.

The fluids' aeration properties were also noted. While some fluids provided good anti-foaming tendencies others took some time to de-aerate. This might be an issue for some systems and fluids that have foaming tendencies might not be the best choice without further additives. Initial optically detected particle counts were also recorded after each test. These findings will be reported in later sections. Fluid viscosities were also tracked and will be reported in later sections.

4.2   Test Methods

The test system can provide flow rates varying between $0.1 < \dot{V}(\text{GPM}) < 48$ through the test cell, and the temperature capabilities range from $40 < \text{T}(°\text{C}) < 120$. Depending on the viscosity of the fluid (tests reported here conducted with an ISO-46 fluid) being tested, the Reynolds numbers that can be generated within the test cell range from $10 < \text{Re} < 40,000$. The heart of the test system is the test cell. Figure 4.2.0.1 shows a schematic and photo of the test cell. The design ensures that the entire surface of the varnish is exposed to the flow of oil. The placement of the coupon in the test cell is such that the top of the coupon, where the varnish resides, is flush with the bottom of the incoming pipe wall. This provides a continuous no slip condition from the pipe wall to the coupon, thereby exposing only the varnish into the flow of oil. This simulates many environments where varnish is formed on the no slip boundary conditions of machinery. The lid of the test cell is made of vapor polished polycarbonate allowing a camera to be positioned above the coupon for recording.

Each test is preceded by flushing the system with the base stock to remove any remaining fluid from the previous test. A fluid is then added to the test system and is circulated through both the main and by-pass lines while the desired fluid temperature is reached. Depending on the flow rate desired for the test one of two methods will be used. For flow rates $\dot{V} > 15\text{GPM}$ the variable area flow meter will be used and the by-pass line will not be needed. For flow rates $\dot{V} < 15\text{GPM}$, and where high accuracy is desired, the by-pass line is employed. The fluid is directed through the by-pass line where the positive displacement flow meter very accurately measures the total flow of the pump. The ball valve is then positioned to remove the desired flow from the by-pass line providing precise flow control over the coupon.

The system is initially run without the coupon until the temperature reaches steady state. Then, the flow is stopped temporarily and a prepared coupon is inserted into the test cell. The camera lighting is turned on and photographic recording begins. The system is turned back on and the desired duration of testing is performed. During the test, images are captured using a 12.0 MP resolution camera set to take a photograph every 10 seconds. The placement of the camera is
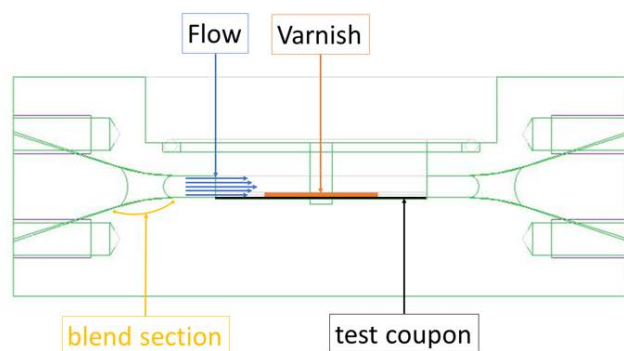
Figure 4.2.0.1: (a) Wireframe CAD model of test cell showing location of coupon and varnish. (b) Photo of the test cell without the polycarbonate lid. The varnish coupon prior to testing can be seen in the center of the cell. Dimensions on both figures correspond to the scale bar shown in the lower right corner of (b).

fixed so that the position of the varnish is the same for all tests. Upon completion of the test, the coupon is removed from the test cell and dried in heptane to remove any oil from the sample prior to weighing. An initial post-test mass recording is done and 24 hours later another is performed to ensure no further change occurred due to evaporating heptane. The difference between the pre-test and post-test mass is identified as mass loss, one of the metrics used to characterize varnish removal.

In the Methods Section, the test system is demonstrated with two fluids, Fluid D and Fluid E, both of which are known to have varnish removal capabilities. This will help to identify the removal metrics used in Chapter 5. All tests are conducted at a temperature of 90°C, a flow rate of 4.5GPM and a duration of 120 minutes. With a flow rate of 4.5GPM, an average velocity of 10.12 ft/s (3.08 m/s) is created within the test cell. The viscosities of the two fluids tested are 17.27 and 12.82 centi-Stokes (cSt) at 90°C, which correspond to Reynolds numbers in

the high laminar flow regime (Re_D=1,442 and Re_E=1,944). These conditions are selected to approximate lubrication conditions in a gas turbine engine, as well as other components. Two tests are run for each fluid under these conditions.

4.3   Test Metrics

The initial testing metrics were mass loss and filter inspection. The varnish mass was recorded pre and post testing to find removed mass in %. The filter was used to help identify the type of mechanism responsible for the removal (diffusion or convection discussed later). Filter characterizations included not only the size of removed particles but their shape. More aggressive chemicals would dissolve the varnish into particles smaller than 5μm and pass through the filter entirely just giving a hint of brown on the filter. The filter will be discussed further in Section 4.3.3.

These two metrics, mass loss and filter inspection, became the initial basis for characterizing varnish removal and although these two metrics were valuable in characterizing the chemical cleaners removal abilities further metrics such as the removal rate were desired. A clear test cell lid was incorporated into the design prior to test 41. This allowed real time images of the varnish removal process to be captured in situ. This allowed further metrics to be found including the removal rate through the entire test, the maximum removal rate, the time of maximum removal rate and the time at which no further varnish was being removed. These will be discussed in Section 4.3.2.

At the present time there are four primary, three secondary and two tertiary metrics. The primary metrics are used to characterize the varnish removal process and include maximum removal rate (mg/min), maximum removal rate time (min), steady state removal (min) and maximum removed varnish (%). The first three primary metrics are found using numerically analyzed time-lapse photography while the fourth is found using mass loss. The three secondary testing metrics include analyzing the removed particles in the filter, tracking the viscosities and identifying the ISO codes of the fluids. The two tertiary metrics include odor and aeration properties.

The combination of primary, secondary and tertiary metrics allows for a very comprehensive comparison from fluid to fluid. The primary metrics are used to quantify the varnish removal process and provide information on the capability of each fluid to remove the varnish. The secondary metrics are used to accurately identify how the cleaner will affect the system. Analyzing the removed varnish will provide information on the size of the varnish particles that will be circulating through the system and helps to properly size the filter system for each fluid. Identifying the viscosities of the fluids initial viscosity, and tracking them through use, allows confidence that the proper viscosity will be used in a given system. Furthermore, identifying the initial cleanliness of the fluid, and tracking it through use,

helps to ensure that cleaners conform to end user standards of cleanliness as well as properly sizing the filter system to remove varnish but not the cleaner.

4.3.1   Mass Loss

The mass loss metric is used to track the total mass loss from the coupon. The coupons are weighed before any varnish is applied to the coupon and then again after the varnish has been applied to the coupon. The start of test (SOT) mass weight is the weight of the coupon plus the varnish minus the coupon weight. This allows tracking of the actual mass loss. After each test the coupon is stood on end, on a soft shop towel, to allow the bulk of cleaner fluid to drain from the coupon. The coupon is then taken to a vented fume hood. In the fume hood the coupon is submerged in heptane, for up to 5 minutes, to remove any remaining chemical cleaner. The coupon is then dried, using compressed air, and weighed. This weight is recorded and the coupon is then re-submerged in heptane for 1 minute, blown dry and re-weighed. The two weights are then compared to ensure no residual chemical cleaner remains on the coupon. When the masses are within 0.25% of each other the final mass is recorded. To further ensure that there is no mass change the mass is weighed again 24 hours later. Fluids D and E are shown in comparison for mass loss in Figure 4.3.1.1 and illustrate how mass comparisons are viewed in Chapter 5.
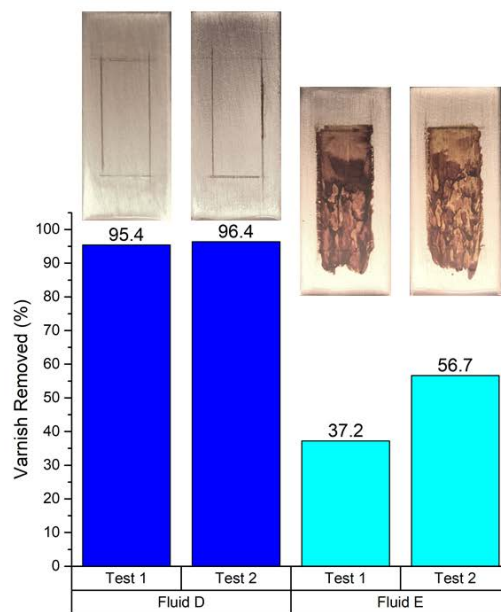
Figure 4.3.1.1: Percent varnish mass removed during the 120-minute tests on Fluid D and E. Insets show photos of the coupons after each of the tests

4.3.2 Time-lapse Photography

Time-lapse photography is used to image the real time varnish removal process from the coupon. Time-lapse photography was first proposed after failed attempts to photograph, and record mass loss, during testing. Initially testing was stopped and the coupon was removed from the test cell for heptane drying and weighing at specified intervals. Not only did the temperature drop substantially, the heptane had adverse effects on the testing process. Implementing a clear lid would provide uninterrupted imagining during testing. A polycarbonate lid was machined and implemented prior to test 41. Once the polycarbonate lid was manufactured imaging parameters needed to be established. A Gopro camera, with 12Mpx resolution was purchased and testing was performed that identified the best parameters for the camera distance from the lid and how many images per minute. A 5cm distance and 10 images per minutes were found to provide the best results.

The system of lights include two Neewer, NL - 660s. These lights have 660 LEDs (330 White and 330 Yellow) to illuminate a variable white balance from tungsten to daylight (3200 to 5600K). The lighting will ensure that a consistent image will be recorded by the camera regardless of the conditions in the lab. The lighting will be mounted on tripods that will be located in the same position from test to test. The lighting system is shown in Figure 4.3.2.1.

Figure 4.3.2.1: Test cell shown with Neewer NL-660 lighting

4.3.2.1   Algorithmic Processing

The mass loss results are informative and clearly illustrate a difference between the two fluids. However, the images taken during testing can be used to provide more information about varnish removal. An algorithm is developed to analyze the images of the varnish coupons taken during the test using the CMKY color scale. Specifically, the K value (the blackness value) is the exclusive color analyzed for this process. An illustration of this algorithm is shown in Figure 4.3.2.2. First, an image of the test cell before the test is taken and the image is cropped to include just the coupon. Then, a region with no varnish is identified and the average K value is calculated from that region to use as the no-varnish reference (K_{min}). This is repeated for a region with only varnish (K_{max}). Then, during the test, the average K value of the varnish region is obtained. After the test, the K values at each time are normalized using the references K_{min} (no varnish) and K_{max} (maximum amount of varnish). This step ensures that the algorithm can be applied for any varnish or fluid, i.e. having any initial appearance or color. Each test had an average of 723 images over the 120 minute test duration so the cropping allowed faster run-times for the algorithm.

The results of this analysis for the two fluids are shown in the top panels of Figure 4.3.2.3. The normalized K value necessarily starts at 1 and then decreases as the varnish is removed as the test proceeds. It can be observed that the rate of change of the K factor with time is faster for Fluid D, indicating that this fluid removes varnish more quickly. Fluid D also reaches steady state varnish removal sooner than Fluid E. These observations can be quantified by taking the derivative of the K factor vs. time data, as shown in the lower panels of Figure 4.3.2.3.

It was found that taking the slope over just two points created a very jagged 1st derivative. This would cause very large negative numbers which were not indicative of the actual maximum rate of varnish removal. Extending this to include 3,5,7 and 9 points smoothed the graph of the 1st derivative. The problem was that the values decreased slightly as the number of points increased. It was found that a very accurate 1st derivative plot could be found using 7 points while only decreasing the values by 2%. Taking the derivative over 7 points helped to smooth the first derivative graphs and eliminate phantom removal rates caused by differences in K values.

First, the time of the maximum varnish removal rate can be identified from the maximum negative value of the derivative. Second, the time at which the magnitude of the derivative decreases to below -5E-3 for at least 2 minutes is identified as steady state, i.e. after this time, very little additional varnish is removed with continued flow. Using this approach, we can determine that Fluid D's maximum varnish removal rate occurs, on average, 6.5 min after the test started and reached steady state at 17 min. For Fluid E, the maximum removal rate occurs at 12.2 min and reaches steady state at 48 min. This indicates that Fluid D reached its
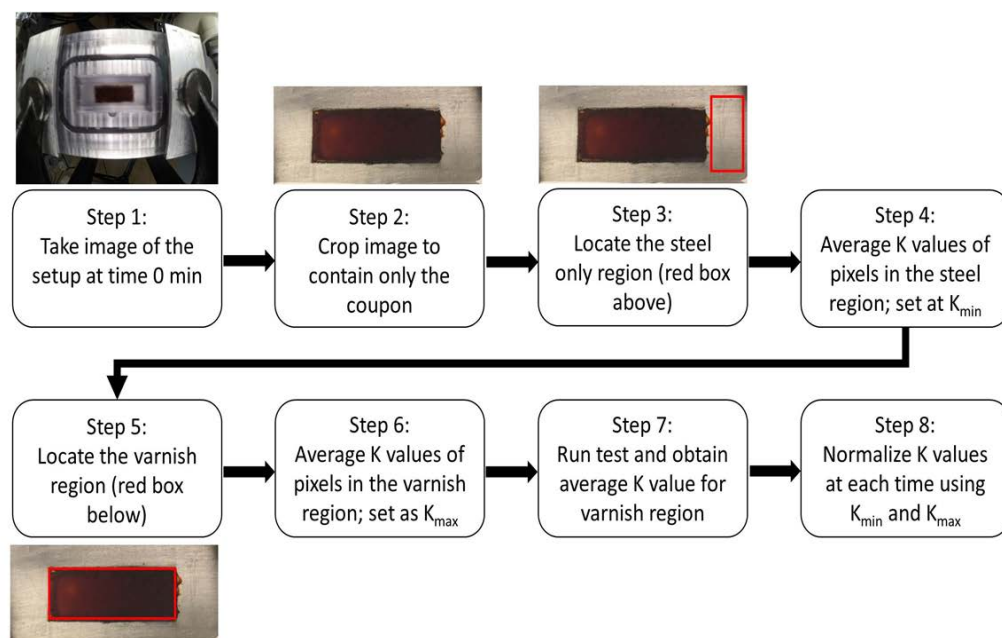
Figure 4.3.2.2: Algorithm used to quantify varnish removal including: 1-original image, 2-cropped image, 3-location of steel reference site, 4-averaging steel values, 5-locating varnish region, 6-averaging varnish K (black value from CMKY color scale) values, 7-collect data during test and 8-normalize data to generate a plot of the amount of varnish as a function of time.

maximum removal rate and steady state removal sooner than Fluid E.

The analysis above enables quantitative comparison of times, but only qualitative comparison of the mass loss and rate of mass loss. To address this, the K values in Figure 4.3.2.3 need to be associated with mass removed. To determine the validity of this approach, the percent change of the normalized K value during the test is compared to the percent change of the coupon mass. The results are shown in Figure 4.3.2.4. The difference between the mass loss change and K value change is less than 2%, indicating that these two measures of total varnish removed are quite consistent. Based on this consistency, we can multiply the normalized K values by the start of test masses to general plots of varnish mass removed as a function of time.

Figure 4.3.2.5 shows the varnish removal in terms of mass as a function of time. In this work, the data points at each time are calculated as an average from the two tests on each fluid. This result enables quantitative comparison of the fluids varnish removal performance. This is the pattern followed throughout Chapter 5. Initially, three parameters were identified to fully characterize the varnish removal:
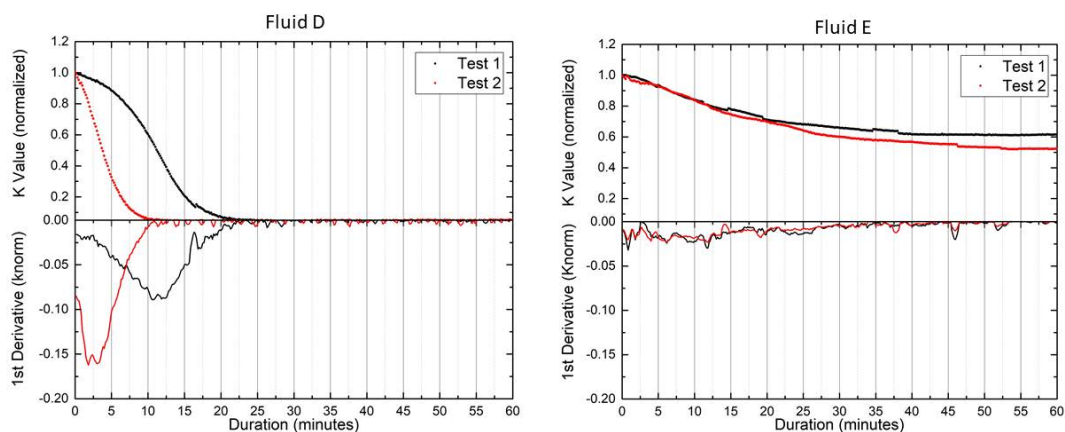
Figure 4.3.2.3: Time-lapse photographic results for Fluid D and Fluid E. Top graphs display the normalized K value from the algorithm shown in Figure 4.3.2.2 while the bottom graph shows the 1st derivative of the normalized data. The derivative provides a means of identifying the time at which the varnish removal rate is a maximum and of steady state removal.

maximum varnish removed, time at which the maximum varnish has been removed and maximum rate of varnish removal. These three parameters have been updated to include a fourth: the time of maximum varnish removal rate. With these four parameters, characterizing each fluid becomes simplistic and comprehensive.

Using the four characterization parameters mentioned above, a direct comparison between Fluid D and E can be made, as shown in Figure 4.3.2.6. In all cases, the parameters are averages from the two tests performed on each fluid. First, Fluid D removed substantially more varnish from the coupon than did Fluid E (95.9% vs 46.94%). The time required to reach steady state varnish removal is also shorter for Fluid D than Fluid E (17 min vs 48 min). Finally, Fluid D has a much larger maximum varnish removal rate than Fluid E (6.42 mg/min vs. 1.62 mg/min). Taken together, the comparison of these parameters shows that Fluid D is a much more aggressive chemical compound than Fluid E, removing twice as much varnish in half of the time.

74
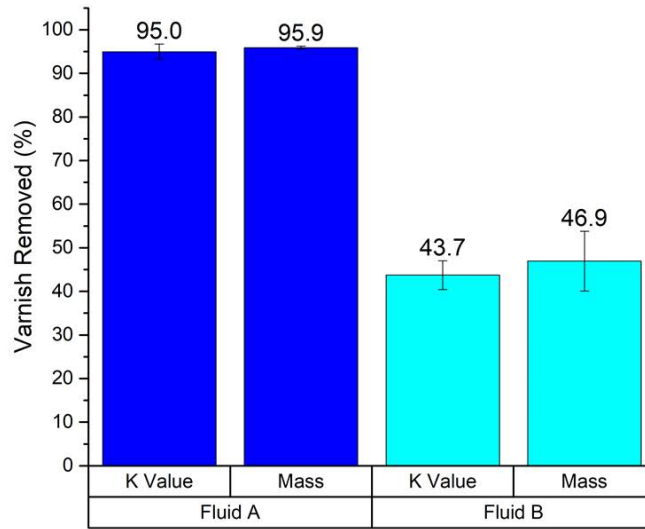
Figure 4.3.2.4: Percent varnish removed quantified by the total change in the normalized K factor during the test and the difference between the coupon mass at the start and end of the test for Fluids D and E.

4.3.3   Filter

The filter provides valuable information on the mechanism of removal for each cleaner. The filter shown in Figure 3.3.9.1 houses a 10 micron stainless steel cylindrical filter. Initially this metal filter was used to inspect how varnish was being removed. The filter would be removed after each test and then a photograph would be taken of the inside of the filter as shown in Figure 4.3.3.1.

This metal filter was then cut open to further inspect the varnish removed from the coupon. During the process of cutting and un-rolling the filter, significant damage was caused to the varnish contained in the filter prompting another method of filter inspection. It was decided that the metal filter would be lined with 5 micron polypropylene filter paper. The filter paper is cut in rectangles that fit just inside the rubber seals on either end of the metal filter. The filter paper is marked with testing information including test number, coupon number and fluid number. There is also a 1in^2 marked on the paper to allow varnish particle counts to be made within the square and related to the entire filter area. The filter paper is shown in Figure 4.3.3.2. This has become the standard for inspecting the varnish removed from the coupon.

The paper filter allows easy removal and inspection of the removed varnish
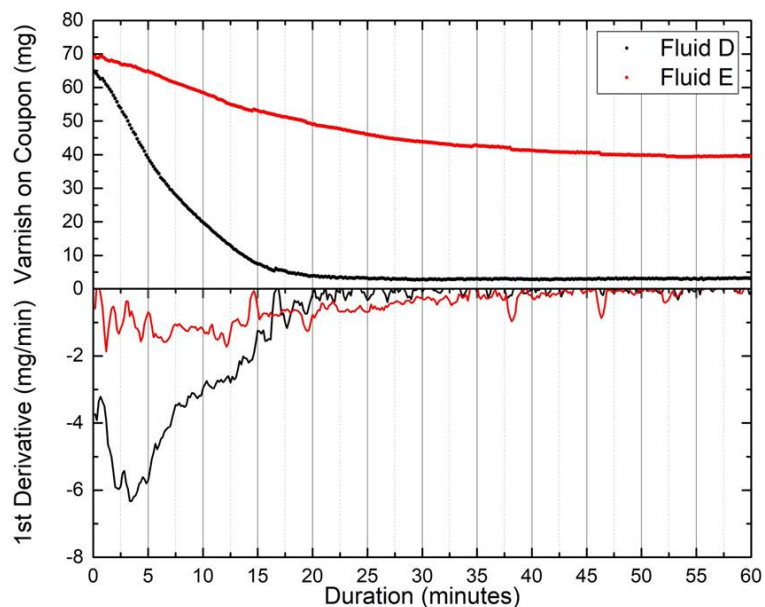
Figure 4.3.2.5: Top plot shows the average values for both fluids using the normalized K value multiplied by the original start of test varnish weight showing the actual weight of removal. The bottom plot shows the derivative of the varnish removal data.

without damaging the varnish in the process. The paper filter allows for easy photography and microscopy to characterize how the varnish is removed from the coupon. This has provided insight into whether shear forces or chemical breakdown play a larger roll in the removal process. It has also helped to correlate the Schmidt number discussed in Chapter 6.

4.3.4 Viscosity

Viscosity was not an initial test metric and is not used in the current characterization of the cleaner fluids. However, viscosity is an important property of any lubricant and therefore should be considered when evaluating cleaner fluids. If the viscosity of the cleaner fluid isn't close to that of the fluid used in service detrimental results could occur. The viscosities were tracked prior to test 78 but new fluid viscosities for these fluids were not captured. The only viscosities that will be reported are for the tests in which the fluid was tested when new and tracked during testing. This will cover tests 100 through 117.

The viscosities are measured using an ATS STRESSTECH rheometer capable of both parallel plate and concentric cylinder measuring systems. The ATS rheometer can provide temperature measurements ranging from 5-100°C and shear rates
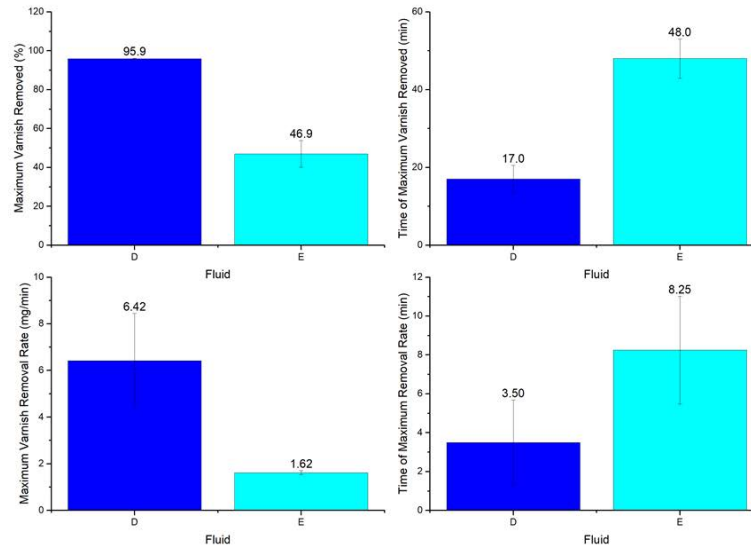
Figure 4.3.2.6: Comparison of Fluids D and E in terms of four varnish removal performance metrics. Upper left: maximum percent varnish removed. Upper right: time required to achieve steady state varnish removal. Bottom left: maximum varnish removal rate. Bottom right: time of maximum removal rate.

of 0.1-4000 1/s. All viscosities for this work were measured using the concentric cylinder configuration at 40°C and at an average shear rate of 100 1/s.

4.3.5   Optically Detected Particle Counts

Optically detected particle counts are an important part of oil monitoring and shouldn't be overlooked. Optically detected particle counts are widely used in industry and is one method of quickly determining if there is a problem with the system. The most common unit of reporting optically detected particle counts is the International Organization for Standardization ISO Code System. This convention is covered under the ISO standard 4406:2017 [150]. Optically detected particle counts for this work is done using a Beckman Coulter (HIAC-ROC) optical particle counter. Optical particle counting is covered under ISO 11500 [151] and is one of the most widely used methods today for determining fluid cleanliness. Optically detected particle counts were not an initial test metric and was instituted at the same time as viscosity tracking. It became apparent that the particle counts were substantially different between the chemical cleaners. The particle counts provided valuable information for correctly sizing a filter that would remove varnish from the
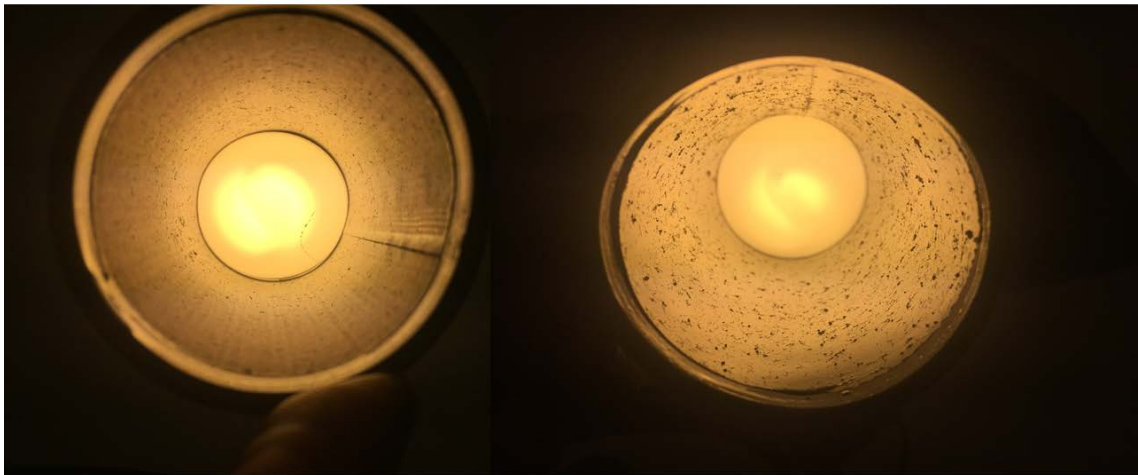
Figure 4.3.3.1: Initial filter inspection performed using visual/photographic imaging. Left: filter showing a base fluid varnish trappings. Right: filter showing a cleaner fluid trappings.

fluid while allowing the cleaner to remain in circulation. While optically detected particle counts wasn't used to characterize the cleaner fluid in this paper the results will be shown and discussed in the scope of tests 100-117.

4.3.6   Fluid Odor and De-aeration

Characterizing each fluid for odor included ranking the strength and unpleasantness of the smell at both ambient (23°C) and operating temperature (90°C). While this is open to individual interpretation several lab members were polled and in 95% of the fluids the results were unanimous. The ranking for each category ranged from 1-5 with 1 identifying a strength or smell that was not strong or unpleasant and 5 identifying a smell that was strong or unpleasant.

Foam was able to be tracked due to air being introduced to the test cell chamber during installation of the coupon. This air would be purged during the first 10 seconds of operation after insertion of the coupon and would foam the fluid in the reservoir. Depending on the chemical cleaner the foam would vary. This variation was tracked using a scale from 1-5 with 1 identifying a fluid with very little foam and 5 identifying a fluid with substantial foam. The results for Fluid D and E are shown in Table
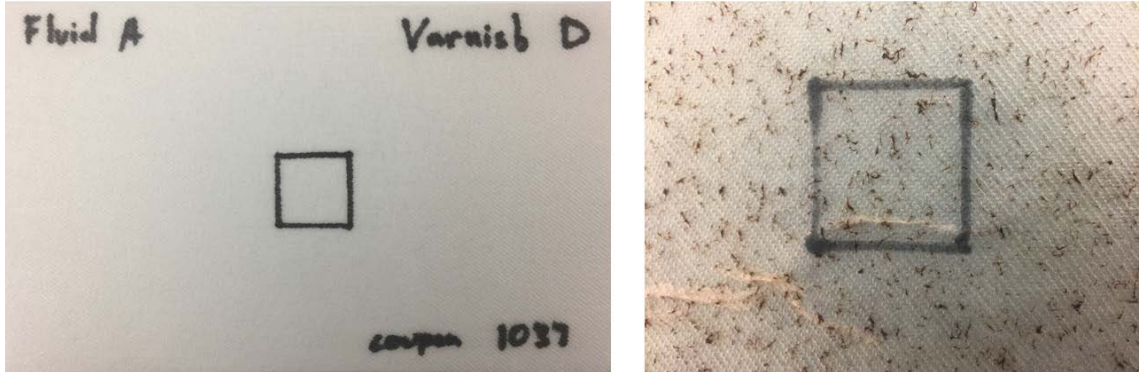
Figure 4.3.3.2: Current polypropylene filter paper used for filter inspection. Left: pretest paper with markings for fluid, coupon, test number and a 1in^2 area marked on its surface. Right: post test filter (Test 74) paper showing varnish removed

4.3.7 Mass Diffusion

While not initially classified as a test metric, the mass diffusion coefficient (D) has become invaluable in comparing fluids at differing temperatures and flow rates. Mass diffusion helps to characterize the fluid's ability to dissolve the varnish under differing conditions. The Schmidt number (Sc) is used to determine whether convective or mass diffusion is driving the varnish removal process. Fluids can behave very differently under varying conditions of flow and temperature and the Schmidt number is one of the best indicators of fluid performance. Mass and convective processes will be discussed in Chapter 6.

Fluid	23°C Smell	23°C Strength	90°C Smell	90°C Strength	Foam
Fluid D	3	3	5	5	3
Fluid E	2	1	3	1	2

Table 4.3.6.1: Identifying the fluid odor (as unpleasantness), strength (in permeation) and foam tendency (for the ability to de-aerate) for Fluid D and E on a scale from 1-5. 1 is a low value for strength, smell and foam, while 5 is a high value for strength, smell and foam.

4.4 Summary

The initial test metrics of mass loss and filter inspection proved inadequate to characterize the performance of the cleaner fluids. However, with introduction of the clear test lid, non-intrusive photographic data was collected that allowed varnish removal rates to be calculated using algorithmic processing. This allowed the majority of the current work to progress using the 4 characterization parameters discussed previously. With the addition of viscometry and optically detected particle counts, further characterizations are allowed. The viscosities ensure that the fluid falls into the range expected for in service systems. Optically detected particle counting ensures that chemical cleaner compounds, containing large particles, won't inadvertently cause concern by appearing as contaminated fluid. The performance of the fluid used in the test system, as well as the characterizations discussed previously, will be discussed in Chapter 5.

Chapter 5

RESULTS

5.1 Introduction

Over 140 individual varnish removal tests were run, as summarized in the Appendix. Initially, tests were designed to provide information about the testing conditions that provided consistent and high varnish mass removal amounts. Over the course of these initial tests, it was found that not enough varnish was removed. This was addressed by changing the test conditions and varnish preparation and storage. Then, testing metrics were expanded from just mass removal to several test metrics, including mass removal rates, time of maximum removal rate and when the removal process reached steady state. This was enabled by the addition of updated components to the test system as discussed in Chapter 3. Moreover, during these tests, unexpected phenomena occurred that prompted the investigation of varnish composition, varnish preparation conditions and varnish mass control on the coupon. What follows is a chronological description of each test series along with what information was gained, how that information was used to improve the tests, which test metrics became the standard, and final results for a series of test fluids evaluated using the developed standard metrics.

5.2 Test Method Evaluation

During design and construction of the varnish test system, significant consideration was given to flow rate and temperature control. These two parameters provide a method of simulating the conditions that exist for in service systems. Furthermore, the varnish on the surface of the coupon was exposed to the flow of oil on the no slip boundary condition at the pipe walls. This simulated environment allows confidence in the varnish removal process by accurately mimicking real systems. In doing so, it is important that conditions such as flow within journal bearings and heat transfer units can be reproduced.

Reynolds numbers for common, hydrodynamic, journal bearings were investigated and found to be very low (Re = 10-100) in the laminar regime [152]. The transition to turbulent flow in common journal bearings is estimated to be Re = 1300 using a bearing ratio (R/C) of 1000, where R is the radius of the journal and C is the oil film thickness. This provided some insight into flow numbers needed

to simulate common journal bearings. Flow rates in typical piping systems, such as heat transfer systems, are designed to remain in the laminar flow regime to keep friction as low as possible. This fact is apparent from observing the Moody Diagram which shows the friction factor in terms of the Reynolds number and pipe roughness [153]. Flow within lubrication passages and drain-back channels are also typically in the laminar regime [154]. For cams and lifters, the Reynolds numbers are known to be low within the journal bearing and even lower on the cam surface. For these reasons, tests should be performed with laminar flow to reproduce the conditions in many components.

The first 45 tests were run using only mass loss and filter inspection. However, these two metrics provided no information about the *rate* of removal as well as *when* the varnish removal process ended. A series of tests were designed to identify rates of removal and the steady state condition. In the following sections, the term steady state refers to a condition where the varnish is not appreciably losing mass with additional flow. While varnish mass will continually be removed, the rate of removal has reach its lowest point and further testing would not help to characterize fluid performance. During these tests, the coupon was removed at specific intervals to be weighed and imaged. This caused several problems, explained later, and the process was discontinued.

However, the observations prompted the use of a clear lid to enable photographic imaging during testing. This allowed the varnish removal process to be photographed in situ and the results using real time photographic imaging proved invaluable. It was then possible to record, non-intrusively, the varnish removal process. The imaging data was combined with the mass loss data to provide rates of removal in mg/min. The result became a primary metric for chemical cleaner performance.

Initially, three tests were used for each fluid. This provided a means to check the accuracy and precision of the tests by finding the average values, standard deviations and errors. When confidence was established in the testing process, and in the interest of time, only two tests were run for each fluid. Moreover, tests were run for extended durations to determine where steady state exists for base oils and provide an upper time limit on testing. We expected the chemical cleaners to outperform the base oils and remove the varnish in shorter periods of time. That is, the time to reach steady state for cleaner fluids was expected to be less than the time it takes base oils reach steady state.

After each test, the filter was imaged to help understand how the varnish was being removed i.e. small/large particles, flaking or rolling. Attempts were made to cut the stainless-steel filter open to allow it to lay flat for inspection and imaging. It was found that the process of cutting the metal filter and rolling it open damaged the varnish on the filter. Much of the varnish was contained between the layers of steel mesh so the varnish was squeezed into different shapes as well as broken into

smaller pieces when the mesh was cut, making evaluation difficult. Furthermore, the varnish became dislodged from the filter during the cutting process. Therefore, this process was discontinued and polypropylene paper was placed inside the metal filter which allowed for quick and easy inspection of the removed varnish.

The first 12 tests were run using a variable area flow meter on the by-pass line. The accuracy of the variable area flow meter was deemed insufficient for this test system and a high precision, positive displacement, flow meter was installed on the by-pass line. This provided accurate and repeatable flow across the coupon in the test cell.

The varnish removal results are divided into three main categories: (1) initial testing and identification of testing parameters and trends, (2) identifying varnish aging characteristics, and (3) final testing of chemical cleaners using standard metrics.

5.3 Initial Testing
5.3.1 Tests 1-2: 70°C, 9GPM, Varnish A, Base Fluid A

Tests 1-2 were conducted with Base Fluid A, which has a density of 0.862g/cm^3 (7.19lbs/gal) and a viscosity of 45.87cSt at 40°C (104°F). Using a test temperature of 70°C (158°F) and 34LPM (9GPM), an average velocity of 6.18m/s (20.3ft/s) was generated in the test cell, providing a Reynolds number of 3707. This is in the turbulent flow regime and the goal was to determine the maximum amount of varnish that could be removed using base oil.

During Test 1, the coupon was removed from the test cell at 10, 15, 25, 45, 65, 105 and 165 minutes, visually inspected, and photographed. The total flow across the coupon was 5621L (1485gal). There was drastic movement of varnish during the first 10 minutes (as shown in Figure 5.3.1.1), prompting closer interval inspection in subsequent tests. It was determined that the steady state removal condition was met at 165 minutes and testing was concluded at that time. Initially, the final weight was found by drying the coupon in an oven at 90°C (194°F). This caused the varnish to flow on the coupon and required considerable time (>100min) to completely dry the oil from the coupon. The start of test varnish weight (SOT) for test 1 was 86.5mg, so 64.4mg of the varnish was removed during testing. This gives a percentage-based varnish removal of 74.5%. However, there was a temperature drop of 5°C (41°F) during each visual inspection which might have had an effect on the removal process.

Test 2 used the same parameters and fluid as test 1, but the photographic data was taken every minute during the first 9 minutes (to catch the process of varnish removal lost in test 1) and then at 14, 24, 84 and 165 minutes. These initial photographs were taken by removing the stainless steel test cell lid and taking a picture. The lid was replaced and testing continued. The varnish removal process is shown in Figure 5.3.1.2. The temperature of the fluid dropped from the desired
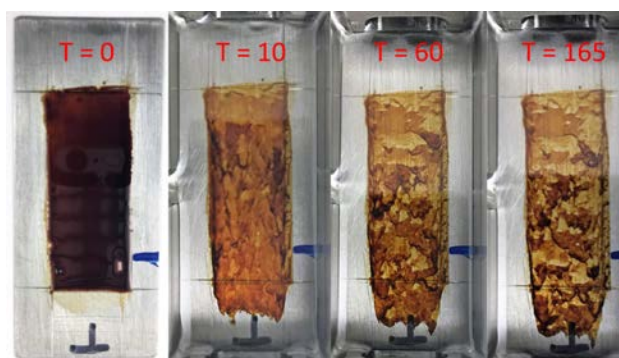
Figure 5.3.1.1: Test 1 showing the movement of varnish on the coupon at 0, 10, 60, and 165 minutes. The test cell lid was removed and the coupon was imaged in the test cell while covered in fluid.

70°C (158°F) to slightly below 62°C (144°F) during the first 10 minutes of testing. At 165 minutes, the test was concluded, providing a direct comparison between test 1 and 2. Test 2 was found to remove 68.6% of the varnish on the coupon. The average removal for tests 1 and 2 was found to be 71.5%.

Figure 5.3.1.2: Test 2 showing the movement of varnish on the coupon at 0, 1, 5, and 165 minutes. The test cell lid was removed and the coupon was imaged in the test cell while covered in fluid.

Test 2 was dried using two methods. First, the coupon was immersed in heptane for 2 minutes and dried using compressed air. The weight was recorded. The coupon was then placed in the oven to dry for 100 minutes at 90°C (194°F). When the weights of the two methods were compared, it was found that there was only a 0.25% difference. It was decided that, at the conclusion of further tests, the coupon would be dried with heptane exclusively and weighed.

5.3.2   Tests 3-5: 70°C, 0.5GPM, Varnish A, Base Fluid A

Tests 3-5 were run to determine the removal of varnish at 0.5GPM, using the same varnish batch as tests 1-2. At this flow rate, a flow velocity of 0.3424m/s was generated in the test cell, providing a Reynolds number of 205. These tests were run for 531 minutes for a total flow of 265.5 gallons and showed an average removal of 23.8%. These coupons were heptane dried and weighed in the same fashion as tests 1-2. From this comparison it was determined that higher flow rates removed more varnish.

5.3.3   Tests 6-7: 70°C, 0.5 and 10GPM, Varnish B, Base Fluid B

The next tests were designed to compare Varnish batch A from tests 1-5 to Varnish Batch B, which was high in metal content. Tests 6-7 used Base Fluid B, which had a density of 7.19lbs/gal and a kinematic viscosity of 46.02cSt at 40°C. Test 6 had a flow rate of 10GPM, a temperature of 70°C and a duration of 360 minutes for a total flow of 3600 gallons. This generated a flow velocity of 6.88m/s and a Reynolds number of 2098. Test 6 removed 4.6% of the varnish on the coupon. Test 7 had a flow rate of 0.5GPM, a temperature of 70°C and a duration of 430 minutes, for a total flow of 215 gallons. This generated a flow velocity of 0.3424m/s and a Reynolds number of 104. Test 7 removed 0.74% of the varnish on the coupon.

Test 6 was compared to Tests 1 and 2. The flow rate, temperature and use of a base fluid were identical providing a direct comparison. Test 6 removed 4.60% of the varnish on the coupon while Tests 1-2 removed an average of 71.5%. This is substantially less varnish (only 6.43% of tests 1-2). Test 7 was compared to Tests 3-5. Again, the flow rate, temperature and use of a base fluid provided a direct comparison. Test 7 removed 0.74% while Test 3-5 removed an average of 23.8% of the varnish on the coupon. This was also substantially less varnish (only 3.09% of tests 3-5). It was apparent that varnish high in metal content (as shown in Section 3.2.1) was harder for the chemicals to remove. The use of high metal content varnish was discontinued to facilitate quicker removal of varnish during testing.

5.3.4   Tests 9, 10, 14 and 17-25: 70°C, 0.5GPM, Varnish C, Base Fluid B and 4 Cleaner Fluids

Tests 9, 10 and 14 attempted to validate that chemical cleaners could indeed outperform base fluids. Chemical cleaner J was tested for 220 minutes (110 gallons of flow) and showed an average of 7.53% varnish removed from the coupon. This was slightly lower than expected, so another series of tests was designed to directly compare three fluids over the same time and flow parameters.

Tests 17-25 consisted of Base Fluid B and two cleaner fluids (K and H). The fluids were run for a total time of 220 minutes (110 gallons of flow). The coupons were removed from the test cell, cleaned with heptane, weighed, photographed and reinstalled into the test cell at 5, 15, 30, 60 and 110 gallons of flow. This provided

insight into the performance of the cleaners, on a rate of removal basis, throughout the duration of the test. This process was repeated for each test. The results for tests 17-25 are shown in Figure 5.3.4.1. While the removal exhibited similar trends with increasing flow, there were large differences in the amount of varnish removed by each fluid from test-to-test. This was unexpected and further investigation was needed to identify the cause of the anomaly.
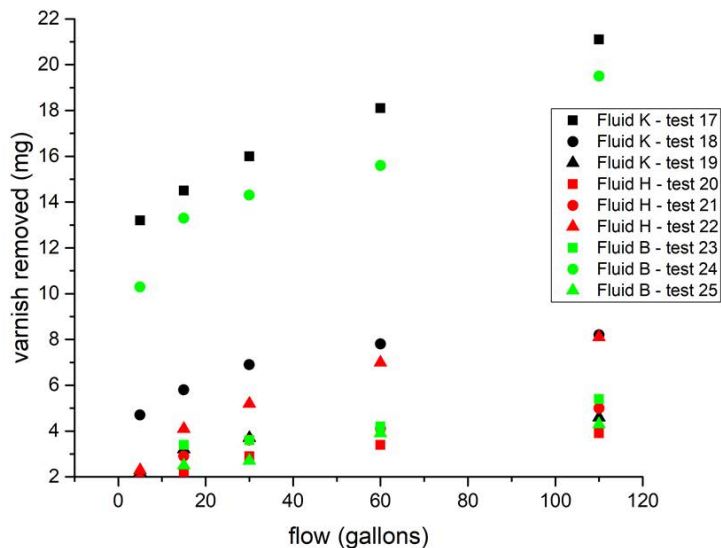
Figure 5.3.4.1: Tests 17-25 where three fluids K, H and Base Fluid B were compared for varnish removal at 5, 15, 30, 60 and 110 gallons of flow with heptane being used to remove oil for weighing.

The observation that heptane might influence the chemistry of the varnish during testing prompted re-testing of the three fluids from Tests 17-25, with no interruption to weigh the coupons during testing, and only recording the final weight of varnish removed after 220 minutes (110 gallons of flow). Tests 26-34, which were not washed with heptane, are shown in comparison to tests 17-25 in Figure 5.3.4.2.

The results showed that, indeed, the heptane had an influence on overall varnish removal from each fluid. Fluid K showed a decrease from a heptane washed 13.3% (11.30mg) removed to an unwashed 10.5% (10.42mg) removed. Fluid H showed an increase from a heptane washed 8.71% (5.67mg) removed to an unwashed 14.5% (10.47mg) removed. Finally, Base Fluid B showed a decrease from a heptane washed 10.5% (9.73mg) removed to an unwashed 7.94% (5.48mg) removed. This shows that the heptane wash affected the fluids in different ways. While heptane
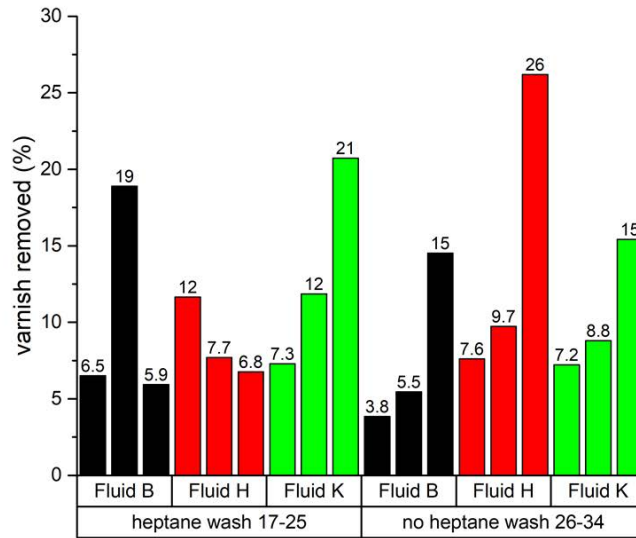
Figure 5.3.4.2: Tests 17-34 where three fluids K, H and Base Fluid B were compared for varnish removal at 110 gallons of flow with and without heptane wash.

increased removal for some fluids, it decreased removal for others. Therefore, using heptane to remove oil, and any weighing which would interrupt testing, was discontinued for all future tests.

It was also observed that the results in Figures 5.3.4.1 and 5.3.4.2 exhibited large differences in removed varnish mass % for the same fluid and the same test procedure. These findings will be addressed in the following sections.

5.3.5 Tests 8, 11-13: 70°C, 10GPM, Varnish C, Base Fluid B and Cleaner Fluid J

Test 8 used Base Fluid B and ran for 150 minutes, giving a total flow of 1500 gallons. The flow velocity was 6.88m/s for a Reynolds number of 2098. Test 8 removed 61.8% of the varnish by weight. Tests 11-13 used the same testing conditions and cleaner Fluid J. Tests 11-13 removed an average of 40.1% of varnish by weight. The observation that Test 8 (base fluid) removed more varnish than tests 11-13 (Fluid J) was unexpected. Further comparison to similar flow rates was desired to ensure this observation was correct. Tests 1-2 used a flow rate of 9GPM and Base Fluid A. The average removal amount of Tests 1-2 was 71.5%. When compared to Test 8, Tests 1-2 removed more varnish with less flow. An explanation for this will be provided in the following sections.

87

To address the discrepancies found in testing at this point, the precision of the test system was improved. The original flow meter, located on the by-pass line, was a variable area flow meter with an accuracy of $\pm$ 2%, and relied on visual methods to read the flow. Because the by-pass line was used to obtain specific flows ranges through the test cell, it was replaced with a very accurate, positive displacement flow meter with an accuracy of $\pm$ 0.25% and digitally displayed flow rate. This new flow meter was installed prior to Test 13.

5.3.6   Test 29a: 90°C, 0.5GPM, Varnish C, Fluid H

There are a few tests that were identified by a number followed by a letter. This convention was to signify a test that reused a coupon from a previous test. Test 29a reused the coupon from test 29 to test the same flow and fluid against higher temperatures. Test 29a compared 0.5GMP at 70°C to the elevated temperature of 90°C at the same flow rate to help find the parameters that would give the best results in the shortest time period. The Reynolds number for a flow of 0.5GPM and a temperature of 90°C is Re = 209. Fluid H was used and tested for 220 minutes (110 gallons total flow) at 0.5GPM and 90°C.

Test 29a showed a varnish removal of 33.1mg (44.6%), which is significantly more than the average of tests 29-31 (5.67mg or 8.71%) or the average of tests 29-31 (10.5mg or 14.5%). This was not unexpected because molecular activity increases with temperature and higher flow rates should remove more material [155].

5.3.7   Tests 26a and 36: 90°C, 10GPM, Varnish C, Fluid H

Tests 26a, which reused the coupon from test 26, and test 36 were run with Cleaner Fluid H and a flow rate of 10GPM at 90°C which generated a Reynolds number of Re = 4214. While this is into the turbulent regime, a direct comparison between 0.5GPM and 10GMP, at 90°C was desired. Test 26a was performed for 11 minutes (110 gallons of total flow) and showed a total removal of 33.6% (29.6mg). Test 36 was performed for 240 minutes (2400 gallons of total flow) and showed a removal of 60.7mg (93.3%).

Tests 26a and 36 were compared to tests 20-22 which were run using Fluid H at 0.5GPM and 70°C. This comparison provided insight into a flow rate *and* temperature change using the same fluid. The average removal from tests 20-22 was 5.67mg (8.71%) while tests 29-31 removed 10.47mg (14.5%). These results are a significant improvement. This substantial difference prompted a series of tests that would use 90°C and a flow rate set to ensure laminar flow.

5.3.8   Tests 32b and 37-63: 90°C, 4.5GPM, Varnish C, 6 Cleaner Fluids

This series of tests was designed to remain in the laminar regime while providing maximum flow rates. Equation 3.3 will allow a velocity to be found that kept

the flow in the laminar regime (Re<2300). From this the flow rate was found to be 5.5GPM. To ensure that the system would be well below the transitional regime, a flow rate of 4.5GPM was chosen. This provided a flow velocity of 3.08m/s and average Reynolds numbers of Re $= 1843 \pm 150$, depending on viscosity. Tests 37-63 were performed with various durations, using Base Fluid B and six different cleaners at 4.5GPM and 90°C. Tests 37-63 were performed three times for each coupon. The average results for Tests 37-63 are shown in Figure 5.3.8.1.
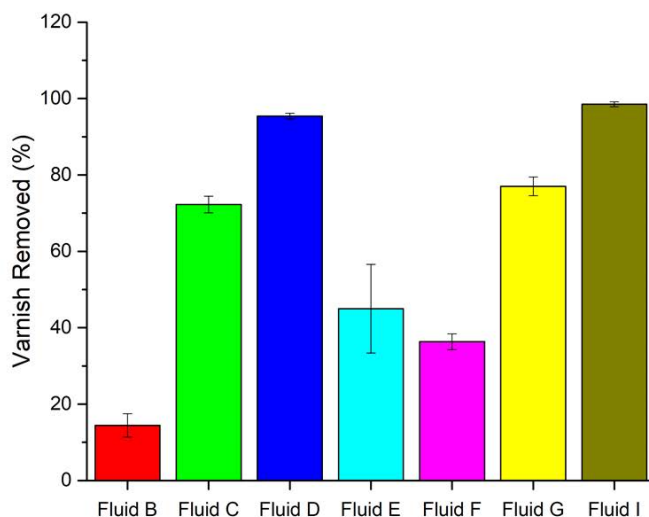
Figure 5.3.8.1: Tests 37-63 where one base fluid and six cleaner fluids were compared at 4.5GPM at 90°C. The large error associated with Fluid E gave cause for concern and prompted further analysis of this anomaly.

This series of tests also includes Test 32b, which reused the coupon from Test 32, and was the first time-lapse photography used in the test system. A vapor polished, polycarbonate lid was machined to provide real time imaging of the varnish removal process. A Go-pro camera was mounted over the test cell lid, at a distance of 5cm, and set to provide images every 10 seconds.

While the durations of Tests 37-63 were not the same, they were all within 60 minutes of each other. The first of the three tests with each cleaner fluid was slightly longer to ensure steady state was captured on the digital recording system. Once steady state was reached, the duration of the next two tests was scaled down to record 15 minutes after steady state was reached. This ensure steady state was achieved for most tests while facilitating multiple tests each day. The large error

associated with Fluid E was unexpected and prompted investigation of cause. This difference will be discussed in later sections.

5.3.9 Start of Test (SOT) vs End of Test (EOT) Trend

Referring back to Figure 5.3.4.1 and Figure 5.3.4.2, there are large differences in varnish removal for the same fluid under the same conditions. When this is analyzed in terms of varnish present at the start of test (SOT) and varnish present at the end of test (EOT), a trend can be found. Figure 5.3.9.1 shows the effect of initial varnish weight (SOT) on the amount of varnish removed from the coupon (EOT).
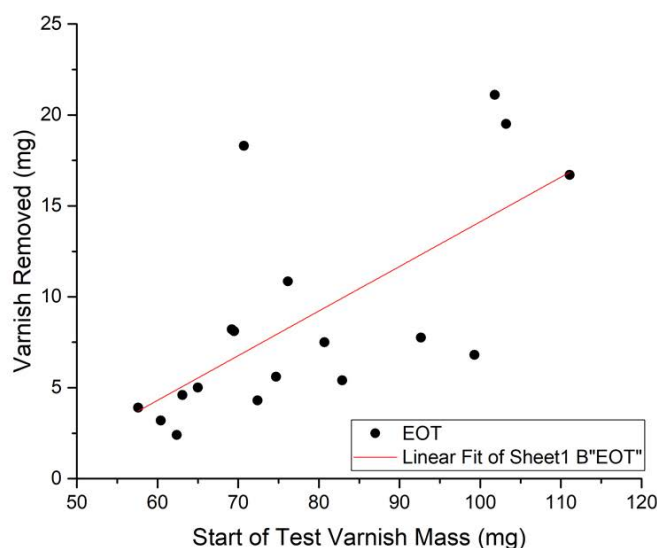
Figure 5.3.9.1: Tests 17-34 showing the trend between the start of test (SOT) mass and the end of test (EOT) mass.

Figure 5.3.9.1 confirms that, if the varnish coupon has more varnish initially, then more varnish will be removed from the coupon. Linear fitting of the SOT-EOT results showed that this relationship was exhibited by all fluids, regardless of testing conditions. Several attempts were made to standardize the SOT-EOT effects observed. This included both linearization of the data to extrapolate varnish removal amounts and finding a relationship that would describe the SOT/EOT dependence. Neither of these methods proved successful.

To limit the effects of EOT/SOT dependence on test results, it was decided to control the SOT weight on the coupon within specific tolerances. Prior to test 37, the average mass of the varnish on the coupon was 87.8mg and the standard

deviation was 12.2mg. The coupons produced for tests 37-78 had an average mass of 67.1mg and a standard deviation of 7.80mg. The smaller standard deviation was better and the ability to control the variation of SOT varnish mass improved as the techniques of applying the varnish to the coupon were further honed. This minimized the effect of SOT mass on results obtained from test 37 onward.

5.4 Varnish Aging
5.4.1 Chemical Changes in Varnish Over Time

After minimizing the effect of variable SOT, as described in the previous section, inconsistent results continued to be observed. Looking back at Figure 5.3.4.1 and Figure 5.3.4.2, it is apparent that, for the same fluid under the same conditions, a range of varnish removal was observed in different tests. It was thought that, after controlling the SOT varnish weight, the results would exhibit similar mass removal. To evaluate this, tests 50-54 were performed with Fluid E using the same test conditions of 4.5 GPM and 90°C. Figure 5.4.1.1 shows there is still variation between the tests, which demonstrated that additional varnish dependence mechanisms needed to be explored.
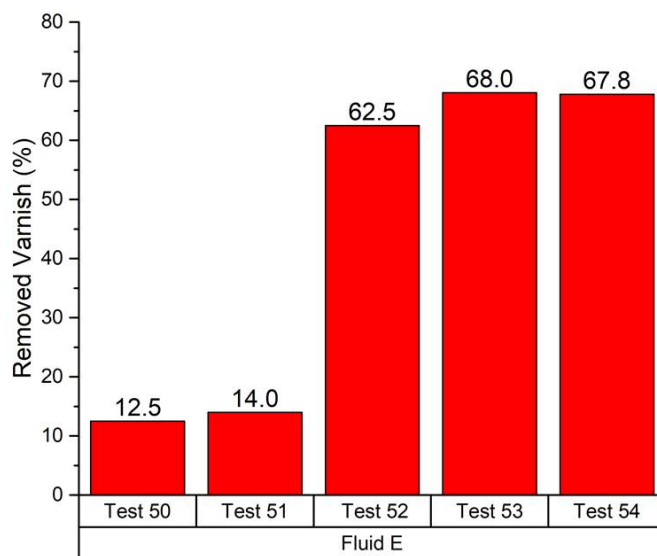
Figure 5.4.1.1: Tests 50-54 showing a large discrepancy of % varnish removed with the same fluid and test parameters

Attempting to eliminate variation in the data, a comparison of all testing parameters for Fluid E (tests 50-4) was done. This included comparing the SOT mass, the total flow over the coupon and the total varnish removed. This comparison

is shown in Table 5.4.1.1. If the mass removal phenomena could be explained by the SOT-EOT trend discussed previously, then Tests 51 and 54 could be compared. The total flow over the coupon was virtually the same (1398 gallons to 1359 gallons respectively) and Test 51, with a much larger SOT, should have removed more varnish. This is not the case since Test 54 removed far more varnish than Test 51. A further comparison was made to eliminate the SOT-EOT trend by comparing Test 50 with Test 53. The flow over the coupon is identical (1809 gallons) while the removal amounts are very different (12.5% to 68.1%). These two comparisons can readily eliminate the SOT-EOT trend as the source of the discrepancy. If total flow over the coupon is considered as the possible reason for the removal differences, then Test 50 and Test 54 can be compared. Test 50 had a total flow of 1809 gallons while Test 54 had only 1359 gallons of total flow. Test 50 should have removed more varnish, but Test 54 removed substantially more. This anomalous behavior is not due to SOT-EOT or total flow over the coupon. Therefore, there must be another explanation for the observations.

test number	% removed	total time	total flow	SOT (mg)	mg removed
test 50	12.50	402	1809	64.00	8.00
test 51	14.00	311	1398	80.00	11.20
test 52	62.50	364	1638	57.60	36.00
test 53	68.05	402	1809	67.60	46.00
test 54	67.80	302	1359	64.90	44.00

Table 5.4.1.1: Results for tests 50-54, where a comparison is made between all testing parameters and mass removed to explain the difference in mass removed between tests. Neither the SOT-EOT trend or total flow over the coupon can explain the difference.

After eliminating SOT-EOT dependence, as well as any flow differences, other potential factors that might affect the removal of vanish were discussed. The varnish was produced in fairly large quantities and kept from further light, heat and atmospheric oxygen by storing the varnish in sealed containers in a lab. However, this did not eliminate oxidation of hydrocarbons [104]. It first proposed that the oxidation continued after the varnish was applied to the coupon due to bulk oxidation processes and further exposure to oxygen in the atmosphere. This process could continue over time such that the age of the varnish may affect results. Table 5.4.1.2 shows tests 50-54. Less varnish is removed for the older coupons, suggesting that physiochemical varnish changes were taking place while the coupons were stored.

Based on this, it was decided that tests should be performed as soon as possible after the varnish was applied to the coupons. Once the varnish coupons arrived at the lab, they were covered with a neutral base oil to prevent further exposure to the atmosphere and minimize any resulting oxidation that might occur

Test number	% Removed	Age of varnish (days)
test 52	62.50	52
test 53	68.05	53
test 54	67.80	63
test 50	12.50	128
test 51	14.00	132

Table 5.4.1.2: Results for tests 50-54 showing the age of Varnish C during testing

to the varnish on the coupon. The time between application of the varnish on the coupon and submergence in base oil was recorded, as well as the time between being covered in base oil and the time of testing.

5.4.2 Tests 64-78: 90°C, 4.5GPM, Varnish C, Base Fluid B and 6 Cleaner Fluids

To test the theory of varnish change over time, tests 64-78 recorded the date of varnish application, shipping time, as well as the date the varnish was covered in base oil. Also, two tests (64-65) were performed as soon as the new varnish coupons arrived in the lab using Base Fluid B and followed immediately by testing of the six cleaner fluids (66-77). The final test (78) was run using the same base oil, Base Fluid B, with a coupon that had been covered in base oil for the duration of the other six cleaner fluid tests. Tests 64-78 included the same base oil and cleaner fluids as Tests 37-63, but the time was set at 120 minutes, giving a total of 540 gallons of flow over the coupon. This choice was made because steady state was already known for this series of fluids. Tests 37-63 were performed three times for each fluid while tests 64-78 were performed twice. The results for tests 37-63 and the results for tests 64-78 are shown together in Figure 5.4.2.1.

The results in Figure 5.4.2.1 show definitively that physiochemical changes to the varnish are taking place over time. Base Fluid B was used as a reference for the aging process and demonstrated that the varnish was harder to remove as time progressed (removed less mass). However, the cleaner fluids exhibited a range of abilities in removing aged varnish, depending on the chemical composition of the fluid. The aging process had very little effect for Fluid D, while Fluids C, G and I removed more mass as the varnish aged. Finally, Fluids E and F follow the trend of Base Fluid B where less varnish is removed from older coupons. To quantify the effect of varnish aging, the tests with Base Fluid B were analyzed. The results of the initial and the final Base Fluid tests are shown in Table 5.4.2.1.

The large difference between Tests 64-5 and Test 78 seen in Table 5.4.2.1 is indicative of varnish change over time. This is an aspect of varnish properties that had not previously been explored. Therefore, further testing of varnish removal using only base oil was performed to provide insight into the rate of varnish change.
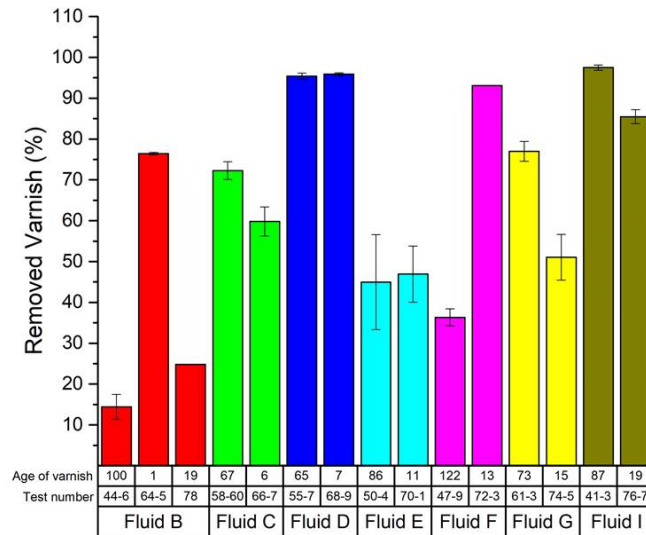
Figure 5.4.2.1: Base Fluid B and six cleaner fluids compared at 4.5 GPM at 90°C over tests 37-63 and 64-78. The bottom rows show the varnish age at the time of testing along with the test number and fluid used.

test number	% removed	days exposed to air	days covered in base oil
test 64	76.0	6	1
test 65	76.9	6	1
test 78	24.8	6	19

Table 5.4.2.1: Results for tests 64, 65 and 78, using the same Base Fluid B and testing conditions, showing the varnish change over time.

5.4.3 Tests 82-93: 90°C, 4.5GPM, Varnish D at Various Preparation Conditions, Base Fluid B

To try to minimize the effects of varnish aging, several steps were taken. First: a new Base Fluid B was selected to be used exclusively during this series of tests. Second: in this series of tests, a new batch of varnish was used with the designation Varnish D. Third: the average mass on the coupon was controlled to help to minimize any SOT-EOT trends. The average mass of each coupon was 77.3mg and the standard deviation was 6.87mg, which provided an improvement over previous tests. Fourth: several varnish preparation conditions were tested.

For tests 82-93, which were designed to identify the varnish preparation conditions that minimize the aging phenomena, three different conditions were used. Furthermore, some of the coupons were covered in a neutral base fluid while others

were exposed to the air. The four preparation conditions will be called Preparation 1 Air (P1A), Preparation 1 Oil (P1O), Preparation 2 Oil (P2O) and Preparation 3 Oil (P3O). The preparations differed by the amount of time the varnish coupon spent in the oven and the temperature of the oven. A full description of the preparation conditions is given in Table 3.2.1.2.

P1A had three coupons exposed to the atmosphere while P1O had eleven coupons covered in base oil the day after varnish application on the coupon. P2O had three coupons covered in base oil (again a day after application) and P3O had 5 coupons (1 day after application) covered in base oil. The tests were designed to identify whether covering the varnish in base oil, as compared to exposing the coupon to air, would limit the aging phenomena. The differing preparation conditions were used to identify a varnish that would minimize the effect of varnish aging on test results.

The tests were performed on one coupon from each preparation category, and began the day after the samples arrived in the testing facility. The same tests were then performed again 7 and 14 days later. The results of tests 82-93 are shown in Figure 5.4.3.1.
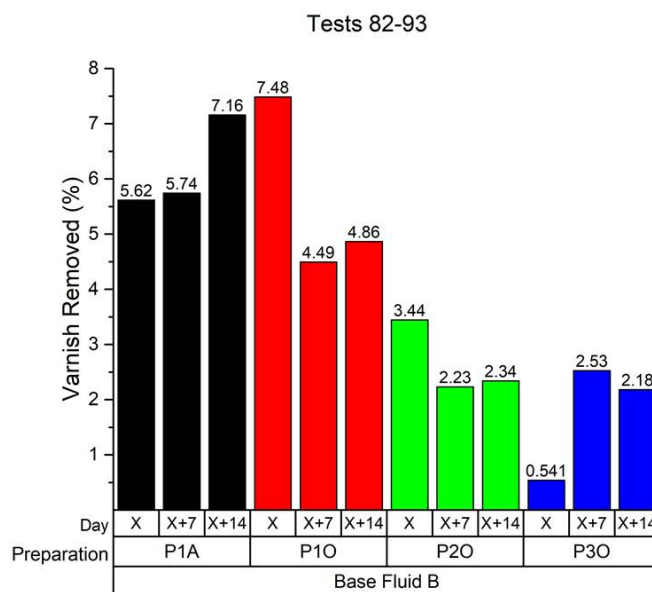
Figure 5.4.3.1: Base Fluid B tested with 4 different preparation conditions at 4.5 GPM, 90°C and 120 minutes. The bottom rows show the varnish age at the time of testing along with the preparation condition.

Figure 5.4.3.1 demonstrates that, not only the age of the varnish, but the conditions it was prepared under, had an effect on the removal amounts. The ideal

95

varnish, including preparation conditions and aging characteristics, would have no aging pattern. However, each preparation condition exhibits differences in varnish removal over time for the same varnish batch. Therefore, the ideal preparation condition minimized the aging effects and consistently increased or decreased over time. This eliminated preparation conditions P1O, P2O and P3O due to their inability to maintain a consistent increase or decrease over time. For example, P1O exhibited a large decrease of varnish removal over the first seven days and then a small increase, while P3O exhibited a large increase and then a small decrease.

The choice was made to use preparation conditions P1A because of the minimal change observed over the first seven days of testing. Furthermore, P1A did not need to be covered in base fluid or stored in sealed containers to prevent leaking. The next step was to ascertain the rate of increase of varnish removed over time (quantified by the slope, m) for P1A between the first and subsequent tests in Figure 5.4.3.1. The slope would be compared to later tests to ensure that the varnish aging phenomena falls within the values found from Figure 5.4.3.1. The slope for the first seven days of P1A (X→X+7) it was found to be 0.018%/day. The slope for the next seven days of P1A (X+7→X+14) was found to be 0.202%/day. Finally, the slope (m) for the entire test period of P1A (X→X+14) was found to be 0.110%/day. These values will be used for comparison to future test results that exhibit an increase in varnish removed with coupon age.

5.5 Final Testing of 8 Fluids

All final tests were performed using Varnish D, testing conditions P1A, a flow rate of 4.5GPM, a testing temperature of 90°C and a duration of 120 minutes. The final tests were also conducted within 5 days of receiving the coupons in the lab. Flow through the test cell was kept within ±0.01GPM throughout the duration of each test and temperature was maintained at an average temperature of 90±3°C. Each test was preceded by running the system with new base fluid for 10 minutes to ensure that all components in the test system were flushed. Each test was brought up to operating temperature prior to testing and the time to install the coupon into the test cell was kept below 1 minute. Fluid was allowed to flow across each coupon for ten seconds at the beginning of each test to ensure any air was purged from the lines.

5.5.1 Mass Removal (%)

The first metric found was the mass loss percent. Mass loss percent is a characterization that gives the overall performance of the fluid and was used to identify good candidate cleaners. The results for the eight fluids tested are shown in Figure 5.5.1.1. It is observed that two of the fluids (Fluid M and O) removed significantly more varnish than the other six fluids. It is also observed that Fluids Q and S removed more varnish than control Fluid R and cleaner Fluids L, N and P.

Therefore, Fluids Q and S might be good candidates for long term use in a system, depending on the remaining characterizations.
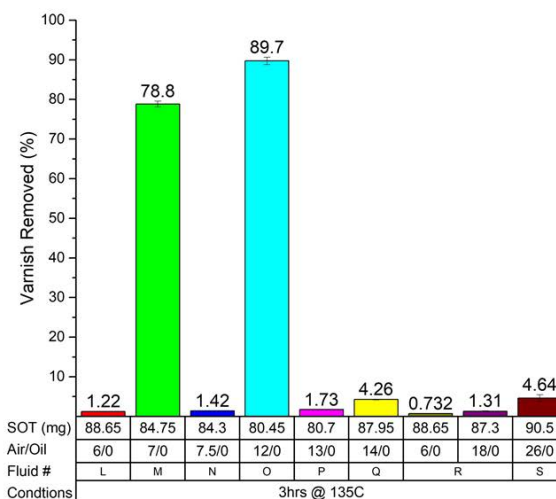
Figure 5.5.1.1: Mass removal results for base Fluid R and 7 cleaner fluids using Varnish D and preparation conditions P1A.

5.5.2 Trends and Aging

Control of both the SOT/EOT trend and varnish aging is imperative to ensure accurate and reliable test results. To minimize the effect of SOT/EOT, the weights of the coupons were kept within strict limits. The average SOT weight of the final batch of coupons was 86.6mg and the deviation was reduced to only 4.72mg. This is a drastic improvement over the prior measurements given in Section 5.3.9.

After the mass removal data was found (Figure 5.5.1.1) the results needed to be analyzed to determine if varnish aging had an effect. Fluid R (a base fluid) was tested at the beginning and end of this test series to track any varnish aging that might have occurred. Fluid R, shown in Figure 5.5.1.1, was tested with varnish aged for 6 days and then again at 18 days. The slope (m) for this time period (twelve days) is found to be 0.048%/day. Table 5.5.2.1 summarizes the comparison between the values from the previous varnish aging tests (Figure 5.4.3.1) and the current series of tests.

Table 5.5.2.1 shows that the slope of Fluid R fits nicely between the slopes of Fluid B. This indicates that the aging process falls in the range expected from the

Fluid	X→X+7	X→X+12	X→X+14
Fluid B	0.018	N/A	0.110
Fluid R	N/A	0.048	N/A

Table 5.5.2.1: Varnish aging for Fluid B and R using preparation conditions P1A. Values shown in %/day.

tests shown in Figure 5.4.3.1. This allows further characterization of the fluids with confidence that the varnish aging phenomena will have little affect on the results.

5.5.3   Time-Lapse Photographic Results

Following the approach outlined in Section 4.3, the results from the time-lapse photography need to be compared to the actual mass removed. This comparison is shown in Figure 5.5.3.1.

The varnish removal calculated from K_{norm} and from mass measurements were in good agreement, with the maximum standard error being less than 1.5%. This then enabled the next step of the process outlined in Section 4.3. The average K_{norm} was multiplied by the average SOT to provide a plot of mass removal vs. time. The plots of $K_{norm}*$SOT and the 1st derivative of $K_{norm}*$SOT with respect to time for each fluid are shown in Figure 5.5.3.2. These plots are then used to calculate the remaining test metrics.

5.5.4   Fluid Characterization Using Primary Metrics

The primary test metrics include the maximum rate of varnish removal (mg/min), the time of maximum varnish removal rate (min), the actual amount of varnish removed (%) and the time when steady state varnish removal is reached. Each of these primary metrics was discussed in detail in Section 4.3. These metrics are shown in Figure 5.5.4.1. Fluids M and O are shown to remove most of the varnish on the coupon, although the removal process is very different between the two fluids.

Looking at the top left panel in Figure 5.5.4.1, we see that Fluid O displays a much higher maximum removal rate than Fluid M (2.40 vs 1.05 mg/min respectively). This indicates that Fluid O is much more aggressive at removing varnish than Fluid M. The top right panel of Figure 5.5.4.1 corroborates this finding by showing that the maximum removal rate time occurred much sooner for Fluid O than for Fluid M (25.8 vs 120 minutes respectively). These two findings indicate that Fluid O not only removed varnish at a quicker rate but also reached this rate much sooner. This supports the fact that Fluid O is a much more aggressive cleaner than Fluid M, even though both fluids removed most of the varnish on the coupon during the test.
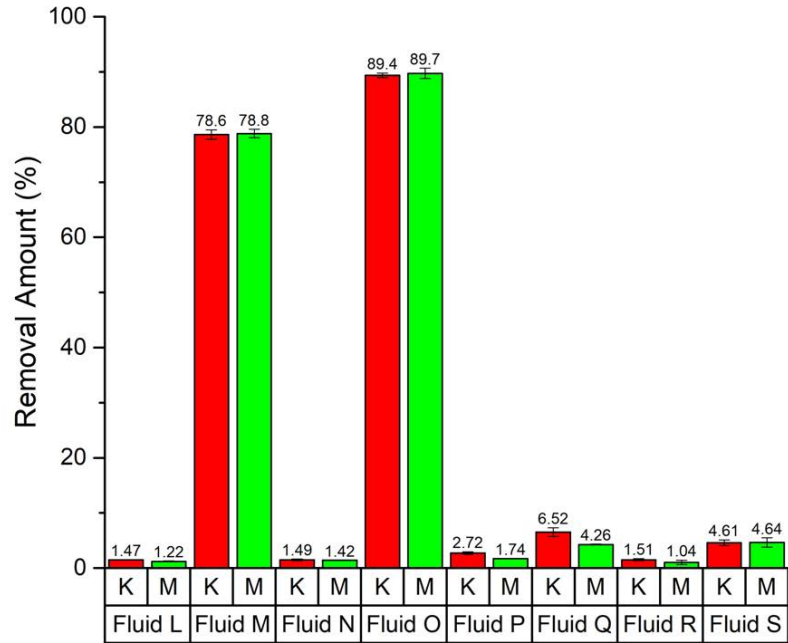
Figure 5.5.3.1: Removal amounts obtained from video processing and actual mass loss. The good correlation between these two measurements enables use of the normalized K values to find the maximum rate of removal, time of maximum rate of removal and steady state removal.

Both fluids (M and O) might be under consideration for removing large amounts of varnish in short time durations. Correctly sizing the pore size and surface area of the filter will be crucial for maximum performance with high removal fluids. These fluids will be discussed further in the context of the secondary and tertiary metrics in later sections.

Of the six fluids (Fluids L, N, P, Q, R and S) that exhibited less varnish removal, it is apparent from Figure 5.5.3.2 that these fluids were at steady state throughout test according to our definition of steady state. While the plot shown in Figure 5.5.4.1 has values for maximum removal rate, they were obtained from the maximum of the 1st derivative of the varnish removed. This means that any non-linearity in the data might give falsely inflated values.

To address this problem, Fluids L, N, P, Q, R and S were reevaluated in terms of average varnish removal rates. The two rates that were compared were the actual average mass removal rate (mass removed/duration) and average K value removal
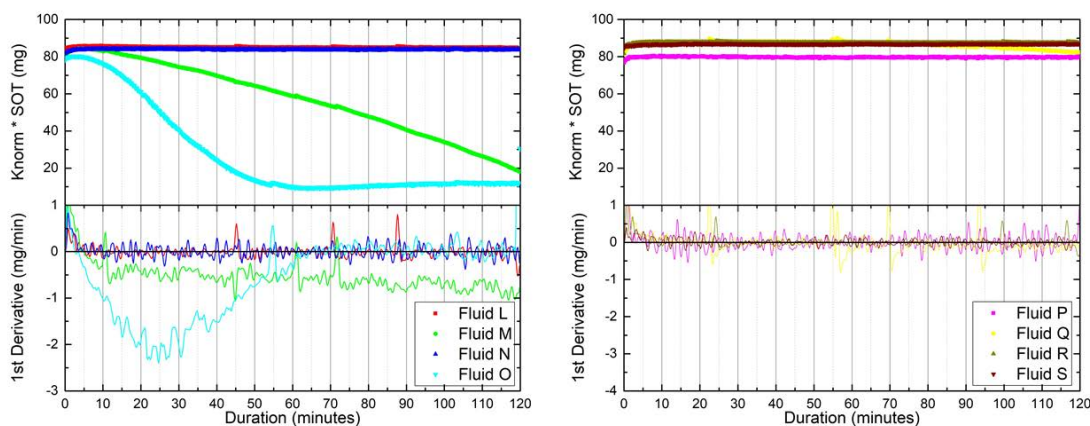
Figure 5.5.3.2: Upper panels: Normalized K value multiplied by SOT for Fluids L, M, N, O, P, Q, R and S. Lower panels: 1st derivative of data in upper panel with respect to time.

rate $((K_{norm})_{min}/\text{duration})$. These two rates should be very similar since the change in mass and the change in K value from the start and end of the test were found to be comparable. The results for mass removal rate and K value removal rate are shown in Figure 5.5.4.2.

The removal rates in Figure 5.5.4.2 are very consistent between the two methods, with a maximum error of only 0.82%. This provides another technique of analyzing the varnish removal process for cleaners that remove less varnish. This process will be incorporated for any fluid that exhibits steady state removal conditions throughout the duration of testing. To quantify the removal process for these cleaners, we will use the averaged values in Figure 5.5.4.3 and mass removed.

Figure 5.5.4.3 shows the metrics considered for the low removal chemical cleaners. It is apparent now that Fluids Q and S exhibit varnish removal capabilities and might be considered for further analysis. Fluid R is known to be base fluid and exhibits the lowest removal of the six fluids shown in Figure 5.5.4.3, as expected. The remaining fluids (L, N and P) do not exhibit any substantial varnish removal potential. For systems that might use chemical cleaners for extended durations, cleaner Fluids such as Q and R might be considered. These fluids will be discussed later in terms of the secondary and tertiary metrics.

100
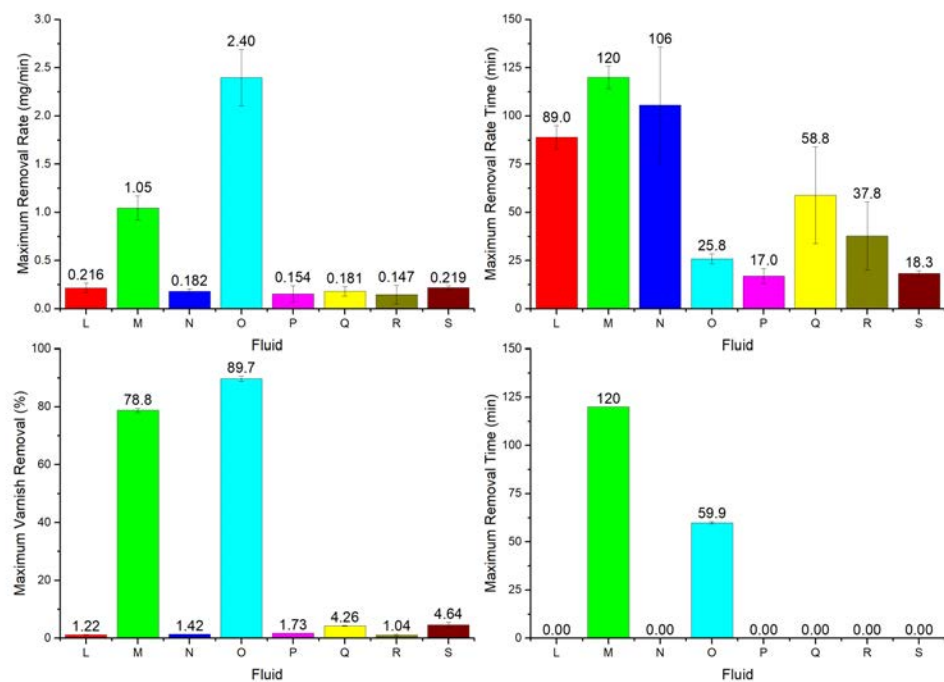
Figure 5.5.4.1: Left upper: Maximum removal rates in mg/min. Right upper: Maximum removal rate time in min. Left lower: Maximum varnish removed in %. Right lower: Maximum removal time (or steady state) in min.

5.5.5 Filter

The filter provides valuable information about the varnish removal process, and showed that the fluids removed varnish from the coupon in different ways. Two images of the filter paper were taken for each test. One image was taken at standard magnification while another was taken at 10x magnification. The filter paper was marked with a 1in^2 area located in the middle. The 10x magnification images includes about 34% of the 1in^2 area and were taken in the upper right corner of the square. The permanent marker was still visible on the magnified area on most filter papers. The results for Fluids L, M, N and O are shown in Figure 5.5.5.1 while the results for Fluids P, Q, R and S are shown in Figure 5.5.5.2.

Figure 5.5.5.1 shows that Fluid L, which only removed 1.22% of the varnish on the coupon, displays very little varnish in the filter. The color has changed only slightly in some parts of the originally white filter. The inset shows no varnish particles, indicating that the varnish particles removed were much smaller than 5
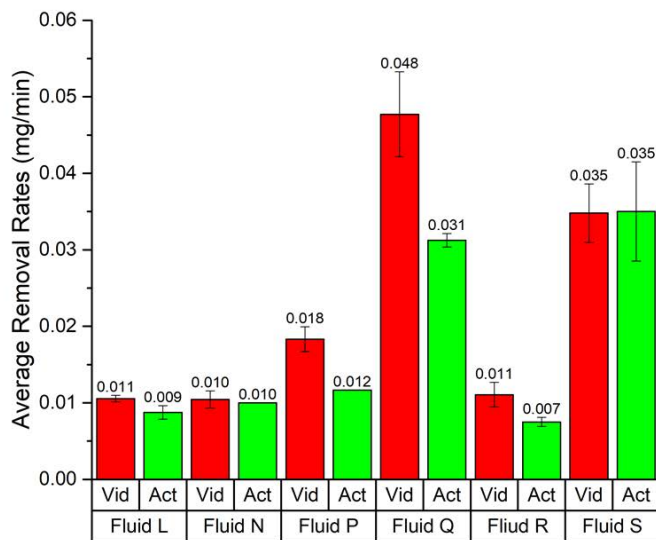
Figure 5.5.4.2: K$_{norm}$ average removal rate compared to actual mass average removal rate. Average removal rates shown for Fluids L, M, N, O, P, Q, R and S.

micron. Fluid M, which removed 78.7% of the varnish on the coupon, turned the filter a light shade of brown when viewed at standard magnification and removed most of the permanent marker. When viewed at 10x magnification, the filter looked almost white again with no visible varnish present. This indicated that most of the removed varnish was smaller than 5 micron in size but there was enough mass to darken the filter. Fluid N, which removed 1.42% of the varnish on the coupon, displayed a slight brown shade while showing no visible varnish in the inset, indicating that the removed varnish was smaller than 5 micron. Fluid O, which removed 89.7% of the varnish on the coupon, displayed sporadic, light brown, darkening of the filter with spherical varnish particles present in the filter. The inset shows varnish particles trapped in the filter. Fluids P and R showed very little varnish or color change, in either the standard or magnified images. Fluid Q, which removed 4.26% of the varnish on the coupon, displayed an abundance of removed varnish larger than 5 micron in both the standard and magnified images. The varnish was removed in circular and disk-shaped pieces over a range of sizes.

The filter data suggests that Fluid M removed varnish by dissolving it into very small, suspendible particles. That would indicate the need for a filter smaller than 5 micron to catch the removed varnish circulating in the system. Fluids L, N, P and R removed so little varnish that filter sizing is unlikely to be the main concern
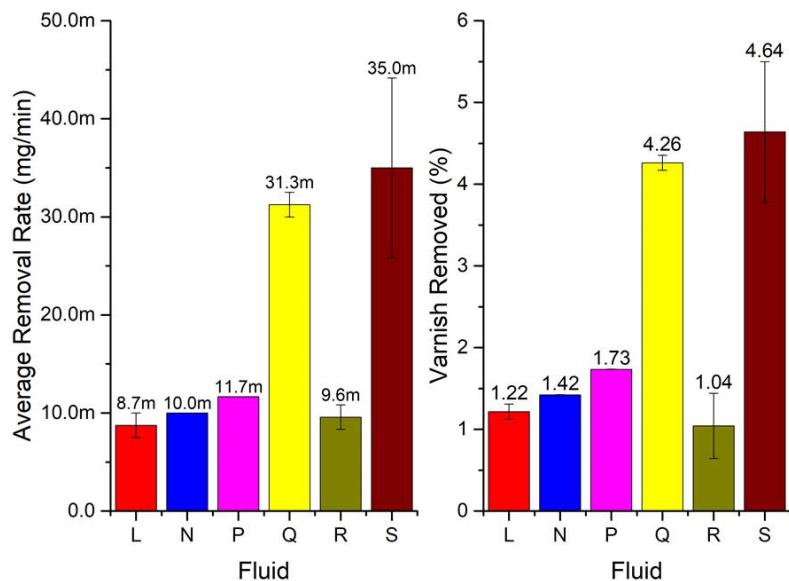
Figure 5.5.4.3: Left: average removal rates. Right: mass percent removed. Results shown for Fluids L, M, N, O, P, Q, R and S.

with these particular cleaners. Fluid Q, which removed 4.26% of the varnish on the coupon, removed varnish in particles larger than 5 micron, indicating that this filter size is appropriate for use. Finally, Fluid S, which removed 4.64% of the varnish on the coupon, had very little varnish trapped in the 5 micron filter, indicating that a smaller filter pore sized is needed to remove suspended varnish in the system.

The filter has proved invaluable in characterizing not only the size of the removed particles but sizing the appropriate filter to the cleaner. The filter indicates the mechanism of removal by inspecting the size and shape of the removed varnish. The varnish has two methods of removal: mass diffusion and convective diffusion. Both of these methods are discussed in detail in Chapter 6. The process of mass diffusion softens the varnish until discrete particles are suspended in the chemical cleaner. This process is defined by Fick's first law. The process of convective diffusion creates shear forces on the surface of the varnish. This pulls varnish off in a mechanical way and typically removes the varnish in larger pieces. When combined, convective mass-diffusion can remove varnish in differently sized and shaped pieces as discussed previously. In conjunction with the primary metrics, the filter allows further characterization of the removal process.
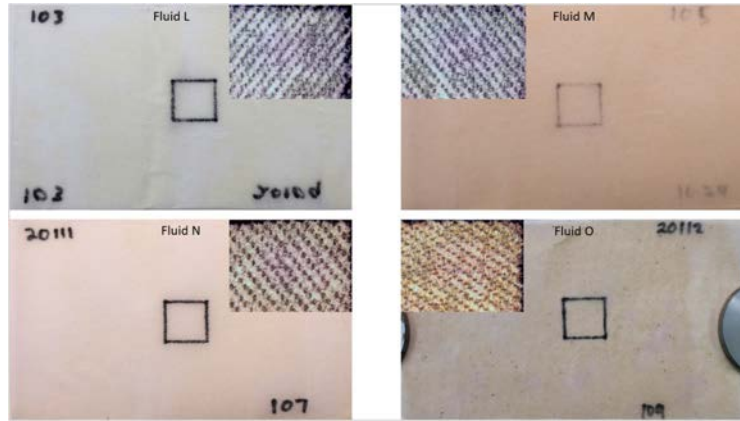
Figure 5.5.5.1: Filter images for Fluids L, M, N, and O shown at standard magnification and at 10x magnification in the insets.
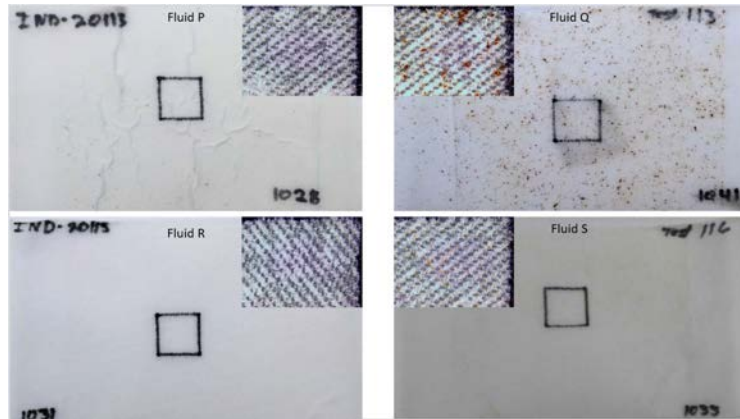
Figure 5.5.5.2: Filter images for Fluids P, Q, R and S shown at standard magnification and at 10x magnification in the insets.

5.5.6 Viscosity

The viscosity of a fluid is highly dependent on temperature and pressure, as discussed in Section 1.2. Moreover, viscosity can also undergo temporary and/or permanent viscosity changes when exposed to high shear rates and shear stresses [156]. Most hydraulic and lubricating fluids are composed of a base fluid and additive package. Base fluids have molecular chains that are around 30-40 carbons long and are very shear stable because the molecules are not prone to dissociation or breakage by mechanical forces. However, additives can have substantially longer, and more complex, chains that are easier to break and can cause viscosity changes [80].

The chemical cleaners used in this work have unknown chemical compositions, so inferences about their viscometric performance are purely speculative. However,

polymer chains can range up to thousands of molecules in length and do experience temporary and/or permanent viscosity loss under conditions of high shear rate and stress. We would expect to see very little viscosity loss (if any) in the base fluid (Fluid R) and possible viscosity loss in the other fluids depending on chemical makeup. The main idea in tracking viscosities was to ensure that the cleaner fluids would be in the range of typical turbine lubricating oils, which can range from 32-68 cSt [157], both pre and post testing. The viscosities of Fluids L-R were measured before testing (new fluid) and then again after each test. The results are shown in Figure 5.5.6.1.
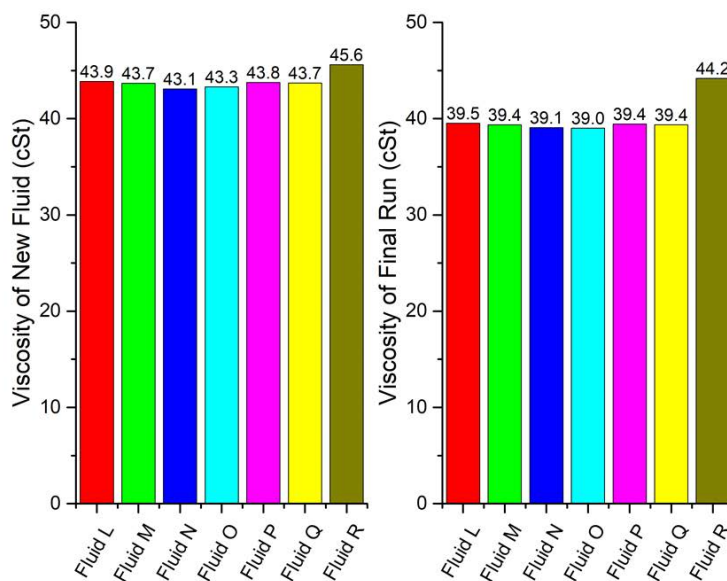
Figure 5.5.6.1: Left: viscosity of new fluids. Right: viscosity after 2 tests.

Figure 5.5.6.1 indeed shows viscosity decreases for all of the fluids except Fluid R (base fluid). The viscosity results indicate that, while there may be some permanent viscosity loss, the post-test viscosity is still acceptable (i.e. between 32-68 cSt) for each fluid tested [157]. However, typical rheometric measurements are only accurate to about $\pm 5\%$ [63]. When finding the viscosity of fluids, using a rotational rheometer, it is important to ensure that the results are accurate. The rheometer used in this work was calibrated using the Cannon viscosity reference standard N44 which is known to have a viscosity of 42.58 cSt at 40°C. The rheometer used in this work showed less a 2% error when checked against this standard. This provides confidence in the viscosity values reported in this work.

5.5.7 Optically Detected Particle Counts

Optically detected particle counts provided further insight into the composition of the cleaner fluids. The particle counts recorded in this work were all performed at 25°C with a Beckman-Coulter, HI-ROC optical counter. Each test used 1 liter of fluid which took six minutes to completely flow through the particle counter giving a total of 35 readings for each ISO code. The particle counter has an accuracy of ±0.5 ISO code and a minimum resolution, at a flow rate of 0.278mL/s, of an ISO code of 9. Figure 5.5.7.1 shows the new and final particle counts for fluids.
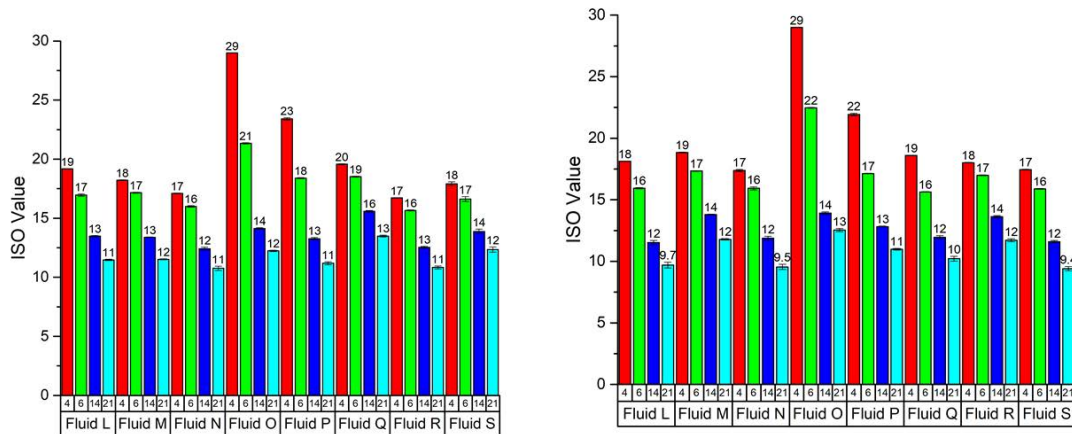
Figure 5.5.7.1: Left: particle counts of new fluids. Right: particle counts of the fluids after 2 tests.

Two fluids (Fluid O and P) exhibited high levels of 4 and 6 micron particle counts. In fact, Fluid O had 4 micron particle counts that were higher than ISO 28 because the optical particle counter used in this work was only capable of recording particle counts up to ISO 28. This information can be helpful for correctly sizing the filter to each cleaner fluid and will include identifying the size of the cleaner chemicals and properly sizing the filter to remove varnish. Therefore, it was desired to compare the mass removal amounts to the particle counts and this comparison is shown in Table 5.5.7.1.

Although the accuracy of the particle counter is ±0.5 ISO code the results in Table 5.5.7.1 show a correlation between mass removed and increasing particle counts. Moreover, it also relates the size of the removed varnish particles by showing an increase in specific ranges. One would expect the particle counts to decrease over

Fluid	Varnish Removed (%)	ISO 4	ISO 6	ISO 14	ISO 21
L	1.22	-1.1	-1.1	-2.0	-1.8
M	78.8	<1	<1	<1	<1
N	1.42	<1	<1	<1	-1.3
O	98.7	N/A	<1	<1	<1
P	1.73	-1.5	-1.3	<1	<1
Q	4.26	-1.0	-1.9	-3.6	-3.5
R	1.04	+1.1	<1	-1.0	-1.7
S	4.64	<1	<1	-1.7	-2.1

Table 5.5.7.1: Fluid mass removal shown with each ISO count recorded. A negative value is a decrease of ISO count while a positive value is an increase of ISO count. Fluids where high mass was removed showed an increase of ISO counts while fluids that removed low amounts show a decrease. The filter used in this work was 5 micron polypropylene paper. Fluid O had particle counts higher than 29 for ISO 4 which could not be recorded by the counter used in this work.

time using a 5 micron filter size but this was not always the case. Fluid M, which removed 78.8%, showed an increase of particle counts over all ISO codes recorded. This would suggest a range of varnish particles removed. Figure 5.5.5.1 would seem to refute this by showing no trapped varnish in the inset of Fluid M. It is possible that the varnish agglomerates again due to temperature decrease (when the fluid cools and is tested in the particle counter) or other mechanisms.

Refereing again to Figure 5.5.5.1 it is apparent that no large varnish parities are trapped in the inset, for Fluid N, but the filter is a light brownish color indicating that particles smaller than 4 micron were removed. This might explain the increase in ISO 4 counts of Fluid N. Fluid Q, which removed 4.64%, shows a substantial decrease of particle counts over the range of ISO codes. Looking at Figure 5.5.5.2, it is apparent that this fluid removed varnish in larger pieces and that the filter trapped most of this varnish. This explains why Fluid Q has a decrease of particle count data while other fluids did not. This particle count data, when used in conjunction with filter imaging, can provide a range of insights into the varnish removal process.

5.5.8   Fluid Odor, De-aeration and Seal/O-ring Swelling

Fluid odor isn't a metric of concern for a mechanical system, but for the people using these chemicals, it is vitally important. Odor and chemical volatility typically go hand in hand. Characterizing each fluid for odor included ranking the strength and unpleasantness of the smell at both ambient (23°C) and operating temperature (90°C). The ranking for each category ranged from 1-5, with 1 identifying

a strength or smell that was not strong or unpleasant and 5 identifying a smell that was strong or unpleasant.

The ability of a fluid to resist foaming is an important property for lubricating fluids. Foam can prevent the lubricating oil from coming into contact with the surfaces it's trying to protect as well as cause pump cavitation, increased oil temperature due to implosion and a host of other problems. In this study, foam formed due to air being introduced to the test cell chamber during installation of the coupon. This air would be purged during the first 10 seconds of operation after insertion of the coupon and would foam the fluid in the reservoir. The amount of foam varied depending on the chemical cleaner. Foam performance is typically characterized according to ASTM D892 [158]. However, in this study foam was tracked by observation of the foam in the reservoir using a scale from 1-5, with 1 identifying a fluid with very little foam and 5 identifying a fluid with substantial foam. The results for all fluids are shown in Table 5.5.8.1.

Fluid	23°C Smell	23°C Strength	90°C Smell	90°C Strength	Foam
Fluid L	1	1	2	2	1
Fluid M	4	4	5	5	2
Fluid N	1	1	2	2	3
Fluid O	1	1	2	2	4
Fluid P	1	1	2	2	3
Fluid Q	1	2	2	2	2
Fluid R	1	1	1	1	1
Fluid S	2	1	2	1	2

Table 5.5.8.1: Identifying the fluid odor (as unpleasantness), strength (in permeation) and foam tendency (for the ability to de-aerate) for Fluid D and E on a scale from 1-5. 1 is a low value for strength, smell and foam, while 5 is a high value for strength, smell and foam.

Chemicals can have adverse effects on rubber based components and some of the early fluids tested caused slight swelling of the o-ring on the test cell lid. Because machines are composed of rotating and sealed components it will be important to track any swelling or shrinking of seals to identify cleaners that cause these adverse effects. The final eight fluids tested exhibited no swelling or shrinking of seals and o-rings.

5.6   Summary

This work developed processes to characterize chemical cleaner performance in removing varnish from mechanical systems. Primary metrics included mass removed (%), maximum mass removal rate (mg/min), maximum mass removal rate

time (min), average mass removal rate (mg/min) and steady state removal conditions (min). Secondary metrics included filter inspection, particle count data and viscosity. Tertiary metrics include fluid odor and foam performance.

The current test metrics are combined to form comprehensive fluid characterizations. The combination of mass removal and mass rate removal provides definitive information about the capabilities of the chemical cleaner to remove varnish. Mass and rate of removal succinctly characterize the *aggressiveness* of the chemical cleaner by providing real time data of the mass removal process. The filter and particle count data further characterize the size of the removed varnish which provides valuable information to help properly size the filter. Viscosity data tracks the performance of the fluid on a molecular level while tracking foam performance will ensure proper steps are taken to ensure air entrainment is avoided. Finally, odor is recorded to help end users choose a chemical cleaner that not only removes varnish, but do not require the use of a breathing apparatus. The complete overview of the testing metrics are shown for the final eight fluids in Figure 5.6.0.1.

Metric\Fluid	L	M	N	O	P	Q	R	S
Varnish Removed (%)	1.22	78.8	1.42	89.7	1.73	4.26	0.732	4.64
Max Removal Rate (mg/min)	N/A	1.0500	N/A	2.4000	N/A	N/A	N/A	N/A
Average Removal Rate (mg/min)	0.0087	0.5510	0.0100	06030	0.0117	0.0313	0.0096	0.3500
Max Removal Rate Time (min)	N/A	>120	N/A	25.8	N/A	N/A	N/A	N/A
Steady State (min)	N/A	>120	N/A	60	N/A	N/A	N/A	N/A
Filter Particle Size (ps) micron	ps < 5	ps < 5	ps < 5	ps > 5	ps < 5	ps > 5	ps < 5	ps > 5
Viscosity Change (cSt)	-4.5	-4.3	-4.0	-4.3	-4.4	-4.3	-1.4	N/A
Particle Counts (4, 6, 14, 21)	19, 17, 13, 11	18, 17, 13, 12	17, 16, 12, 11	>29, 21, 14, 12	23, 18, 13, 11	20, 19, 16, 13	17, 16, 13, 11	18, 17, 14, 12
Smell/Strength	1.5	4.5	1.5	1.5	1.5	1.75	1	1.5
Foam	1	2	3	4	3	2	1	2

Figure 5.6.0.1: Complete overview of testing metrics for each of the eight fluids tested.

From Figure 5.6.0.1 one can begin to evaluate each fluid based on individual performance. In the first row we can compare the varnish removed (in %) for each fluid and then move down the rows to compare maximum removal rate, average removal rate, maximum removal rate time, steady state removal, generated particle size, viscosity change, initial optical particle counts, smell and strength and foam

production. For the end user, each of these categories will provide significant insight into the performance of the fluid as well as expected filter requirement and working environment.

Furthermore, the characterization of varnish aging will allow the scientific community to understand the effects of varnish composition on chemical cleaner performance. Moreover, the analysis of the effects of varnish preparation conditions provides information about how much varnish might be removed for given curing conditions in a mechanical system. Aspects of the varnish removal process that have not previously been considered have been explored in this work.

Overall, this research provides a new approach to comprehensive characterization of chemical cleaner performance. The approach has been demonstrated with representative cleaner fluids which has revealed previously unexplored trends in varnish removal. The results are therefore valuable to both the scientific community and end users. The two main processes of removal in this work, mass and convective diffusion, will be discussed in the following chapter and help to characterize fluid performance.

Chapter 6

THEORETICAL ANALYSIS

6.1   Introduction

The results presented in the previous chapter are driven by thermal, mechanical and chemical processes. Each of these process are a form of diffusion known as thermal, convective and mass diffusion. This chapter will focus on theoretical analysis of the varnish removal process through these mechanisms.

Thermal diffusivity is caused by temperature differences in a fluid. Thermal diffusion affects the solubility of a solution by causing a temperature gradient. The concentration of the solution in the temperature gradient causes a concentration gradient and affects the diffusion of the solute into the solvent.

Momentum diffusivity is the result of the spread of momentum between particles of a fluid. This transport can occur in any direction relative to the fluid flow and is typically attributed to external pressure and/or shear stress. When a pressure is applied on an incompressible fluid in a pipe with open ends, the velocity of the fluid will change. The fluid will accelerate, or decelerate, depending on the relative direction of the pressure.

Shear stress is always present in pipe flow because of the no slip condition due to the adhesive forces between the fluid and the pipe wall. The shear stress has the effect of slowing the fluid down as it nears the pipe wall. As the velocity of the fluid increases from zero at the pipe wall to the free stream velocity it creates what is known as the boundary layer. Layers of fluid that are not in contact with the wall are then sandwiched between the boundary layers. The result is that some layers are flowing with greater velocity than others. Viscosity is the property that determines the amount of cohesive force transmitted from one layer to another.

Mass diffusivity is the process of a substance moving from an area of higher concentration to an area of lower concentration. The substance spreads out evenly to fill an area or environment. In a fluid, the solute is the substance which is diffusing while the solvent is the area of lower concentration to which the solute diffuses. Mass diffusion is the result of the kinetic properties of matter where the particles will mix until evenly distributed. Mass diffusivity may be thought of, in mathematical terms, as movement down a concentration gradient. Diffusion also can be the result of a chemical softening of a substance, causing it to diffuse into a solvent.

In this work all three types of diffusion - mass, momentum and thermal - are present. The chemical cleaners cause the varnish to soften and diffuse into the fluid. The momentum diffusion causes shear stress along the surface of the varnish to pull the softened particles off. Thermal diffusion causes a temperature gradient, which in turn affects the solubility of the varnish in the fluid. The units for diffusivity are (length)^2/(time) for all three types of diffusion.

6.1.1 Thermal Diffusion

Thermal effects on fluid behavior (such as viscosity) are well documented [159, 160]. Molecular activity increases with temperature [161] and the viscosity-temperature relationship was discussed in Chapter 1. Therefore, any thermal effects on the varnish removal process must be quantified for a complete understanding of varnish removal.

The heater for the test system is located in the return line near the reservoir and, while the average temperature is 90°C, the instantaneous temperature fluctuated by ± 3°C between heater cycles. The heater is trying to compensate for the heat lost from the test system through convection and radiation. Although there are three types of heat loss (convection, radiation and conduction) the test system has limited solid contact with its surroundings limiting conduction. Therefore, radiation (though limited at the operating temperatures of the test system) and convection are responsible for the majority of the heat lost. The surroundings are at a nearly constant temperature of 23°C while the fluid is kept near 90°C. The equations for radiation and convection are well known and shown as Equations 6.1 and 6.2

$$Q = \epsilon \sigma A (T_{pipe}^4 - T_{envrionment}^4) \tag{6.1}$$

$$Q = hA(T_{pipe} - T_{envrionment}) \tag{6.2}$$

where Q (W) is power, ϵ (dimensionless) is emissivity, σ ($W/(m^2K^4)$) is the Stefan-Boltzman constant, A (m^2) is the area of radiation and h ($W/(m^2K)$) is the convective heat transfer coefficient. To simplify the process of calculating heat transfer, the Biot number was found using Equation 6.3

$$Bi = \frac{L_c h}{k} \tag{6.3}$$

where L_c is a characteristic length (typically the volume of a body divided by its surface area) and k ($W/(mK)$) is the thermal conductivity of the body. The Biot number provides a simple way of determining if the temperature inside the body will vary significantly in space as the body is cooled. If the Biot number is small ($<<1$) the body can be treated as one constant temperature. The test cell has a characteristic length of 0.0149m, h for free convection air is typically $10(W/(m^2K))$

[162] and k for 316 stainless steel is $16.3(W/(mK))$ [163]. The Biot number was found to be 0.009, which is much smaller than one. To confirm this result, i.e. that the temperature of the test cell was constant in space, a simulation was done in COMSOL. The COMSOL simulation was performed on a full scale model of the test cell (3.2in, x 2.5in x 7in) with the port shape (from Figure 3.3.2.1) shown in the center. The parameters in COMSOL were prescribed as a temperature of 90°C for the fluid and convective surface flux with 23°C for ambient temperature. The results are shown in Figure 6.1.1.1.
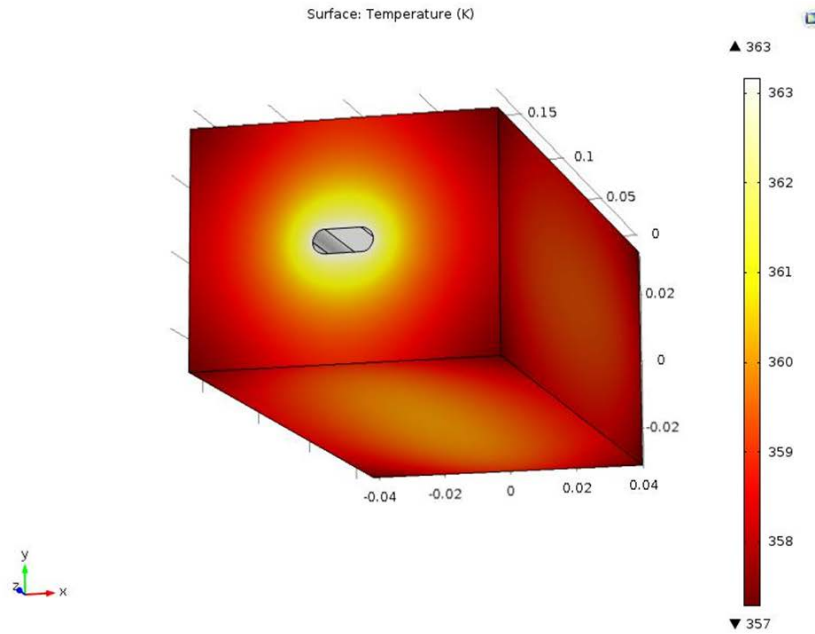
Figure 6.1.1.1: COMSOL simulation to verify that the test cell can be treated as being at one temperature. The COMSOL simulation was performed on a full scale model of the test cell (3.2in, x 2.5in x 7in) with the port shape (from Figure 3.3.2.1) shown in the center. As the Biot number inferred, the test cell can be treated as one temperature. The temperatures from this simulation are reported in units of Kelvin.

Figure 6.1.1.1 shows that the temperature variation in the test cell is very small (as the Biot number implied) allowing simplification of the heat transfer calculations by allowing the test cell to be treated as one temperature. Using Equation 6.1, the power lost to radiation is found to be $28.9W$ and using Equation 6.2 the power lost to convection is found to be $40.2W$. The mass flow rate of the test system can be found using Equation 6.4.

$$\dot{m} = \rho\dot{V} \tag{6.4}$$

where the flow rate ($\dot{V}$) of the test system is 284e-6m^3/s (4.5GPM) and the average density (ρ) of the fluids is $870kg/m^3$ for a mass flow rate ($\dot{m}$) of $0.247kg/s$. To find the temperature drop across the test cell, Equation 6.5 can be used.

$$Q = \dot{m}C_p(\Delta T) \tag{6.5}$$

where C_p is the specific heat of the fluid and Δ T is the temperature drop across the test cell which is found to be 0.14°C. The Prandtl number, which represents the ratio of momentum to heat diffusion in a fluid, is shown as Equation 6.6)

$$Pr = \frac{\nu}{\alpha} \tag{6.6}$$

where α (m^2/s) is the thermal diffusivity of a standard ISO-46 base fluid at 90°C. For the eight fluids tested, the Prandtl number was found to be 180 ± 20. The Prandtl number indicates that the convection process dominates the thermal diffusion process in the varnish removal test system. The Prandtl number, combined with the very small temperature loss through the test cell, indicates that thermal diffusion has a negligible impact on the varnish removal process and can be neglected.

6.1.2 Momentum Diffusion

Pipe flow is commonly encountered in practice. Round pipes are typically used to transport fluids (due to their ability to resist hoop stresses) while rectangular shapes are used to transport gasses. When a fluid flows through a pipe, friction is generated. This friction is directly related to the pressure drop and/or head loss during flow. The pressure drop is used to find the pumping power needed to push the fluid through the pipe (Section 3.3.4).

In pipe flow, the fluid velocity is zero at the pipe surface (known as the no-slip condition) and the maximum fluid velocity occurs at the center of the pipe. This creates a velocity profile in the fluid that is dependent upon the radial distance from the center of the pipe. For this reason, it is common to use an average fluid velocity when dealing with pipe flow. The average velocity can be calculated from the known flow rate and the cross sectional area of the pipe as shown in Equation 3.2. The relationship between the average velocity and the velocity profile can be found using the principle of mass conservation shown as Equation 6.7.

$$\dot{m} = \rho v_{ave}A_c = \int_{A_c} \rho u(r)dA_c \tag{6.7}$$

The average velocities, combined with the viscosity and a characteristic length, can be used to differentiate between three fluid flow regimes. The three regimes of

fluid flow are laminar, transitional and turbulent. Laminar flow is characterized by very smooth flow with highly ordered motion. Turbulent flow is characterized by flow that is highly disordered where eddies and velocity fluctuations are present. The transitional regime is characterized as possessing varying amounts of laminar and turbulent flow. The well-known dimensionless Reynolds number is used to characterize fluid flow and identifies the regime of operation by comparing the inertial forces to viscous forces as shown in Equation 6.8.

$$Re = \frac{v_{ave}D}{\nu} = \frac{\rho v_{ave}D}{\mu} \tag{6.8}$$

where v_{ave} is the average flow velocity, D is a characteristic length of geometry, and μ and ν are the dynamic and kinematic viscosities respectively. Important Reynolds numbers for pipe flow are as follows: Re<2300 is laminar, 2300≤Re≤4000 is transitional and Re>4000 is turbulent. The characteristic length is either the inside diameter of the pipe for circular pipes, or the hydraulic diameter for non-circular pipes as shown in Equation 3.1.

In fully developed laminar pipe flow of constant cross section, the velocity profile $u(r)$ remains constant in the direction of flow. Figure 6.1.2.1 shows a constant cross section pipe with a fully developed flow profile. A ring shaped volume element of radius r, thickness dr and length dx is shown and only is acted upon by pressure and viscous shear forces.
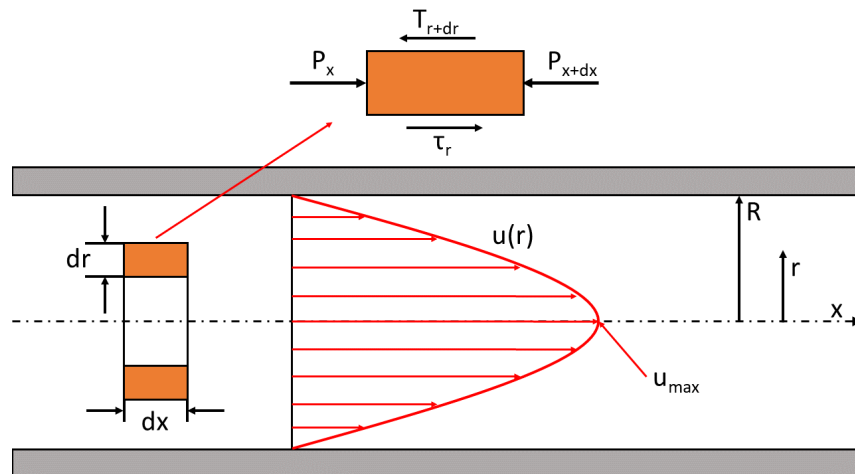
Figure 6.1.2.1: Constant radius (R) pipe flow showing a ring-shaped volume element, with radial thickness dr and length dx, and a parabolic velocity profile. The ring element is shown at the top and is only acted upon by pressure and shear forces.

To find the velocity profile, a force balance is done on the volume element and is shown as Equation 6.9.

$$(2\pi r dr P)_x - (2\pi r dr P)_{x+dx} + (2\pi r dx \tau)_r - (2\pi r dx \tau)_{r+dr} = 0 \qquad (6.9)$$

Solving this equation leads to the very well-known velocity profile equation for circular pipes under the conditions of incompressible, steady state flow. This equation is shown as Equation 6.10.

$$v(r) = 2v_{ave}\left(1 - \frac{r^2}{R^2}\right) \qquad (6.10)$$

However, the test cell is not circular in shape. Although the test cell has a constant cross section across the varnish, the shape is that of two half circles split by a rectangle as shown in Figure 3.3.2.1. Finding an analytical solution for the velocity profile for this geometry would enable the velocity at the surface of the varnish to be calculated. A close approximation for the actual test system port shape was found by using an ellipse. A velocity profile for an ellipse was calculated and then compared to simulations of the actual port geometry in COMSOL to ensure the velocity at the surface of the varnish was the same as obtained for the approximate ellipse geometry. The continuity and Navier-Stokes equations were used to solve this problem and are shown below:

$$\partial_x v_x + \partial_y v_y + \partial_z v_z = 0 \qquad (6.11)$$

$$\begin{aligned}
\rho(v_x\partial_x + v_y\partial_y + v_z\partial_z)v_x &= -\partial_x p v_x + \eta(\partial_x^2 + \partial_y^2 + \partial_z^2)v_x \\
\rho(v_x\partial_x + v_y\partial_y + v_z\partial_z)v_y &= -\partial_x p v_y + \eta(\partial_x^2 + \partial_y^2 + \partial_z^2)v_y \\
\rho(v_x\partial_x + v_y\partial_y + v_z\partial_z)v_z &= -\partial_x p v_z + \eta(\partial_x^2 + \partial_y^2 + \partial_z^2)v_z
\end{aligned} \qquad (6.12)$$

where v_i is the ith component of velocity, ρ is the density, p is the pressure and η is the dynamic viscosity. These equations simplify greatly when considering steady state, incompressible pipe flow where the axis is coincident with the z-axis and v_x and v_y are zero. This also means that the pressure gradients $\partial_x p$ and $\partial_y p$ are zero. The continuity equation from 6.11 then reduces to $\partial_z v_z$=0. When these simplifications are made, the remaining equation describing axis-symmetric pipe flow is shown as Equation 6.13.

$$(\partial_x^2 + \partial_y^2)v_z = \frac{1}{\eta}\partial_z p \qquad (6.13)$$

The equation for an ellipse is shown as Equation 6.14 and will be used in conjunction with the solution of Equation 6.13 to find the velocity profile in an elliptical cross-section.

116

$$\frac{x^2}{a^2} + \frac{y^2}{b^2} = 1 \tag{6.14}$$

A solution of Equation 6.13 that satisfies the boundary conditions of no-slip at the wall and no shear in the center provides the velocity profile and is shown as Equation 6.15.

$$v_z = 2v_{ave}\left(1 - \frac{x^2}{a^2} - \frac{y^2}{b^2}\right) \tag{6.15}$$

This solution is identical to Equation 6.10 with the exception of the geometrical term for a pipe vs an ellipse. The cross sectional area of the test cell port is known to be 0.922cm^2. The height of the port is .635cm and the overall length is 1.59cm, for a length to height ratio of 2.5. Calculating the major and minor axis values for an ellipse that has an area of 0.922cm^2 and a length-to-height ratio of 2.5, we find that a equals 0.857 and b equals 0.343.

The characteristic length for the test cell was given as 0.945cm and the calculated characteristic length for the ellipse is 0.935cm for an error of 1.05%. The characteristic length, d_h, is the hydraulic diameter and is used when calculating the Reynolds number. The Reynolds number for the test cell at 90°C, when used with base Fluid R, is known to be 1843 and the calculated Reynolds number for the elliptical shape is 1823 for an error of 1.09%. Therefore, using an ellipse to find the velocity of the fluid over the varnish in the test cell is acceptable.

The flow rate used in the test system was 4.5GPM ($284\text{cm}^3/\text{s}$) which provides an average flow velocity of 3.08 m/s in the test cell. This average flow velocity is the same for the actual system and the ellipse because the cross sectional areas are the same. However, the velocity profiles will be slightly different and need to be checked against the actual port shape to ensure the velocity profiles are comparable. COMSOL simulations were run using both geometric profiles and the results are shown in Figure 6.1.2.2.

The maximum flow velocity for the varnish test system is 5.31m/s while the maximum velocity for the elliptical shape is 5.86m/s, which is an error of 10.4%. The error is due to the difference in areas at the position of the maximum velocity. From Figure 6.1.2.2 it can be seen that there is a much larger area of high flow rate in the actual test cell than in the elliptical area (as shown in the black elliptical area). The velocity of interest is where the fluid encounters the leading edge of the varnish layer. To ensure that the analytical solution for the velocity profile can indeed be used to find the velocity near the surface of the varnish, the velocity of the COMSOL model was compared to the elliptical model at the average height of the varnish. To find the velocity of the fluid at the average height of the varnish layer, Equation 6.15 was used. The velocity of interest, in the case of an ellipse, occurs where x is zero and y is the average varnish height of 124μm. This gives a
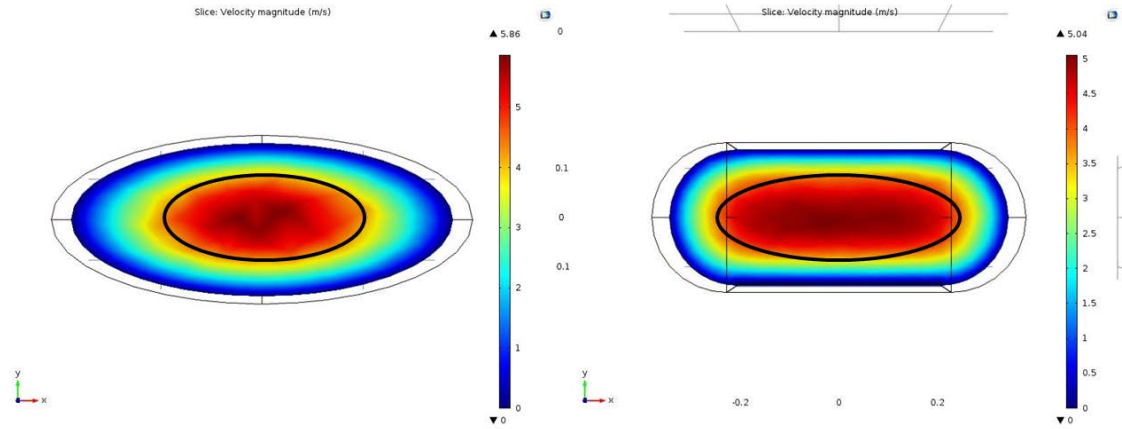
Figure 6.1.2.2: Flow simulations using the actual test cell geometry and the elliptical geometry. These results were used for calculating the velocity of the fluid as it encounters the varnish. The black ellipse is identifying the effective area of maximum velocity for each geometrical shape. The slight difference in area causes differences in the maximum velocity numbers.

velocity of 0.438m/s. The velocity of flow over the varnish from COMSOL for the actual test system was found to be 0.431m/s, for an error of 1.62%. This error is acceptable in flow calculations. Moreover, the flow is fully developed and laminar in either case, allowing the use of the elliptical shape for analytical calculations.

The velocity profile will change slightly as it moves over the leading edge of the varnish and will reach fully developed flow again some distance from the leading edge of the varnish. The distance required to attain the fully developed velocity profile can be found using flat plate boundary theories. Figure 6.1.2.3 shows the laminar boundary layer developed over the varnish stain.

Using the entrance length equation for laminar flow, shown as Equation 6.16, the distance to restore the fully developed profile can be found.

$$L_{h,laminar} \simeq 0.05 ReD \tag{6.16}$$

Using the stream velocity at the surface of the varnish, the Reynolds number is found to be 8.78e-5. The distance for the re-development of the velocity profile
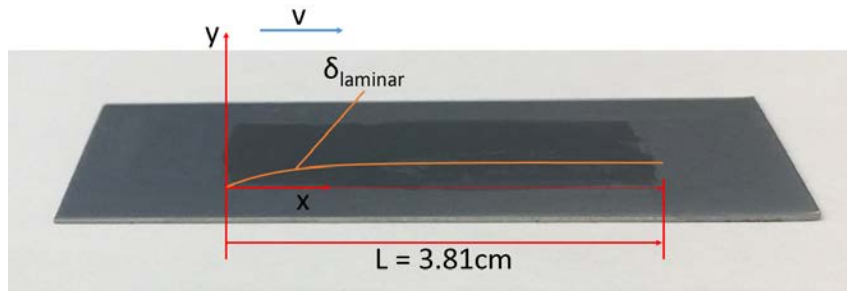
Figure 6.1.2.3: Flat plate boundary layer theory showing the development of a laminar boundary layer over the coupon.

was 4.15μm. This value agrees well with the simulation generated in COMSOL where the length was found to be 3.56μm, as shown in Figure 6.1.2.4.
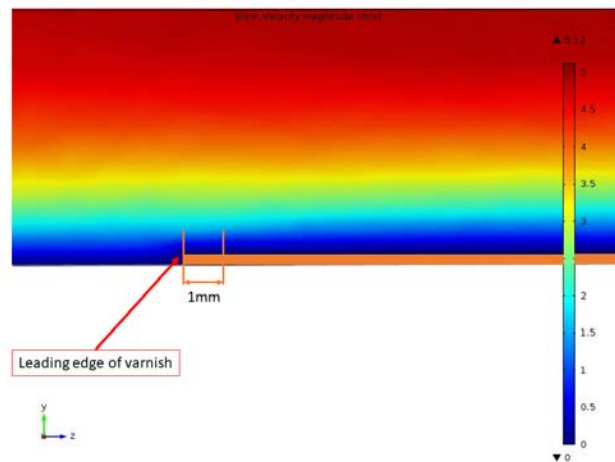
Figure 6.1.2.4: The development of boundary layer over the varnish occurs 4.15μm from the leading edge of the varnish.

With the velocity profile known (Equation 6.15), the shear stress can be calculated at the varnish layer using Equation 6.17.

$$\tau_{varnish} = \eta \frac{du}{dy}\bigg|_{y=b} \tag{6.17}$$

119

Although the velocity at the varnish layer is zero (no-slip condition) the derivative will not be zero. The derivative of the velocity profile is

$$\frac{dv}{dy} = 2v_{ave}\left(-\frac{2y}{b^2}\right) = -4v_{ave}\frac{b}{b^2} \tag{6.18}$$

So at the varnish layer the shear stress is

$$\tau_{varnish} = \eta\left(-4v_{ave}\frac{1}{b}\right) = -4\eta\frac{v_{ave}}{b} \tag{6.19}$$

The total frictional force along the varnish layer is obtained by integrating the shear stress over the area as shown in Equation 6.20.

$$F = \int_A \tau dA = \tau A \tag{6.20}$$

The total shear force along the surface of the varnish is

$$F = -4\eta\frac{v_{ave}}{b}A \tag{6.21}$$

The sign is negative because the shear forces act opposite to the direction of flow. The only difference between shear forces on the varnish samples in the various tests performed in this research is the viscosity of the fluids. Table 6.1.2.1 shows the viscosity of each fluid and the shear forces acting on the surface of the varnish. While diffusion (discussed in the next section) is responsible for softening the varnish, the shear forces are responsible for forcibly removing the varnish.

Fluid	Viscosity (cSt)	Shear Force (N)	Varnish Removed (%)
L	12.94	-40.51	1.22
M	17.27	-54.30	78.8
N	12.18	-38.58	1.42
O	11.79	-37.40	89.7
P	12.50	-37.41	1.73
Q	12.88	-40.49	4.26
R	13.53	-42.04	1.02
S	13.65	-42.41	4.64

Table 6.1.2.1: Each fluid compared for viscosity (cSt), shear forces (N) on varnish surface and varnish removed (%).

From Table 6.1.2.1 is it apparent that the fluids exhibiting the highest shear forces aren't necessarily removing the most varnish. This demonstrates that convective processes may contribute to varnish removal, but do not always drive varnish removal.

6.1.3 Mass Diffusion

Mass diffusion, in liquids, is the process whereby a solute is diffused into a solvent. A concentration gradient is established and is dependent upon the strength of the chemical cleaner, the temperature of the fluid and, if present, convective diffusion. In the varnish test system, the varnish (the solute) is dissolved into the cleaner fluid (the solvent). Fick's first law (shown as Equation 6.22) relates the diffusive flux to the concentration under steady state conditions.

$$J = -D\frac{dc}{dx} \tag{6.22}$$

where J ($g/(m \cdot s)$) is the diffusion flux, D (m^2/s) is the diffusion coefficient, c (g/m^3) is the concentration and x (m) is the position. Fick's second law (shown as Equation 6.23), which is identical to the heat equation in one dimension, predicts how diffusion causes the concentration to change over time.

$$\frac{\partial c}{\partial t} = D\frac{\partial^2 c}{\partial x^2} \tag{6.23}$$

Using Equation 6.23, combined with knowledge of the mass concentration of the varnish over time, the diffusion coefficient for each cleaner can be found. Figure 6.1.3.1 shows the process of mass diffusion from the varnish into the chemical cleaner under steady state convective conditions.

The first step in using Equation 6.23 is to identify the boundary conditions (BCs) and any initial (IC) condition. Figure 6.1.3.1 shows that Neumann boundary conditions can be applied because no flux occurs at $y = 0$ and at $y = L$. The boundary conditions are shown below

$$\frac{\partial c(0,t)}{\partial y} = 0$$
$$\frac{\partial c(L,t)}{\partial y} = 0$$

The initial conditions then need to ensure that, between $y = 0$ and the average varnish height for each test ($y = h_{ave}$), the concentration is c_0 (the mass concentration in g/cm^3) and, between $y = h_{ave}$ and $y = L$, the concentration is 0. These initial conditions are summarized below.

$$c(y,0) = c_0, \quad 0 < y \leq h_{ave}$$
$$c(y,0) = 0, \quad h_{ave} < y \leq L$$
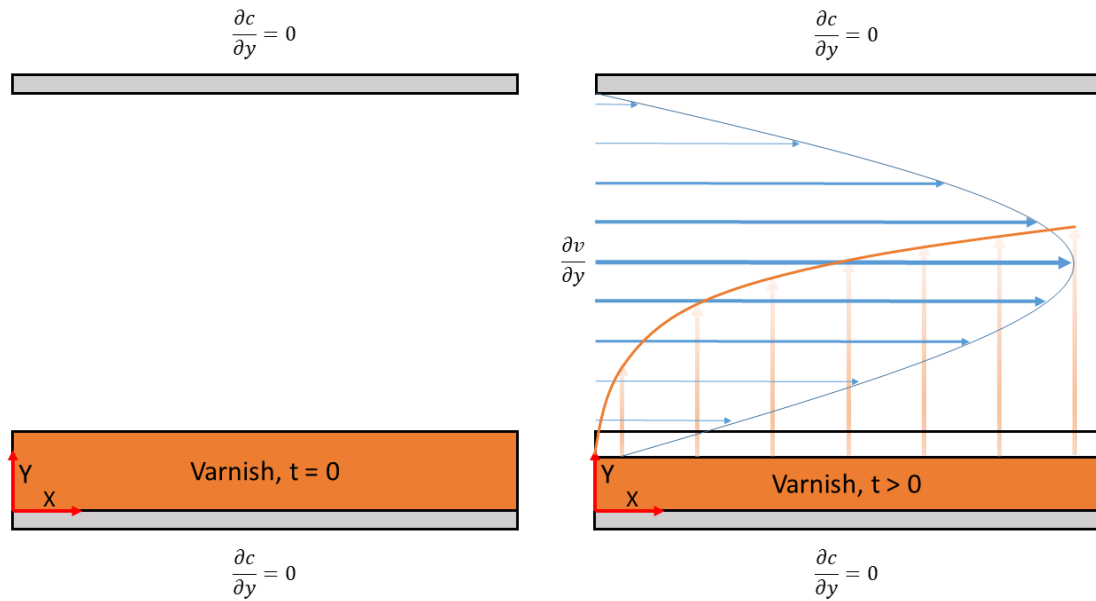
Figure 6.1.3.1: Left: SOT varnish volume element at $t = 0$. Right: The process of testing which shows mass and convective diffusion over the varnish $(t > 0)$.

Here, the assumption of zero varnish in the solution throughout the duration of the test can be justified by finding the mass concentration of varnish in the 18.93 Liters of fluid in the test system as shown in Table 6.1.3.1.

The concentration of interest, c, is defined as the mass present within the original volume of varnish. As the test progresses the mass decreases while the original volume of varnish at SOT does not. This provides a method of tracking the concentration of varnish within the original varnish volume. The length and width of the varnish on the coupon is 3.81cm x 1.27cm. The height of the varnish was found using a DeFelsko PosiTector 6000. This tool measures coating thicknesses using magnetic and eddy current principles on ferrous and non-ferrous metals. Each varnish sample was measured in 6 places across the surface of the varnish and averaged. The volume of varnish present at SOT is found for each test and the initial and final mass loss over time are found using the processes described in Chapter 4. The initial and final average mass concentrations were calculated from the average of the two tests performed for each fluid. The development of the diffusion equation is well known for Neumann boundary conditions. The solution is shown as Equations 6.24 and 6.25.

Fluid	Volume of Cleaner (L)	Mass of Varnish (mg)	Concentration (g/mL)
L	18.93	1.05	5.55e-8
M	18.93	66.8	3.53e-6
N	18.93	1.20	6.34e-8
O	18.93	72.2	3.81e-6
P	18.93	1.40	7.40e-8
Q	18.93	3.75	1.98e-7
R	18.93	0.65	3.43e-8
S	18.93	4.20	2.22e-7

Table 6.1.3.1: Mass concentration at EOT for each fluid tested. The small mass concentrations allowed the boundary condition of no flux at a distance L from the coupon.

$$c(y,t) = a_0 + \sum_{n=1}^{\infty} a_n \cos(\frac{n\pi y}{L}) e^{\left(\frac{-Dn^2\pi^2 t}{L^2}\right)} \qquad (6.24)$$

where

$$a_0 = \frac{1}{L}\int_0^L f(y)dy, \quad a_n = \frac{2}{L}\int_0^L f(y)\cos\left(\frac{n\pi y}{L}\right)dy, \quad n \geq 1 \qquad (6.25)$$

using the initial condition shown previously, the full solution becomes

$$c(y,t) = c_0 + \frac{2c_0}{\pi}\sum_{n=1}^{\infty} \frac{\sin(\frac{n\pi y_{ave}}{L})}{n}\cos\left(\frac{n\pi y}{L}\right)e^{\left(-\frac{Dn^2\pi^2 t}{L^2}\right)} \qquad (6.26)$$

and rearranging Equation 6.26 as shown below

$$\frac{(c(y,t)-c_0)\pi}{2c_0} = \sum_{n=1}^{\infty} \frac{\sin(\frac{n\pi y_{ave}}{L})}{n}\cos\left(\frac{n\pi y}{L}\right)e^{\left(-\frac{Dn^2\pi^2 t}{L^2}\right)} \qquad (6.27)$$

a first term approximation will be applied for this work allowing the summation to be dropped. The coefficient of interest in Equation 6.27 is the diffusion coefficient D. To allow D to be found, Equation 6.27 can be linearized to the familiar equation $y = mx + b$ as shown below

$$ln\left(\frac{(c(y,t)-c_0)\pi}{2c_0}\right) \approx ln\left(\sin\left(\frac{\pi y_{ave}}{L}\right)\right) + ln\left(\cos\left(\frac{\pi y}{L}\right)\right) - \left(\frac{D\pi^2}{L^2}\right)t \qquad (6.28)$$

dropping the constant terms the final equation used to find D is shown below

$$ln\left(\frac{(c(y,t)-c_0)\pi}{2c_0}\right)\frac{L^2}{\pi^2} \approx -Dt \qquad (6.29)$$

Using Equation 6.29, the slope of the line generated by the known mass loss will provide D. Two series of tests were designed to compare the diffusion coefficients generated under low and high flow conditions. The results are shown in the next two sections.

6.1.3.1 High Flow Results ($1700 < \mathrm{Re} < 2000$)

The high flow tests were generated using a flow rate of 4.5GPM, a temperature of 90°C and a test duration of 120 minutes. Figure 6.1.3.2 shows the results for Tests 100-117.
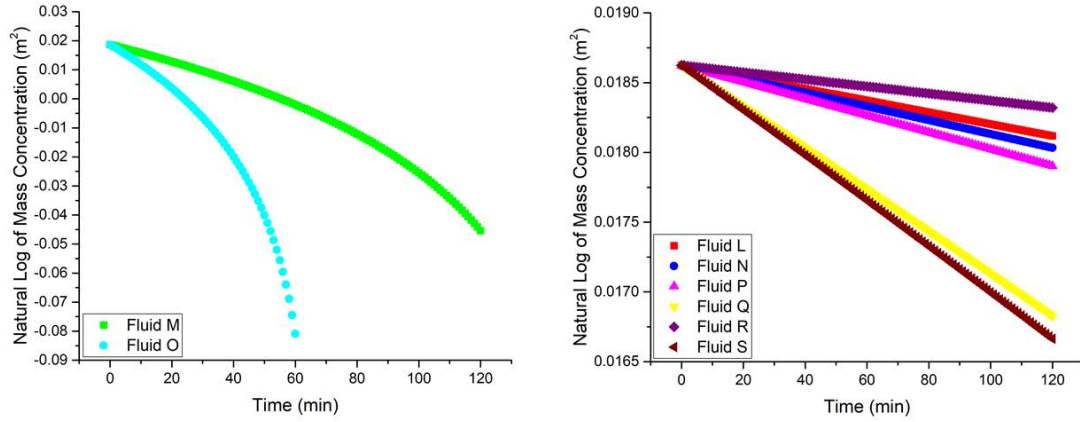
Figure 6.1.3.2: Left: Fluids O and M. Right: Fluids L, N, P, Q, R and S. Both plots show the natural log of mass concentration plotted against the time of mass removal.

The results in this work are averaged values over the two tests performed for each fluid. For fluids that removed most of the varnish on the coupon, only the time where mass removal was occurring was considered. Specifically, after 60 minutes, Fluid O removed no further varnish, so only the first 60 minutes were considered in the calculation. The remaining fluids continued to remove varnish throughout the test duration of 120 minutes. The diffusion coefficient calculated in this work is specifically for convective diffusion. The data used to find the diffusion coefficient

124

was gathered from the test system with a flow rate of 4.5GPM and a temperature of 90°C. The diffusion coefficients for different flow rates, or no flow at all, might be very different.

Once the diffusion coefficients are known, this information can be used to find the Schmidt number. The Schmidt number is defined as the ratio of momentum diffusivity (kinematic viscosity) and mass diffusivity, and is used to characterize fluid flows in which there are simultaneous momentum and mass diffusion convection processes. The Schmidt number is the mass transfer equivalent of the Prandtl number for heat transfer . The Schmidt number is calculated as shown in Equation 6.30.

$$Sc = \frac{\nu}{D} = \frac{\mu}{\rho D} \tag{6.30}$$

A Schmidt number of one indicates that momentum and mass transfer by diffusion are comparable, and velocity and concentration boundary layers almost coincide with each other. Mass diffusion in liquids grows with temperature due to the viscosity decrease with temperature combined with mass diffusion increase with temperature. Therefore, the Schmidt number quickly decreases with temperature. The kinematic viscosities, diffusion coefficients, Schmidt numbers and varnish removed (all calculated or found at 90°C) are shown in Table 6.1.3.2.

Fluid	Diffusion (m^2/s)	ν (St)	Schmidt Number	Mass Removed (mg)
L	4.22e-6	1.29e-5	3.062	1.05
M	4.95e-4	1.73e-5	0.035	66.8
N	4.93e-6	1.22e-5	2.472	1.20
O	1.41e-3	1.20e-5	0.008	72.2
P	6.01e-6	1.25e-5	2.080	1.40
Q	1.50e-5	1.29e-5	0.860	3.75
R	2.53e-6	1.35e-5	5.348	0.65
S	1.63e-5	1.36e-5	0.834	4.20

Table 6.1.3.2: Diffusion coefficient (D), kinematic viscosity (St), Schmidt number (Sc) and mass removed shown for all fluids. All tests run at 4.5GPM and 90°C.

The Schmidt numbers found in Table 6.1.3.2 demonstrate that some cleaners are successful based on the strength of the chemicals while others relied on the convective process to remove varnish at 90°C. Fluid R is known to be a base fluid and has the highest Schmidt number of the final fluids tested. This is expected since mineral base oil has no chemicals to assist in the removal process. Fluids M and O

have very low Schmidt numbers indicating that mass diffusion processes dominated the removal of varnish. The Schmidt number provides a method of comparing mass and convective diffusion and allows direct comparison of a cleaners ability to remove varnish through both processes.

6.1.3.2 Low Flow Results ($175 < \text{Re} < 225$)

To provide further insight into the performance of the chemical cleaners low flow rate tests were performed. These low flow tests were performed on Fluids M, O, P, Q and S using a flow rate of 0.5GPM ($\text{Re} = 205$), a temperature of $90°$C and a test duration of 48 hours. The tests were run for a total time of 48 hours to allow the steady state varnish removal condition to occur. To extract the diffusion coefficient, D, the same method outlined previously was implemented. Figure 6.1.3.3 shows the mass concentration removal plotted against the duration of the tests.
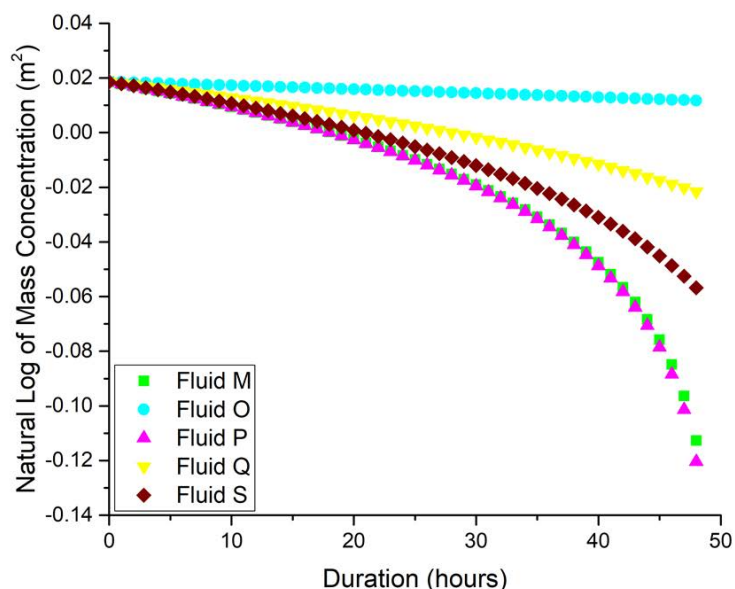
Figure 6.1.3.3: Left: Fluids M, O, P, Q and S. Plots show the natural log of mass concentration plotted against the time of mass removal.

The diffusion coefficient was found using linear interpolation and the results of these tests are shown in Table 6.1.3.3. The low flow rate results show that Fluids P, Q and S exhibited a significant increase (when compared to the high flow rate tests in Table 6.1.3.2) in the overall varnish removal while Fluid M showed a mild increase. Fluid O exhibited a significant decrease of varnish removed. The difference in removed varnish between the high and low flow rates is significant and provides insight into the ability of the cleaner to perform under varying conditions.

Fluid	Diffusion (m²/s)	ν (St)	Schmidt Number	Mass Removed (mg)
M	2.10e-3	1.73e-5	0.0082	95.9
O	1.44e-4	1.20e-5	0.0833	15.4
P	2.17e-3	1.25e-5	0.0058	96.6
Q	8.13e-4	1.29e-5	0.0159	62.2
S	1.42e-3	1.36e-5	0.0096	83.9

Table 6.1.3.3: Diffusion coefficient (D), kinematic viscosity (St), Schmidt number (Sc) and mass removed shown 5 fluids. All tests run at 0.5GPM and 90°C.

6.1.4   High and Low Flow Comparison

From inspection, the Schmidt number is a function of viscosity, which is highly dependent on temperature. Mass diffusion is also dependent upon temperature and higher temperatures lead to increased mass diffusion while lower temperatures decrease mass diffusion [160, 161]. The convective contribution (flow rate) provided significantly different results when varied. Table 6.1.4.1 compares the high and low flow results and exemplifies the convective contribution effect on varnish removal.

Fluid	M	O	P	Q	S
High Flow Diffusion	4.95e-4	1.41e-3	6.01e-6	1.50e-5	1.63e-5
High Flow Schmidt	0.0349	0.0085	2.0799	0.8600	0.8344
Varnish Removed (%)	78.8	89.7	1.73	4.26	4.64
Low Flow Diffusion	2.10e-3	1.44e-4	2.17e-3	8.13e-4	1.42e-3
Low Flow Schmidt	0.0082	0.0833	0.0058	0.0159	0.0096
Varnish Removed (%)	95.9	15.4	96.6	62.2	84.0

Table 6.1.4.1: Diffusion coefficient (D) and Schmidt number (Sc) compared for the high (4.5GPM) and low (0.5GPM) flow results.

When the results from Table 6.1.4.1 are plotted using the flow rate on the abscissa and removed varnish as the ordinate a very comprehensive look can be taken at the performance of the fluids based on flow rate. Figure 6.1.4.1 shows the performance of the fluid based on flow rate and it is apparent that flow rate has a very significant effect on the vanish removal process. The difference might stem from the fact that two specific chemical processes occur for varnish removal. A solvent is typically employed to soften (or loosen) the varnish while other chemicals are

127

employed to cut the side chains and lessen the mass of the polymer. From Figure 6.1.4.1 it can be observed that only one fluid (Fluid M) appears to have chemicals that can perform this function at varying flow rates.
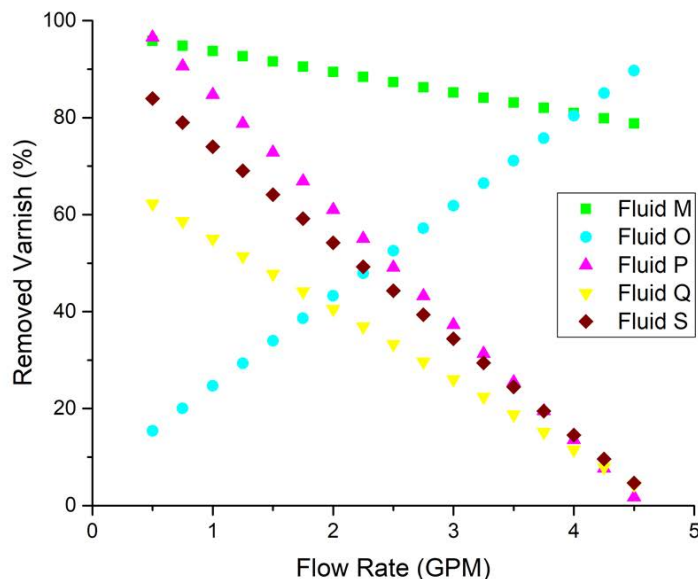
Figure 6.1.4.1: Left: Fluids M, O, P, Q and S graphed in terms of flow rate and removed varnish.

6.2 Summary

Thermal, convective and mass diffusion processes were discussed and compared. Each might have had an impact on varnish removal in the test system. To simplify the process of thermal investigation the Biot number was calculated and found to be very low. This was verified using COMSOL simulations where the temperature variation of the test cell was found to be very small. The Prandtl number provided evidence that thermal diffusion had a negligible effect on varnish removal. Convective effects were investigated by first estimating the velocity profile. The velocity profile was calculated analytically and compared to COMSOL simulations which showed that the analytical result was very accurate. The velocity profile allowed calculation of the shear forces on the surface of the varnish. These forces are responsible for mechanically removing the varnish.

The mass diffusion coefficients were found by manipulating the heat equation into a linear representation of mass concentration loss of varnish from the coupon. Extraction of the diffusion coefficient allowed Schmidt numbers to be found. The Schmidt number provided a direct comparison of mass and convective diffusion.

These numbers showed that some fluids relied on convection to remove varnish while others used powerful chemicals to loosen the varnish and allow mass diffusion to dominate. Therefore, mass and convective diffusion can be expected to be the primary mechanisms of removing varnish.

The chemical aspect of varnish removal relies on solvents to soften the varnish and chemicals to cut the varnish polymers into shorter lengths. The mechanical process removes the softened and shortened polymers by force when the shear forces on the surface of the varnish overcome the surface energy holding the polymer in place. The analysis of the combined effects of convective, mass and thermal diffusion demonstrated here can be applied to other cases to determine varnish removal mechanisms and provide a broad understanding of the varnish removal process in general.

Chapter 7

SUMMARY AND RECOMMENDATIONS FOR FUTURE RESEARCH

7.1 Summary

The work done for this dissertation directly addressed the lack of performance data for chemical cleaners used to flush varnish from gas turbine engines. This thesis reports the first scientific method for characterizing varnish removal performance. A varnish removal test system was designed and manufactured which facilitates the process of testing by using a blank steel coupon which can be covered with artificial varnish. This coupon is easily accessed and changed between tests. The test system can create fluid flows from very low laminar to very high turbulent regimes. This allows virtually every type of system to be simulated within the test cell. The test system can also produce temperatures ranging from ambient (25°C) to 120°C, which allows temperatures common to gas turbine engine, and other mechanical systems, to be generated in the fluid. A filter, located downstream from the test cell, facilitates inspection of the removed varnish to characterize how the chemical is removing the varnish. The filter allows quick and easy changing of pore size using polypropylene filter paper.

This test system is the first of its kind to begin the process of characterizing chemical cleaners. Initially, two parameters were used to characterize the performance of the chemical cleaners (mass loss and filter inspection). This was extended to include four primary test metrics: rate of removal, time of maximum removal rate, steady state varnish removal and mass percent varnish removal. The combination of time-lapse photography and mass removal has allowed a unique method of quantifying varnish removal in terms of color change. This provides a real time plot of the varnish removal process to be generated. This data can be further processed by taking the slope of the color value as a function of time to obtain a removal rate. This is the first scientific evaluation of chemical cleaners designed for removing varnish.

Secondary test metrics include preliminary work on optical particle counting and changes in viscosity over the duration of testing. Initial optical counts were recorded and then again after each test. This data allows insight into the varnish removal process by identifying increases and decreases in optical particle counts.

This will provide invaluable information when sizing a filter to trap removed varnish from a system. Initial viscosities are also recorded and then again after each test. This allows insight into what the varnish is doing to the chemical cleaner during use. Any change in viscosity can be attributed to molecular composition and/or introduced impurities.

Theoretical work has been performed to characterize the thermal, convective and mass diffusion processes. Thermal effects were found to be negligible. Convective and mass diffusion were found to compete in the varnish removal process at 4.5GPM and 90°C. While the investigation into convective and mass diffusion was only performed on the final series of tests, this information will prove invaluable when compared to future testing. Moreover, future work needs to be done in the area of tribological performance of chemical cleaners to round out the complete characterization of cleaner fluids.

This work has made valuable contributions to the scientific community and has provided important practical information for optimizing removal of varnish. The use of this test system will continue to provide data, not only for the gas turbine industry, but for the lubrication industry as a whole. Removing varnish using chemical cleaners may become a more commonly used method if end users have confidence in expected performance of the product, enabled by this research.

7.2 Recommendations for Future Research
7.2.1 Artificial Varnish

Varnish is a complicated substance with a multitude of compositions. Some of the influencing factors in varnish formation are base oil, additive package, metallic components in the machine, atmospheric conditions, operational parameters and filtration, just to name a few. Each system has a unique makeup of materials and parameters that contribute to the eventual and inevitable formation of varnish. With such a plethora of possible varnish compositions, it is imperative that the artificial varnish be given special attention.

In the scope of this work, the artificial varnish was designed to simulate varnish formed within the gas turbine engine. Therefore, the findings reported here are most applicable to that system. The new test method and trends reported are also likely to be relevant to other mechanical components, but quantitative results for a specific component would require testing with varnish from that component. The formation of artificial varnish is the crucial first step in being able to identify the best cleaners for each specific application. Using methods, such as ASTM D7873, artificial varnish can be formed that accurately simulates the chemistry of any desired varnish. This can be done going forward using methods such as FTIR to identify the composition, of in service varnish, and allow similar varnish to be artificially produced. Then, using methods, such as ASTM D7873, artificial varnish

can be formed that accurately simulates the chemistry of any desired varnish. Controlling the exposure to differing metals, temperatures and atmospheres needs to be done with precision and accuracy to ensure test results are beneficial. Future work should include the ability to produce varnish in a lab, under strictly controlled conditions, to enable tests directly applicable to a wide variety of mechanical systems with confidence.

Producing the artificial varnish is just the first of many steps in providing the best testing environment possible. Characterizing any aging effects that happen during storage will help to ensure that test results are interpreted correctly. Application of the varnish on the coupon, including any temperature variations, duration of baking and controlling the mass on the coupon are just as important. This work has demonstrated that differing conditions of application can produce vastly different results which, if not characterized, can lead to inconsistent results.

The production, storage, application and testing of varnish are all critical to accurate chemical cleaner comparison. Controlling artificial varnish production is the first step toward achieving useful results. An application process that provides a varnish that is soft enough to be removed, but not so hard as to render chemical cleaners powerless, should be identified. Beyond what has been done here, additional work can be done to fine tune the varnish application process. Moreover, controlling the mass of varnish on the coupon, to ensure that any SOT-EOT dependence is removed, is of utmost importance. It is imperative that consistently weighted coupons are produced with a minimum of deviation. Future work should include steps to accurately simulate in-service varnish and identify the conditions that provide the best possible varnish for testing a wide variety of chemical cleaners.

7.2.2 Chemical Cleaner Properties

The performance of the chemical cleaners in removing varnish is not the only property of these chemicals that should be considered. Future work should include testing the chemical cleaners for tribological performance. This includes, but is not limited to, finding the coefficient of friction for metals sliding with a cleaner fluid as lubricant under varying loads and speeds. Having a chemical cleaner that removes 100% of varnish present in a system is useless if the cleaner is not capable of acting as a lubricant when the system is operating.

It is also relevant to identify the rheological properties of chemical cleaning agents. Journal bearings, thrust pads, pumps and servo valves are designed and built to operate effectively over a narrow range of viscosities. Altering fluid viscosities might have unintended consequences and negatively impact future machine performance. Preliminary viscosity characterization (in results chapter) has been performed during the scope of this work but much more needs to be done to understand cleaner fluid viscosity and how it varies as varnish is removed.

Future work on fluid cleanliness and filter sizing needs to be performed. Preliminary work has been performed (in results chapter) characterizing fluid cleanliness but further research needs to be done to identify just how much varnish can be suspended in a particular fluid. If these chemical cleaners are to perform their tasks effectively, an understanding of their saturation points and removed varnish particle size should be known. This will help to find the correct filter size for each fluid. A filter sized to large (pore-size) will allow varnish to continue to circulate while an undersized filter might remove the very compounds responsible for removal. In this work it has been documented that cleaners remove varnish through very different mechanisms. Future work should include identifying candidate cleaners and suggesting a proper filter size to assist in varnish removal.

Only chemical removing properties were truly considered in this work but a logical progression of chemical cleaner characterization will include understanding the performance in each regime of lubrication as well as documenting any viscosity change over time. Fluid cleanliness and filter sizing should be considered as the work of varnish testing continues.

The chemical cleaners are a complex mixture of compounds that either soften or cleave the varnish. The softening of the varnish is performed by solvents that separate the polymeric layers of varnish and allow the shear forces to remove it. The shortening of the varnish polymer chains is performed by scission, or bond cleavage, which break the molecular chains into smaller pieces and allows the varnish to be removed by smaller shear forces. The filter results, shown in Figure 5.5.5.1 and 5.5.5.2 demonstrate that some cleaners only soften the varnish, allowing large pieces to be removed, others break the varnish polymers into small pieces much smaller than 5 micron.

Future investigation of the performance between the chemicals that soften the varnish and the chemicals that cleave the varnish should be performed. The flow rate results demonstrate that some chemicals perform better at specific flow rates. The convective flow definitely impacts the performance of the chemicals chosen to perform as a solvent and as a bond cleaver. The ideal fluid will balance performance at low and high flow rates. It is suggested that future work investigate this complex chemical relationship.

7.2.3   Testing Parameters

The current testing parameters (90C, 4.5 GPM and 1800 Re) were selected to remove the most varnish under laminar flow conditions. While these parameters simulate many in-service components, there are a myriad of flow rates within a given system. For example, differing flow rates are present in journal bearings (10-100 Re), servo valves (1000-40,000 Re), pumping components (2000-50,000 Re), heat exchangers and many others. Therefore, the test system can generate very broad range of Reynolds numbers (40<Re<40,000), a range that includes most of these

in-service operational conditions. However, a comprehensive investigation into flow parameters for different components needs to be performed to identify conditions for future testing. This will result in a more complete understanding of chemical cleaner behavior.

7.2.4   Photographic Data

The photographic data has proven invaluable in characterizing the varnish removal process. The ability to view, in real time, the varnish removal process has allowed removal rates and steady state values to be found. Improvement in photographic data can be realized in several ways. The polycarbonate lid, while effective, might be improved with the use of a more transparent material. There are glares and soft spots that limit the resolution of the results obtained thus far.

The lighting plays a major role in ensuring there are no shadows, glares and other detrimental factors in photography. The position of the lighting has been adjusted to minimize these issues, but there is room for improvement. There are camera adjustments available that have not yet been explored which could lead to improvements in imaging. Lighting positions need to be explored that might offer improved imaging. The lights on the current test system have two sources that include bright white and yellow bulbs. The balance of the two, as well as their intensity, should be explored.

During the scope of this work, a record has been made of camera height, lighting position and intensity. The camera has recently been upgraded and the new camera offers many features not offered in the previous model. The combination of camera settings, lighting positioning, intensity and color might further minimize shadow and glare without a change of lid materials. Future work should include optimization of camera and lighting.

7.2.5   Algorithmic Improvement

The algorithm used in processing the time-lapse photography is relatively quick and easy to use. Prior to test 79, the camera was attached to a flex stick that was clamped to one of the light stands. After test 79, a camera mount was fabricated that fixed the camera frame to the test cell lid. This improved the algorithmic data by allowing the same area to be cropped from test to test. However, th algorithm does not search intelligently for the varnish or the steel reference on the coupon and relies on fixed coordinates to assume the position of each.

Even though the fixed position greatly reduces errors in imaging the coupon, there are still slight variations in where the varnish is located on the coupon. This means that, for each test, the algorithm is divided into two sections. The first section finds all the images in the folder and categorizes the information into a matrix. The algorithm then displays four images: the whole image captured from the camera, the cropped image that includes the varnish and steel reference spots, the cropped

varnish image and finally the cropped steel reference image. The images must be visually inspected to ensure that the correct cropping dimensions are applied. The second part of the algorithm then calculates the averaged, max and min K values and stores them in a text file for analyzing.

Upgrades to the algorithm would greatly facilitate the image analysis process. The algorithm could be upgraded to search for the boundaries of the varnish by comparing the dark varnish K values with the lighter steel color that surrounds the varnish. When the boundaries of the varnish are found, they can be used in all subsequent images for varnish reference. The algorithm would then find the brightest steel section located just to the right, or left, of the varnish coupon. Future work should include these algorithmic upgrades to facilitate image processing.

7.2.6   Improved By-Pass Control

The by-pass line is a crucial component of the test system because it regulates the fluid through the test cell. Currently, the ball valve is adjusted by hand and eye to adjust the flow over the test coupon. The ball valve has 4lb·ft of resistance and typically it remains in position once set. This is a very simple method of setting the flow rate through the test cell but does not guarantee that the flow will remain in this position through the test. A method of ensuring that the flow will remain constant at a precise value would be beneficial.

The 3-way ball valve could be upgraded to a 3-way motorized electric ball valve that receives its signal from the positive displacement flow meter. The flow meter is capable of supplying a signal which can be read by an Arduino Board which will control the motorized ball valve. This would be a drastic improvement over the current method of flow control and would allow for pump variations, temperature fluctuations and movement of the manual control ball valve. Future work could include upgrading the manual 3-way control valve to accurately meter the flow over the coupon.

7.2.7   Improved Heater Control

The heater is currently controlled by a thermostat with an accuracy of $\pm$ 3°C. This allows a temperature variation of 87   93°C when 90°C is desired. This work has shown that temperatures of 20°C can drastically affect the removal of varnish far greater that flow variations. For example, Tests 29 and 29a used a flow rate of 0.5GPM, a duration of 220 minutes, and 70°C and 90°C respectively. Test 29 removed 10% of the varnish on the coupon while Test 29a removed 44%. Test 30a used a flow rate of 10GPM, a duration of 11 minutes and a temperature of 70°C. Test 30a only removed 30% of the varnish on the coupon. Each of these tests had a total flow of 110 gallons across the coupon. This demonstrates that temperature has a larger affect on varnish removal than flow rate. Future work should include upgrading the temperature control system to provide greater accuracy. Durex, the

OEM of the current heater, makes a digital control system that can directly replace the rheostat type thermostat currently in use. This would provide increased confidence in the results of the varnish removal test system.

7.2.8 Particle Counting

This test system might benefit from the addition of a particle counter, located in the return line pre-filter. This would give great insight to the size and distribution of particles in the fluid before and during testing. It would also help to quantify the size of the varnish particles removed from the coupon. The varnish removal process is more complicated than just using chemicals to loosen the varnish. The total of the forces at work to remove the varnish include thermal, convective and mass diffusion effects. The mass diffusion effects are chemically driven but rely on the filter to keep the fluid clean. The particle counter would provide insight into correctly sizing the filter for candidate fluids.

7.2.9 Expanded Test Conditions

Additional testing at differing flow rates and temperatures will help to characterize chemical cleaners in a very comprehensive way. For the five fluids tested using varying flow rates, the diffusion coefficient was affected. This, in turn, changed the values of Schmidt numbers. There is no consistent pattern to the diffusion change, indicating that the role of convection is different for each chemical cleaner. This difference in Schmidt number, when investigated, will undoubtedly provide insight into the chemical interaction between the varnish and the cleaner. It would appear that some cleaners need time to dwell on the surface of the varnish for the chemical softening process to occur. This was exemplified by cleaners P and S, where the Schmidt numbers decrease significantly with increasing flow rate. Only cleaner O showed an increase of Schmidt number, indicating that shear forces play a major role in removing the varnish.

This preliminary investigation suggests the need for further testing of differing flow rates to map the mass-convection diffusion relationship. Furthermore, varying the temperature of tests will provide new results when viewed in terms of the Schmidt and Prandtl numbers. There will be a point where the convective and mass diffusion coefficients are equal for varying flow rates and temperatures. Where these coefficients cross will determine which fluids perform better under low or high flow conditions. This will allow cleaners to be selected based on their performance under a broad range of conditions. While some cleaners might be selected for low flow reservoir applications, others will provide increased varnish removal under high flow conditions. The same holds true for temperature variations.

7.2.10 Quantify Smell and Strength

The smell and strength of the chemical cleaner is an important characteristic. In this work, a qualitative approach was used to characterize the smell and strength of each cleaner. This needs to be improved by using scientific methods of quantifying the smell and strength values. Future work should include finding methods of quantifying these metrics that are not subject to individual interpretation. An olfactometer combined with thermal desorption and Mass Spectrometry might offer methods of characterizing smell and strength.

7.2.11 Foam Production

The foam rating was developed using the time required to de-aerate the fluid in the reservoir. The method of characterizing foam performance should be upgraded to include ASTM methods of accurately identifying the foaming tendencies of each chemical cleaner. Future work should include characterizing foam performance in this manner.

7.3 Conclusions

Going forward, the system and testing approach developed in this study can become the standard for characterizing chemical cleaner varnish removing performance. The test system may also be modified to include varnish removal by filter adsorption or electrostatic cleaning. Finally, the system can be used to remove more than varnish. For example, beneficial tribochemistry films (formed from additives such as MoDDP, DLC and ZDDP) can be tested in this system to ensure they can endure the very high Reynolds numbers experienced during turbulent flow. Furthermore, air can be injected into the test system to simulate micro implosion and other cavitation-based issues over the test coupon. Moreover, virtually any hydrocarbon base fluid can be used in the test system. If the desired substance can be attached to the steel coupon (or any material that can be cut in the desired shape and can handle the temperature of testing), the parameters and chemicals that best remove that substance can be found.

I hope research on characterizing varnish removal and understanding removal mechanisms continues to develop. The oxidation of hydrocarbon fluids, and the varnish that forms, is an inevitable process that requires a chemical removal process. Therefore, this work is the starting point for standardizing chemical cleaners and provides valuable information for the scientific community and the end user. Characterizing chemical cleaners using the methods developed in this work will allow greater understanding for the varnish removal process as well as the chemical interactions between varnish and cleaner. A complete understanding of the complex interactions between chemical and varnish, and the convective-mass diffusion process, will take the continued collaboration of chemists, tribologists and engineers.

The information generated will advance our understanding of varnish, varnish removal and the chemicals designed to remove varnish.

BIBLIOGRAPHY

[1] C. S. C. Davison, Wear prevention in early history, Wear 1 (2) (1957) 155–159.

[2] R. G. Bayer, Wear analysis for engineers, Hnb Pub., 2002.

[3] H. A. Barnes, A handbook of elementary rheology.

[4] R. M. Mortier, S. T. Orszulik, M. F. Fox, Chemistry and technology of lubricants, Vol. 107115, Springer, 2010.

[5] J. Fitch, Using oil analysis to control varnish and sludge, Practicing Oil Analysis May.

[6] J. Fitch, S. Gebarin, Review of degradation mechanisms leading to sludge and varnish in modern turbine oil formulations, in: Oxidation and the Testing of Turbine Oils, ASTM International, 2008.

[7] M. Johnson, M. Spurlock, Strategic oil analysis: Estimating remaining lubricant life, Tribology & Lubrication Technology 66 (1) (2010) 22.

[8] AirTECH, How the pump works, [Online; accessed September 20, 2016]. URL http://www.airtechpumps.eu/

[9] Mechanical Engineering Community, Diiference Between Working of Centrifugal pump & Reciprocating Pump, [Online; accessed September 20, 2016]. URL https://mechanical-engg.com

[10] R. B. Erickson, Hydraulic pump technology and selection, Design World for Eaton Corporation.

[11] I. Hutchings, P. Shipway, Tribology: friction and wear of engineering materials, Butterworth-Heinemann, 2017.

[12] American Petroleum Institute, Api base oil interchangeabiltiy guidelines for passenger car motor oils and diesel engine oils (2017).

[13] D. M. Pirro, M. Webster, E. Daschner, Lubrication Fundamentals, Revised and Expanded, CRC Press, 2016.

[14] T. R. Lynch, Process chemistry of lubricant base stocks, CRC Press, 2007.

[15] H. P. Vowles, Early evolution of power engineering, Isis 17 (2) (1932) 412–420.

[16] A. Lucas, J. Harris, Ancient Egyptian materials and industries, Courier Corporation, 2012.

[17] D. Dowson, The history of tribology in america, Journal of Lubrication Technology 103 (3) (1981) 323–333.

[18] M. Nosonovsky, Oil as a lubricant in the ancient middle east, Tribology Online 2 (2) (2007) 44–49.

[19] J. Fitch, Lubrication genesis, Machinery Lubrication 3 (2) (2004) 44–49.

[20] R. S. Westfall, Never at rest: A biography of Isaac Newton, Cambridge University Press, 1983.

[21] Standard Terminology for Plastics: Dynamic Mechanical Properties, Standard, ASTM International, West Conshohocken, PA (2013).
URL https://doi.org/10.1520/D4092-07R13

[22] H. W. Dickinson, James Watt: craftsman and engineer, Cambridge University Press, 2010.

[23] D. Dowson, Men of tribology, Journal of Lubrication Technology 101 (1979) 1.

[24] C. J. Campbell, J. H. Laherrère, The end of cheap oil, Scientific American 278 (3) (1998) 60–65.

[25] U.S. Energy Information Administration, American Field Production of Crude Oil (2016).

[26] U.S. Energy Information Administration, Refinery Yield (2016).

[27] U.S. Energy Information Administration, U.S. Energy Generation (2016).

[28] Bureau of Transportation Statistics, Number of U.S. Vehicles 2015 (2015).

[29] R. W. Carpick, M. Salmeron, Scratching the surface: fundamental investigations of tribology with atomic force microscopy, Chemical reviews 97 (4) (1997) 1163–1194.

[30] T. Vorburger, J. Raja, Surface finish metrology tutorial, National Inst. of Standards and Technology, 1990.

[31] C. Bovington, Friction, wear and the role of additives in controlling them, in: Chemistry and technology of lubricants, Springer, 2010, pp. 77–105.

[32] H. Yoshizawa, Y. L. Chen, J. Israelachvili, Fundamental mechanisms of interfacial friction. 1. relation between adhesion and friction, The Journal of Physical Chemistry 97 (16) (1993) 4128–4140.

[33] F. P. Bowden, D. Tabor, The friction and lubrication of solids, Vol. 1, Oxford university press, 2001.

[34] E. P. Becker, Trends in tribological materials and engine technology, Tribology International 37 (7) (2004) 569–575.

[35] E. Feyzullahoğlu, N. Şakiroğlu, The wear of aluminium-based journal bearing materials under lubrication, Materials & Design (1980-2015) 31 (5) (2010) 2532–2539.

[36] J.-H. Cho, D. E. Boyce, P. R. Dawson, Modeling strain hardening and texture evolution in friction stir welding of stainless steel, Materials Science and Engineering: A 398 (1) (2005) 146–163.

[37] W. Li, Y. Wang, X. Yang, Frictional hardening and softening of steel 52100 during dry sliding, Tribology Letters 18 (3) (2005) 353–357.

[38] A. Misra, I. Finnie, On the size effect in abrasive and erosive wear, Wear 65 (3) (1981) 359–373.

[39] J. Gates, Two-body and three-body abrasion: a critical discussion, Wear 214 (1) (1998) 139–146.

[40] E. Rabinowicz, L. Dunn, P. Russell, A study of abrasive wear under three-body conditions, Wear 4 (5) (1961) 345–355.

[41] H. Sin, N. Saka, N. Suh, Abrasive wear mechanisms and the grit size effect, Wear 55 (1) (1979) 163–190.

[42] G. Stachowiak, G. Stachowiak, The effects of particle characteristics on three-body abrasive wear, Wear 249 (3) (2001) 201–207.

[43] W. Yi-Ling, W. Zi-Shan, An analysis of the influence of plastic indentation on three-body abrasive wear of metals, Wear 122 (2) (1988) 123–133.

[44] R. Garvey, Wear rates impact maintenance priorities, Machinery Lubrication March.

[45] I. D. Marinescu, W. B. Rowe, B. Dimitrov, I. Inaski, Tribology of abrasive machining processes, Elsevier, 2004.

[46] J. Burwell, C. Strang, On the empirical law of adhesive wear, Journal of Applied Physics 23 (1) (1952) 18–28.

[47] J. N. Israelachvili, Y.-L. Chen, H. Yoshizawa, Relationship between adhesion and friction forces, Journal of adhesion science and technology 8 (11) (1994) 1231–1249.

[48] T. Sasada, M. Oike, N. Emori, The effect of abrasive grain size on the transition between abrasive and adhesive wear, Wear 97 (3) (1984) 291–302.

[49] H. Czichos, Tribology: a systems approach to the science and technology of friction, lubrication, and wear, Vol. 1, Elsevier, 2009.

[50] W. Littmann, R. Widner, Propagation of contact fatigue from surface and subsurface origins, Journal of Basic Engineering 88 (3) (1966) 624–635.

[51] T. Beagley, Severe wear of rolling/sliding contacts, Wear 36 (3) (1976) 317–335.

[52] A. Bower, The influence of crack face friction and trapped fluid on surface initiated rolling contact fatigue cracks, Journal of Tribology 110 (4) (1988) 704–711.

[53] C. Bathias, Relation between endurance limits and thresholds in the field of gigacycle fatigue, in: Fatigue Crack Growth Thresholds, Endurance Limits, and Design, ASTM International, 2000.

[54] O. Umezawa, K. Nagai, Deformation structure and subsurface fatigue crack generation in austenitic steels at low temperature, Metallurgical and materials transactions A 29 (3) (1998) 809–822.

[55] M. Hoeprich, Rolling element bearing fatigue damage propagation, ASME, Transactions, Journal of Tribology 114 (2) (1992) 328–333.

[56] M. Fazal, A. Haseeb, H. Masjuki, Biodiesel feasibility study: an evaluation of material compatibility; performance; emission and engine durability, Renewable and Sustainable Energy Reviews 15 (2) (2011) 1314–1324.

[57] G. Frankel, Pitting corrosion of metals a review of the critical factors, Journal of the Electrochemical Society 145 (6) (1998) 2186–2198.

[58] D. J. Young, High temperature oxidation and corrosion of metals, Vol. 1, Elsevier, 2008.

[59] B. J. Hamrock, S. R. Schmid, B. O. Jacobson, Fundamentals of fluid film lubrication, CRC press, 2004.

[60] B. J. Hamrock, W. J. Anderson, Rolling-element bearings.

[61] F. F. Ling, E. E. Klaus, R. Fein, Boundary lubrication. an appraisal of world literature.

[62] Q. J. Wang, Y.-W. Chung, Encyclopedia of tribology: With 3650 Figures and 493 Tables, Springer, 2013.

[63] T. G. Mezger, The rheology handbook: for users of rotational and oscillatory rheometers, Vincentz Network GmbH & Co KG, 2006.

[64] E. d. C. Andrade, Xli. a theory of the viscosity of liquids.part i, The London, Edinburgh, and Dublin Philosophical Magazine and Journal of Science 17 (112) (1934) 497–511.

[65] C. J. A. Roelands, Correlational aspects of the viscosity-temperature-pressure relationship of lubricating oils.

[66] E. Dean, G. Davis, et al., Viscosity variations of oils with temperature, Chemical and Metallurgical Engineering 36 (1929) 618.

[67] Standard Practice for Calculating Viscosity Index from Kinematic Viscosity at 40°C and 100°C, Standard, ASTM International, West Conshohocken, PA (2016).
URL https://doi.org/10.1520/D2270-10R16

[68] S. Wen, P. Huang, Principles of tribology, John Wiley & Sons, 2012.

[69] R. Prince, Base oils from petroleum, in: Chemistry and Technology of Lubricants, Springer, 2010, pp. 3–33.

[70] J. G. Speight, The chemistry and technology of petroleum, CRC press, 2014.

[71] D. C. Kramer, B. K. Lok, R. R. Krug, The evolution of base oil technology, in: Turbine lubrication in the 21st century, ASTM International, 2001.

[72] G. A. Olah, G. S. Prakash, Hydrocarbon chemistry, John Wiley & Sons, 2017.

[73] S. Korcek, R. Jensen, Relation between base oil composition and oxidation stability at increased temperatures, ASLE TRANSACTIONS 19 (2) (1976) 83–94.

[74] R. M. Zhmud, Boris, New base oils pose a challenge, Tribology & Lubrication Technology 67 (7) (2009) 34–38.

[75] J. Wright, The fundamentals of mineral base oil refining (2012).

[76] W. Dresel, et al., Lubricants and lubrication, John Wiley & Sons, 2007.

[77] A. Sequeira, Lubricant base oil and wax processing, CRC press, 1994.

[78] H. Wiener, Structural determination of paraffin boiling points, Journal of the American Chemical Society 69 (1) (1947) 17–20.

[79] M. Brown, J. Fotheringham, T. Hoyes, R. Mortier, S. Orszulik, S. Randles, P. Stroud, Synthetic base fluids, in: Chemistry and Technology of Lubricants, Springer, 2010, pp. 35–74.

[80] L. R. Rudnick, R. L. Shubkin, Synthetic lubricants and high-performance functional fluids, revised and expanded, Crc Press, 1999.

[81] L. Moore, D. Fels, A. Seay, C. Lopez, et al., Pao-based synthetic lubricants in industrial applications, Tribology & Lubrication Technology 59 (1) (2003) 23.

[82] D. R. Kodali, High performance ester lubricants from natural oils, Industrial lubrication and tribology 54 (4) (2002) 165–170.

[83] N. S. Ahmed, A. M. Nassar, Lubricating oil additives, in: Tribology-Lubricants and Lubrication, InTech, 2011.

[84] S. Q. Rizvi, Lubricant chemistry, technology, selection, and design, ASTM International, Conshohocken.

[85] G. Biresaw, K. L. Mittal, Surfactants in tribology, Vol. 4, CRC Press, 2014.

[86] M. T. Costello, 17 corrosion inhibitors and rust preventatives, Lubricant Additives: Chemistry and Applications (2009) 421.

[87] R. Stone, Introduction to internal combustion engines, Palgrave Macmillan, 2012.

[88] V. P. Astakhov, Tribology of Metal Cutting, Vol. 52, Elsevier, 2006.

[89] Z. Tang, S. Li, A review of recent developments of friction modifiers for liquid lubricants (2007–present), Current Opinion in Solid State and Materials Science 18 (3) (2014) 119–139.

[90] M. Smeeth, H. Spikes, S. Gunsel, Boundary film formation by viscosity index improvers, Tribology Transactions 39 (3) (1996) 726–734.

[91] S. Naidu, E. Klaus, J. Duda, Kinetic model for high-temperature oxidation of lubricants, Industrial & engineering chemistry product research and development 25 (4) (1986) 596–603.

[92] J. Lahijani, F. Lockwood, E. Klaus, The influence of metals on sludge formation, ASLE Transactions 25 (1) (1982) 25–32.

[93] M. Rasberger, Oxidative degradation and stabilisation of mineral oil based lubricants, in: Chemistry and technology of lubricants, Springer, 1997, pp. 98–143.

[94] E. Dimitroff, J. Moffitt, R. Quillian, Why, what, and how: Engine varnish, Journal of Lubrication Technology 91 (3) (1969) 406–416.

[95] J. Dong, C. A. Migdal, 1 antioxidants, Lubricant Additives: Chemistry and Applications (2009) 1.

[96] A. Sasaki, Contaminants in used oils and their behavior, Journal of ASTM International 6 (2) (2009) 1–12.

[97] L. Chen, J. Dong, G. Chen, The study of tribo-induced deposits from a copper-containing antiwear additive, Tribology transactions 40 (2) (1997) 339–345.

[98] C. A. Migdal, A. B. Wardlow, J. L. Ameye, Oxidation and the testing of turbine oils, ASTM, 2008.

[99] F. Rounds, Effects of hydroperoxides on wear as measured in four-ball wear tests, Tribology transactions 36 (2) (1993) 297–303.

[100] B. Atherton, Discovering the root cause of varnish formation, Practicing oil analysis 2 (2007) 22–25.

[101] N. Kumar, P. Besuner, S. Lefton, D. Agan, D. Hilleman, Power plant cycling costs, Tech. rep., National Renewable Energy Laboratory (NREL), Golden, CO. (2012).

[102] A. Sitton, J. Ameye, R. E. Kauffman, Residue analysis on rpvot test samples for single and multiple antioxidants chemistry for turbine lubricants, Journal of ASTM International 3 (6) (2006) 1–15.

[103] M. Diaby, M. Sablier, A. Le Negrate, M. El Fassi, J. Bocquet, Understanding carbonaceous deposit formation resulting from engine oil degradation, Carbon 47 (2) (2009) 355–366.

[104] A. Sasaki, S. Uchiyama, T. Yamamoto, Free radicals and oil auto-oxidation due to spark discharges of static electricity, Tribology & Lubrication Technology 55 (9) (1999) 24.

[105] G. Aguilar, G. Mazzamaro, M. Rasberger, Oxidative degradation and stabilisation of mineral oil-based lubricants, in: Chemistry and Technology of Lubricants, Springer, 2010, pp. 107–152.

[106] M. Lazár, Free radicals in chemistry and biology, CRC press, 1989.

[107] S. Blaine, P. E. Savage, Reaction pathways in lubricant degradation. 3. reaction model for n-hexadecane autoxidation, Industrial & engineering chemistry research 31 (1) (1992) 69–75.

[108] V. F. Lvovich, M. F. Smiechowski, Impedance characterization of industrial lubricants, Electrochimica acta 51 (8) (2006) 1487–1496.

[109] O. D. Livingstone, Greg, The emerging problem of lubricant varnish, Maintenance & Asset Management 25 (2) (2010) 38–42.

[110] Z. Pawlak, Tribochemistry of lubricating oils, Vol. 45, Elsevier, 2003.

[111] P. Antoniewicz, Surface-induced dipole moments of adsorbed atoms, Physical Review Letters 32 (25) (1974) 1424.

[112] W. Kohn, K.-H. Lau, Adatom dipole moments on metals and their interactions, Solid State Communications 18 (5) (1976) 553–555.

[113] N. Emanuel, Z. Maizus, I. Skibida, The catalytic activity of transition metal compounds in the liquid-phase oxidation of hydrocarbons, Angewandte Chemie International Edition 8 (2) (1969) 97–107.

[114] G. V. Fuchs, H. Diamond, Oxidation characteristics of lubricating oils, Industrial & Engineering Chemistry 34 (8) (1942) 927–937.

[115] H. Zuidema, Oxidation of lubricating oils., Chemical reviews 38 (2) (1946) 197–226.

[116] V. J. Gatto, W. E. Moehle, T. W. Cobb, E. R. Schneller, Oxidation fundamentals and its application to turbine oil testing, Journal of ASTM International 3 (4) (2006) 1–20.

[117] J. Pospíšil, Aromatic and heterocyclic amines in polymer stabilization, in: Polysoaps/Stabilizers/Nitrogen-15 NMR, Springer, 1995, pp. 87–189.

[118] T. Colclough, Role of additives and transition metals in lubricating oil oxidation, Industrial & engineering chemistry research 26 (9) (1987) 1888–1895.

[119] K. C. Ludema, Friction, wear, lubrication: a textbook in tribology, CRC press, 1996.

[120] K. Farooq, Varnish removal and control in turbine lubrication systems, in: ASME 2009 Power Conference, American Society of Mechanical Engineers, 2009, pp. 281–287.

[121] J. Fitch, Temperature stability of lubricants and hydraulic fluids, Machinery Lubrication (2002) 22–28.

[122] N. McGuire, Tiny bubbles, Tribology & Lubrication Technology 71 (2) (2015) 34.

[123] J. Wright, Microdieseling and its effects on oil, Machinery Lubrication 12 (2012) 2012.

[124] R. Canavelis, Jet impact and cavitation damage, TRANS ASME–J BASIC ENG– 90 (3) (1968) 355–367.

[125] S. R. G. Avila, C. Song, C.-D. Ohl, Fast transient microjets induced by hemispherical cavitation bubbles, Journal of Fluid Mechanics 767 (2015) 31–51.

[126] T. Harvey, R. Wood, G. Denuault, H. Powrie, Investigation of electrostatic charging mechanisms in oil lubricated tribo-contacts, Tribology International 35 (9) (2002) 605–614.

[127] P. W. Huber, A. A. Sonin, Electric charging in liquid hydrocarbon filtration: A comparison of theory and experiments, Journal of Colloid and Interface Science 61 (1) (1977) 126–145.

[128] A. Sasaki, S. Uchiyama, T. Yamamoto, Generation of static electricity during oil filtration, Tribology & Lubrication Technology 55 (9) (1999) 14.

[129] American Petroleum Institute, Engine Oil Licensing & Certification System (EOLCS) Categories & Documents (2017).

[130] S. Lantz, J. Zakarian, S. Deskin, A. Martini, Filtration effects on foam inhibitors and optically detected oil cleanliness, Tribology Transactions 0 (0) (2017) 1–6.
URL http://dx.doi.org/10.1080/10402004.2017.1285089

[131] B. Phair, L. Bensch, J. Duchowski, M. Khazan, V. Tsalyuk, Overcoming the electrostatic discharge in hydraulic, lubricating and fuel-filtration applications by incorporating novel synthetic filter media, Tribology transactions 48 (3) (2005) 343–351.

[132] J. T. Leonard, H. W. Carhart, Effect of conductivity on charge generation in hydrocarbon fuels flowing through fiber glass filters, Journal of Colloid and Interface Science 32 (3) (1970) 383–394.

[133] T. L. Suratt, J. R. Holtz, Engine cleaning processes, uS Patent 5,232,513 (Aug. 3 1993).

[134] M. Carmichael, J. Binatena, Internal combustion engine scrubber, uS Patent 4,877,043 (Oct. 31 1989).

[135] and others, Flushing device for engine lubricating systems, uS Patent 2,454,585 (Nov. 23 1948).

[136] Standard Test Method for Acid and Base Number by Color-Indicator Titration, Standard, ASTM International, West Conshohocken, PA (2014).
URL https://doi.org/10.1520/D0974-14E02

[137] Standard Test Method for Acid Number of Petroleum Products by Potentiometric Titration, Standard, ASTM International, West Conshohocken, PA (2017).
URL https://doi.org/10.1520/D0664-17

[138] Standard Test Method for Oxidation Stability of Steam Turbine Oils by Rotating Pressure Vessel, Standard, ASTM International, West Conshohocken, PA (2014).
URL https://doi.org/10.1520/D2272-14A

[139] Standard Test Method for Kinematic Viscosity of Transparent and Opaque Liquids (and Calculation of Dynamic Viscosity), Standard, ASTM International, West Conshohocken, PA (2017).
URL https://doi.org/10.1520/D0445-17A

[140] Standard Test Method for Flash and Fire Points by Cleveland Open Cup Tester, Standard, ASTM International, West Conshohocken, PA (2016).
URL https://doi.org/10.1520/D0092-16B

[141] Standard Test Method for Determination of Oxidation Stability and Insolubles Formation of Inhibited Turbine Oils at 120°C Without the Inclusion of Water (Dry TOST Method), Standard, ASTM International, West Conshohocken,

PA (2017).
URL https://doi.org/10.1520/D7873-13R17

[142] Standard Practice for Condition Monitoring of Used Lubricants by Trend Analysis Using Fourier Transform Infrared (FT-IR) Spectrometry, Standard, ASTM International, West Conshohocken, PA (2010).
URL https://doi.org/10.1520/E2412-10

[143] I. J. Karassik, J. P. Messina, P. Cooper, C. Heald, et al., Pump handbook, Vol. 3, McGraw-Hill New York, 1986.

[144] H. Cholet, Progressing cavity pumps, Editions Technip, 1997.

[145] D. Dal Porto, L. Larson, et al., Multiphase-pump field trials demonstrate practical applications for the technology, SPE Production & Facilities 12 (03) (1997) 159–164.

[146] N. D. Manring, S. B. Kasaragadda, The theoretical flow ripple of an external gear pump, Transactions-American Society of Mechanical Engineers Journal of Dynamic Systems Measurment and Control 125 (3) (2003) 396–404.

[147] D. M. Wang, H. Ding, Y. Jiang, X. Xiang, Numerical modeling of vane oil pump with variable displacement, Tech. rep., SAE Technical Paper (2012).

[148] I. Takahashi, T. Noguchi, A new quick-response and high-efficiency control strategy of an induction motor, IEEE Transactions on Industry applications (5) (1986) 820–827.

[149] Hydraulics & Pneumatics, Fundamentals of hydraulic reservoirs.
URL http://hydraulicspneumatics.com

[150] Hydraulic fluid power - Fluids - Method for coding the level of contamination by solid particles, Standard, International Organization for Standardization, Geneva, Switzerland (2017).
URL https://www.iso.org/standard/72618.html

[151] Hydraulic fluid power - Determination of the particulate contamination level of a liquid sample by automatic particle counting using the light-extinction principle, Standard, International Organization for Standardization, Geneva, Switzerland (2008).
URL https://www.iso.org/standard/45552.html

[152] A. Harnoy, Bearing design in machinery: engineering tribology and lubrication, CRC press, 2002.

[153] L. F. Moody, Friction factors for pipe flow, Trans. Asme 66 (1944) 671–684.

[154] J. Happel, H. Brenner, Low Reynolds number hydrodynamics: with special applications to particulate media, Vol. 1, Springer Science & Business Media, 2012.

[155] A. Fredenslund, R. L. Jones, J. M. Prausnitz, Group-contribution estimation of activity coefficients in nonideal liquid mixtures, AIChE Journal 21 (6) (1975) 1086–1099.

[156] P. Michael, M. Cheekolu, P. Panwar, M. Devlin, R. Davidson, D. Johnson, A. Martini, Temporary and permanent viscosity loss correlated to hydraulic system performance, Tribology Transactions (just-accepted).

[157] P. P. Walsh, P. Fletcher, Gas turbine performance, John Wiley & Sons, 2004.

[158] Standard Test Method for Foaming Characteristics of Lubricating Oils, Standard, ASTM International, West Conshohocken, PA (2013).
URL https://doi.org/10.1520/D0892-13E01

[159] H. Eyring, Viscosity, plasticity, and diffusion as examples of absolute reaction rates, The Journal of chemical physics 4 (4) (1936) 283–291.

[160] B. Gebhart, L. Pera, The nature of vertical natural convection flows resulting from the combined buoyancy effects of thermal and mass diffusion, International Journal of Heat and Mass Transfer 14 (12) (1971) 2025–2050.

[161] N. Kafoussias, E. Williams, Thermal-diffusion and diffusion-thermo effects on mixed free-forced convective and mass transfer boundary layer flow with temperature dependent viscosity, International Journal of Engineering Science 33 (9) (1995) 1369–1384.

[162] J. H. Whitelaw, Convective heat transfer, Thermopedia.

[163] AISI Type 316 Stainless Steel, annealed sheet, Tech. rep., ASM Aerospace Specification Metals Inc., Pompano Beach, FL (2016).
URL http://asm.matweb.com/search/SpecificMaterial.asp?bassnum=mq316a

APPENDIX

test	varnish-coupon	fluid	flow rate (GPM)	temp (°C)	duration (min)
1	A-920	A	9	70	165
2	A-921	A	9	70	165
3	A-922	A	0.5	70	531
4	A-923	A	0.5	70	531
5	A-924	A	0.5	70	531
6	B-902	B	10	70	360
7	B-903	B	0.5	70	430
8	C-900	B	10	70	150
9	C-901	J	0.5	70	220
10	C-902	J	0.5	70	220
11	C-903	J	10	70	150
12	C-904	J	10	70	150
13	C-905	J	10	70	150
14	C-907	J	0.5	70	220
15	C-908	J	0.5	70	220
16	C-909	J	10	70	11
17	C-910	K	0.5	70	220
18	C-911	K	0.5	70	220
19	C-912	K	0.5	70	220
20	C-913	H	0.5	70	220
21	C-914	H	0.5	70	220
22	C-915	H	0.5	70	220
23	C-916	B	0.5	70	220
24	C-917	B	0.5	70	220
25	C-918	B	0.5	70	220
26	C-919	B	0.5	70	220
26a	C-919	H	10	90	11
27	C-920	B	0.5	70	220
27a	C-920	H	4.5	90	240

Table 7.3.0.1: Tests 1-27a

EndExpansion

test	varnish-coupon	fluid	flow rate (GPM)	temp (°C)	duration (min)
28	C-921	B	0.5	70	220
29	C-922	B	0.5	70	220
30	C-923	H	0.5	70	220
30a	C-923	H	10	70	11
31	C-924	H	0.5	70	220
32	C-925	K	0.5	70	220
32b	C-925	I	4.5	90	67
33	C-926	K	0.5	70	220
34	C-927	K	0.5	70	220
35	C-928	K	0.5	70	10
36	C-929	H	10	90	240
37	C-941	B	4.5	90	240
38	C-944	I	4.5	90	240
39	C-946	I	4.5	90	240
40	C-930	I	4.5	90	120
41	C-931	I	4.5	90	123
42	C-932	I	4.5	90	252
43	C-933	I	4.5	90	244
44	C-934	B	4.5	90	480
45	C-935	B	4.5	90	416
46	C-936	B	4.5	90	381
47	C-940	F	4.5	90	525
48	C-942	F	4.5	90	374
49	C-943	F	4.5	90	119
50	C-948	E	4.5	90	402
51	C-949	E	4.5	90	311
52	C-950	E	4.5	90	364
53	C-951	E	4.5	90	402
54	C-952	E	4.5	90	302
55	C-953	D	4.5	90	265
56	C-954	D	4.5	90	61
57	C-955	D	4.5	90	86
58	C-956	C	4.5	90	191
59	C-957	C	4.5	90	199
60	C-958	C	4.5	90	162
61	C-959	G	4.5	90	221
62	C-960	G	4.5	90	83
63	C-961	G	4.5	90	139

Table 7.3.0.2: Tests 28-63

test	varnish-coupon	fluid	flow rate (GPM)	temp (°C)	duration (min)
64	C-975	B	4.5	90	120
65	C-976	B	4.5	90	120
66	C-977	C	4.5	90	120
67	C-978	C	4.5	90	120
68	C-979	D	4.5	90	120
69	C-980	D	4.5	90	120
70	C-981	E	4.5	90	120
71	C-982	E	4.5	90	120
72	C-983	F	4.5	90	120
73	C-984	F	4.5	90	120
74	C-985	G	4.5	90	120
75	C-986	G	4.5	90	120
76	C-987	I	4.5	90	120
77	C-988	I	4.5	90	120
78	C-989	B	4.5	90	120
79	C-934	I	4.5	90	120
80	C-935	I	4.5	90	120
81	C-936	I	4.5	90	120
82	D-1008	B	4.5	90	120
83	D-1012	B	4.5	90	120
84	D-1015	B	4.5	90	120
85	D-1018	B	4.5	90	120
86	D-1005	B	4.5	90	120
87	D-1011	B	4.5	90	120
88	D-1013	B	4.5	90	120
89	D-1016	B	4.5	90	120
90	D-1001	B	4.5	90	120
91	D-1010	B	4.5	90	120
92	D-1014	B	4.5	90	120
93	D-1017	B	4.5	90	120
94	D-999	F	4.5	90	120
95	D-1019	F	4.5	90	120
96	D-1000	F	4.5	90	120
97	D-1006	F	4.5	90	120
98	D-1009	F	4.5	90	120
99	D-1004	F	4.5	90	120

Table 7.3.0.3: Tests 64-99

test	varnish-coupon	fluid	flow rate (GPM)	temp (°C)	duration (min)
100	D-1023	R	4.5	90	120
101	D-1027	R	4.5	90	120
102	D-1042	L	4.5	90	120
103	D-1044	L	4.5	90	120
104	D-1022	M	4.5	90	120
105	D-1024	M	4.5	90	120
106	D-1026	N	4.5	90	120
107	D-1040	N	4.5	90	120
108	D-1025	O	4.5	90	120
109	D-1036	O	4.5	90	120
110	D-1028	P	4.5	90	120
111	D-1030	P	4.5	90	120
112	D-1037	Q	4.5	90	120
113	D-1041	Q	4.5	90	120
114	D-1031	R	4.5	90	120
115	D-1032	R	4.5	90	120
116	D-1033	S	4.5	90	120
117	D-1039	S	4.5	90	120

Table 7.3.0.4: Tests 100 - 117